COMSAT
Technical Review

Volume 18 Number 2, Fall 1988

Advisory Board Joel R. Alper
Joseph V. Charyk
John V. Evans
John S. Hannon, Jr.
Willard R. Nichols

Editorial Board Geoffrey Hyde, *Chairman*
Richard A. Arndt
Ali E. Atia
S. Joseph Campanella
Dattakumar M. Chitre
William L. Cook
Russell J. Fang
Howard W. Flieger
Ivor N. Knight
Larry C. Palmer
David V. Rogers
Hans J. Weiss
Daniel R. Wells
Pier L. Bargellini, *Editor Emeritus*

Editorial Staff
MANAGING EDITOR
Margaret B. Jacocks
TECHNICAL EDITOR
Barbara J. Wassell
PRODUCTION
Barbara J. Wassell
Raymond L. Joyner
CIRCULATION
Merilee J. Worsey

COMSAT TECHNICAL REVIEW is published twice a year by Communications Satellite Corporation (COMSAT). Subscriptions, which include the two issues published within a calendar year, are: one year, $15 U.S.; two years, $25; three years, $35; single copies, $10; article reprints, $2.50. Overseas air mail delivery is available at an additional cost of $18 per year. Make checks payable to COMSAT and address to Records Department, Communications Satellite Corporation, 22300 Comsat Drive, Clarksburg, MD 20871-9475, U.S.A.

ISSN 0095-9669

© COMMUNICATIONS SATELLITE CORPORATION 1988
COMSAT IS A TRADE MARK AND SERVICE MARK
OF THE COMMUNICATIONS SATELLITE CORPORATION

COMSAT TECHNICAL REVIEW

Volume 18 Number 2, Fall 1988

Index: intersatellite links, communication satellites, satellite networks, spacecraft communications, payloads, orbit spectrum utilization

Intersatellite link application to commercial communications satellites

Y. S. Lee, A. E. Atia, and D. S. Ponchak

(Manuscript received May 15, 1987)

Abstract

The fundamental characteristics of intersatellite link (ISL) systems, and their application to domestic, regional, and global satellite communications, are described. The quantitative advantages of using ISLs to improve orbit utilization, spectrum occupancy, transmission delay (compared to multi-hop links), coverage, and connectivity, and to reduce the number of earth station antennas, are also presented. Cost-effectiveness and other systems benefits of using ISLs are identified, and the technical and systems planning aspects of ISL systems implementation are addressed.

Introduction

Intersatellite links (ISLs), which have not yet been used in commercial satellite networks, can improve and expand communications satellite services. As the demand increases for orbital slots within prime regions of the geostationary arc, ISLs offer the possibility of using this resource more efficiently, and thus circumventing orbit saturation. ISLs can also conserve the spectral resources allocated to the fixed-satellite services (FSS) by replacing the up/down-link bandwidths of a relay station with the ISL frequency bands. An ISL replacing a multiple-hop system provides reduced signal propagation delay, and consequently improved system quality.

An ISL between a domestic satellite network and an international network allows international traffic from small, remote terminals in a given country

to be directed to the nearest domestic earth station and then to the satellite providing international service. Thus, ISLs between domestic and/or regional satellites could support new satellite network architectures.

ISL technologies have been under study for over a decade (since late 1970) by many organizations [1]–[5], and technologies have been developed for the implementation of ISLs at both microwave and optical frequencies. ISL technology issues are sufficiently well defined, and solutions for space applications either already exist or are expected to become available in the near future [6],[7].

At the current stage of ISL development, the crucial question is whether ISLs can enable the design of cost-effective alternatives to existing satellite communications systems. This paper addresses this question from a broad systems perspective. Potential ISL applications are described through a comprehensive evaluation of fundamental ISL systems characteristics and figure-of-merit factors. For each selected ISL application, typical network architectures and payload configurations are derived, and systems costs and benefits are discussed.

Fundamental ISL system characteristics

This section analyzes the major systems characteristics of ISLs, and their impact on the FSS is assessed. Based on this investigation, potential ISL applications are determined.

Orbital arc expansion capability

The useful geostationary orbital arc length that accommodates FSS satellites can be substantially increased by employing ISLs. This concept was previously investigated by Ponchak and Spence with reference to domestic satellite systems [8].

The orbital arc expansion factor, M_θ, can be defined as the ratio of the total useful arc length of an ISL system to that of a corresponding non-ISL system. The factor M_θ is a function of the following system parameters:

- satellite orbital location;
- coverage area(s);
- geographical distribution of traffic nodes (earth stations) within the coverage area; and
- minimum elevation angle of the earth station, which is determined by frequency band and communications link availability (rain statistics).

To quantify the orbital expansion factor, the following three systems were compared for continental United States (CONUS) ISL applications:

- a single CONUS area coverage (basic non-ISL system);
- double area coverages of CONUS (East- and West-half geographical coverages defined by a 96°W longitude line); and
- four time-zone coverages: Pacific, Mountain, Central, and Eastern.

For each system, the useful geostationary orbital locations of the satellites were computed for C-, K_u-, and K_a-band FSS communications services. The criteria for the useful arc are defined so that the minimum elevation angles of the earth station within the coverage are 5°, 10°, and 30° for the C-, K_u-, and K_a-bands, respectively. A satellite-addressable CONUS traffic matrix (based on the traffic model described in Appendix A) was used in the analysis.

The percentage of satellite traffic accessible using the minimum specified earth station elevation angles within a coverage area is shown in Figures 1 through 3 for various satellite orbital locations. In these figures, the percentage of satellite traffic is defined as the ratio of visible traffic to the total traffic within the prescribed area.

Table 1 summarizes the useful orbital arc length and the orbital arc expansion factor (M_θ) that can provide 100-percent traffic coverage for CONUS. Factor M_θ is the ratio of the arc length useful for accommodating 100-percent CONUS traffic with ISLs to the arc length for the single-coverage case (without ISLs).

TABLE 1. ISL ORBITAL ARC EXPANSION CAPABILITY FOR CONUS*

FREQUENCY	SINGLE COVERAGE WITHOUT ISLs	TWO COVERAGES WITH ISLs		FOUR ZONES WITH ISLs	
	ARC LENGTH	ARC LENGTH	M_θ	ARC LENGTH	M_θ
C-Band	85°	143°	1.68	160°	1.89
K_u-Band	69°	128°	1.86	158°	2.29
K_a-Band	5°	59°	11.80	94°	18.80

*Geosynchronous orbital arc centered around 100°W longitude.

As can be seen from the table, the use of ISLs leads to significant increases in the total useful arc length. Therefore, an ISL provides an increased number of useful orbital slots for FSS satellites. For K_a-band satellites, the ISL arc expansion capability is very significant.

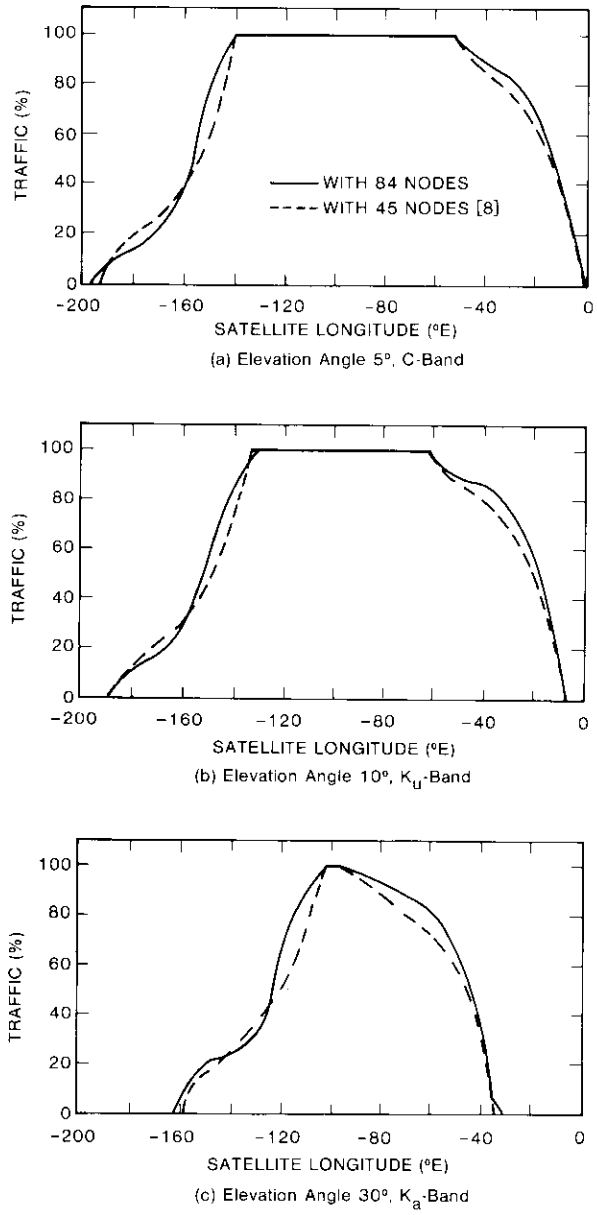

Figure 1. *A Single CONUS Coverage Satellite Orbital Arc Requirement*

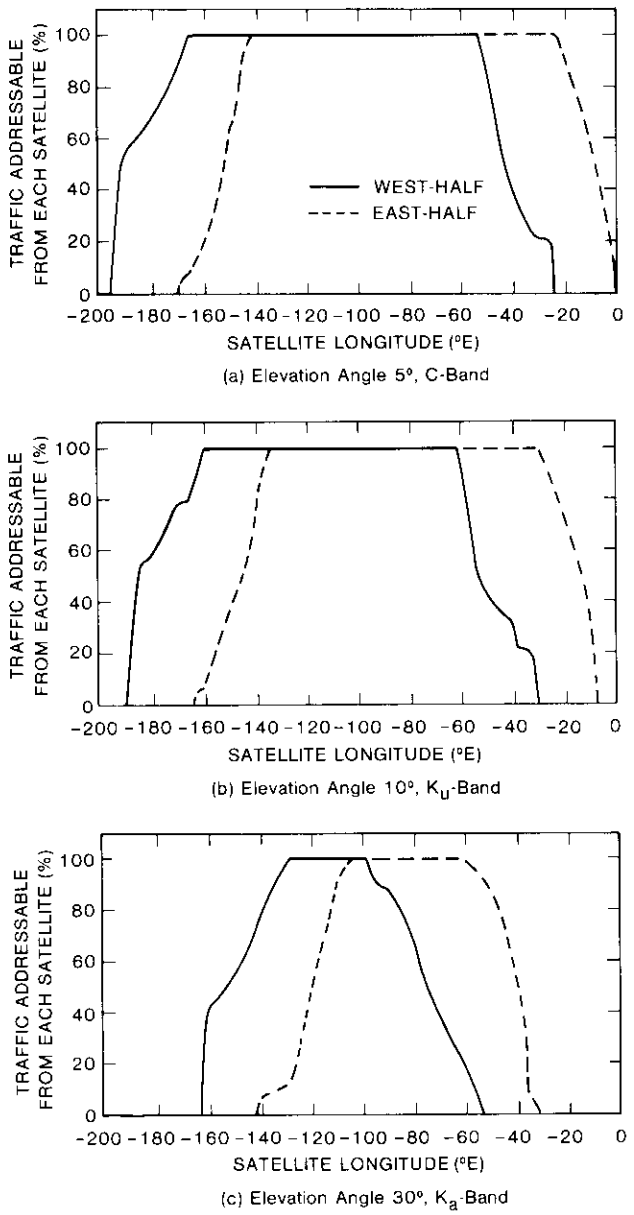

Figure 2. *CONUS East- and West-Half Coverage ISL Orbital Arc Expansion*

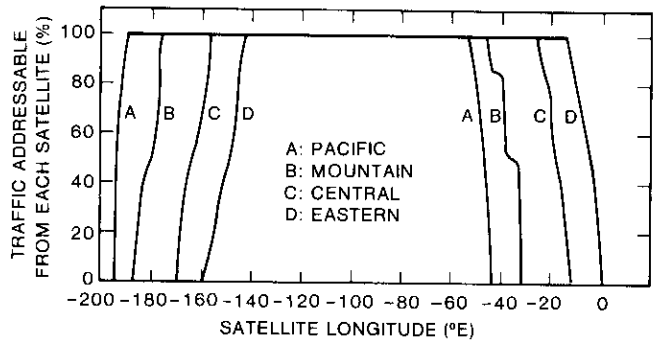

(a) Elevation Angle 5°, C-Band

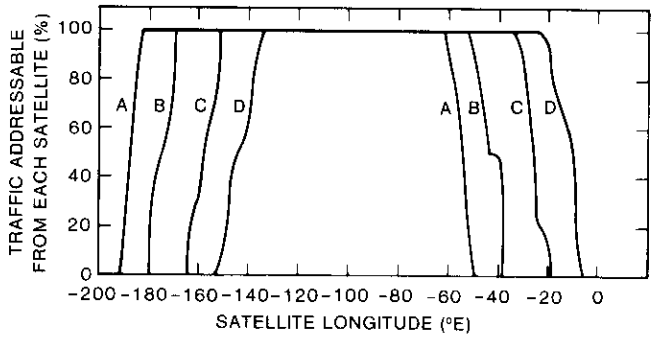

(b) Elevation Angle 10°, K_U-Band

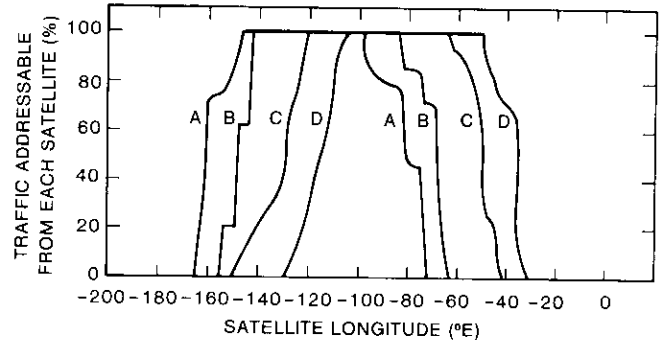

(c) Elevation Angle 30°, K_a-Band

Figure 3. *Four-Time-Zone-Coverage Orbital Expansion Capability of ISL*

Space segment spectrum utilization improvement

Space segment bandwidth savings can be achieved by using an ISL to avoid double-hop transmissions, as shown in Figure 4. The figure depicts two systems that provide identical coverage. In the non-ISL system (Figure 4a), a double hop is needed to interconnect any two stations that are not in the same coverage area. The ISL system of Figure 4b avoids double-hopping. The transponder bandwidth needed by the cross traffic (T_{12} and T_{21}) between coverage areas C_1 and C_2 is indicated for each case by the shaded portions at the top of the figure.

Table 2 lists frequency bands characterized by high atmospheric attenuation (and thus not useful for up- or down-links) which have been assigned to the ISLs by the International Telecommunications Union (ITU) [9]. Because the ISL frequency spectrum is traded for the spectrum of the up- and down-links, the ISLs provide an increased space segment capacity in direct proportion to ISL traffic. The released bandwidth then becomes available for additional up- and down-link traffic.

TABLE 2. ISL FREQUENCY ALLOCATION (ITU)

FREQUENCY BAND (GHz)	BANDWIDTH TOTAL* (GHz)
22.55–23.55	1.00
32.0–33.0	1.00
54.25–58.20	3.95
59.00–64.00	5.00
116–134	18.00
170–182	12.00
185–190	5.00
Total	45.95

*To be shared with other radio services in most of the bands.

The spectrum utilization improvement factor, M_B, is defined as the ratio of total traffic capacity of non-ISL *vs* ISL systems. For a service area encompassing N satellite coverages, M_B is given by

$$M_B = \frac{\text{Total bandwidth of non-ISL system}}{\text{Total up- and down-link bandwidth of ISL system}}$$

$$= 1 + \frac{\sum_{i,j=1}^{N} T_{ij}}{\sum_{i,j=1}^{N} T_{ij}} \quad (i \neq j) \qquad (1)$$

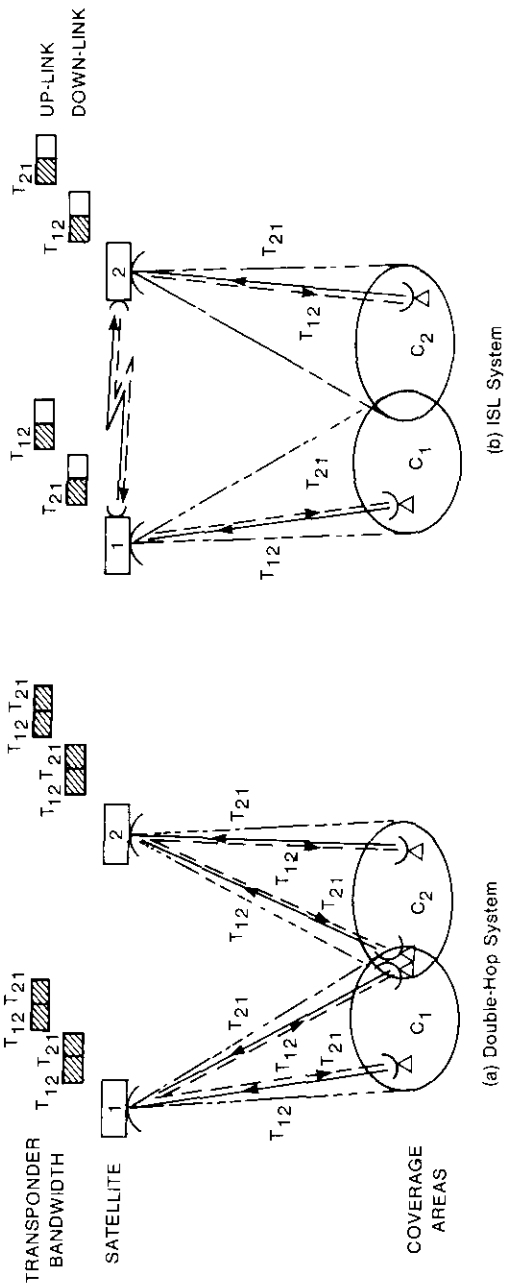

Figure 4. *Bandwidth Utilization Improvement With ISL*

where T_{ij} represents a traffic matrix element between service areas i and j. The numerator in the second term represents the additional bandwidth required for double hops.

For the case of four-time-zone CONUS coverage and four ISL satellites, as discussed previously, the total CONUS traffic based on the model in Appendix A is

$$\sum_{i,j=1}^{N=4} T_{ij} = 10 \times 10^6$$

while the ISL traffic (sum of off-diagonal matrix elements) is

$$\sum_{\substack{i,j=1 \\ (i \neq j)}}^{N=4} T_{ij} = 6.408 \times 10^6$$

Therefore, the spectrum utilization factor for this case is $M_B = 1.641$.

Time delay reduction

Transmission time delay impacts commercial satellite communications for both voice and data. For voice, a user's convenience in carrying out the conversation is inversely proportional to the mean of the end-to-end delay in the satellite communications system [10]. Therefore, increased delay in a double-hop transmission (for example) discourages voice circuit users, resulting in decreased traffic.

The transmission efficiency in a data transmission system is related to the weighting factor, which is proportional to $1/(1 + d)$, where d is the round-trip delay time in blocks for stop-and-wait automatic repeat request (ARQ) error control [11]. Transmission efficiency decreases rapidly when the delay is significant relative to block duration.

ISL usage can eliminate multiple hops and reduce transmission delay. This reduction can be measured by the end-to-end delay reduction factor of an ISL, defined as

$$M_T = \frac{\text{Transmission delay in non-ISL system}}{\text{Transmission delay in ISL system}} .$$

Transmission time delay is determined from the ISL geometry shown in Figure 5. The total one-way time delay of signals originating from a transmit earth station and received by another station within the coverage areas of two ISL satellites includes the delays encountered in the up-link, ISL, and down-link. The up- and down-link delays depend on the elevation angles of the transmit and receive earth stations.

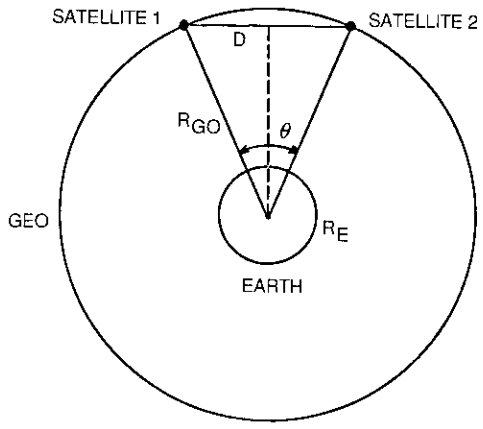

R_E = Earth radius, 6.375×10^6 m

R_{GO} = Geostationary orbit distance from the center of the earth, 4.216×10^7 m

θ = ISL longitudinal separation in degrees

D = ISL distance between two satellites

Figure 5. *Basic Geometry of the ISL*

Figure 6 shows the total one-way transmission delay vs ISL distance in longitudinal degrees. Also shown are single- and double-hop delays of the non-ISL satellite network. The lower bound of delay corresponds to transmit and receive earth stations located near the subsatellite points, while the upper bound corresponds to earth stations having 5° elevation angles within the coverage areas.

An ISL has a definite advantage in reducing delay, compared to a corresponding double-hop network without ISL. ISLs between satellites that are spaced about 50° apart in longitude can meet the International Telegraph and Telephone Consultative Committee (CCITT)-recommended 400-ms criterion of one-way transmission delay for voice traffic. A corresponding double-hop network requires a longer delay, ranging from 477 to 555 ms, and cannot meet the CCITT criterion. The time delay advantage of ISLs can provide improved telephony services to more users in the extended coverage areas, resulting in increased satellite-addressable traffic.

Coverage extension and flexible traffic interconnectivity

Increased geographical coverage and traffic interconnectivity can be achieved with ISLs. Individual satellite orbital locations can be selected to

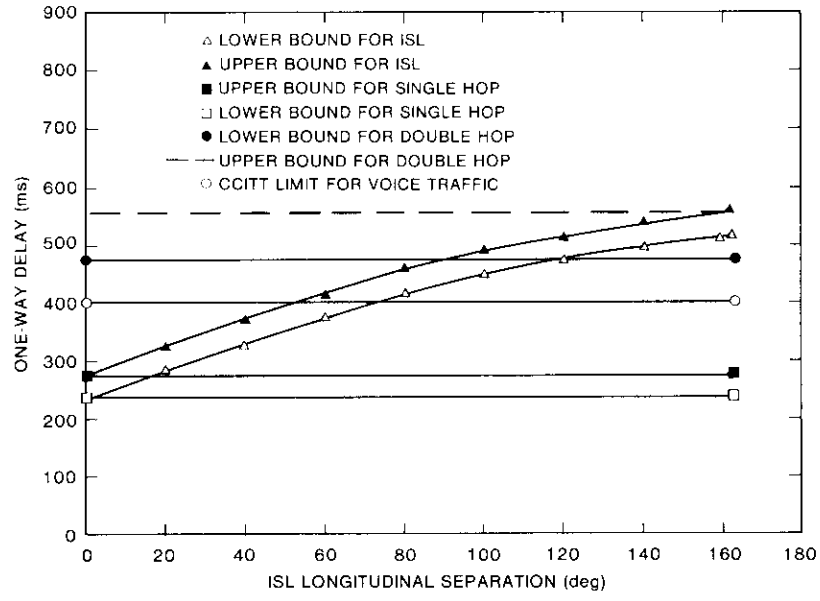

Figure 6. *Transmission Delay of the ISL System*

provide coverage for high-traffic areas. For example, a 50° ISL connecting two satellites located at 10° and 60°W longitude can provide full traffic interconnectivity for all users in the extended joint coverage areas, including CONUS, South America, Europe, the Middle East, and Africa. Figure 7 shows the worldwide coverage achievable with three ITU regional ISL satellites positioned at 15°, 125°, and 250°E, respectively.

An ISL provides a space segment link for flexible traffic interconnectivity between satellites, which allows considerable flexibility in satellite systems network planning. An integrated space segment for domestic, regional, and international communications [12],[13] can be achieved through efficient use of ISLs.

Reduction factor for number of earth station antennas

While multiple earth station antennas are needed for interconnectivity between satellites in conventional multi-hop systems, only one earth station antenna per traffic node is required in ISL systems. The ISL advantage factor related to the reduction of the number of antennas at each earth station is

$$M_E = \frac{N_n}{N_i}$$

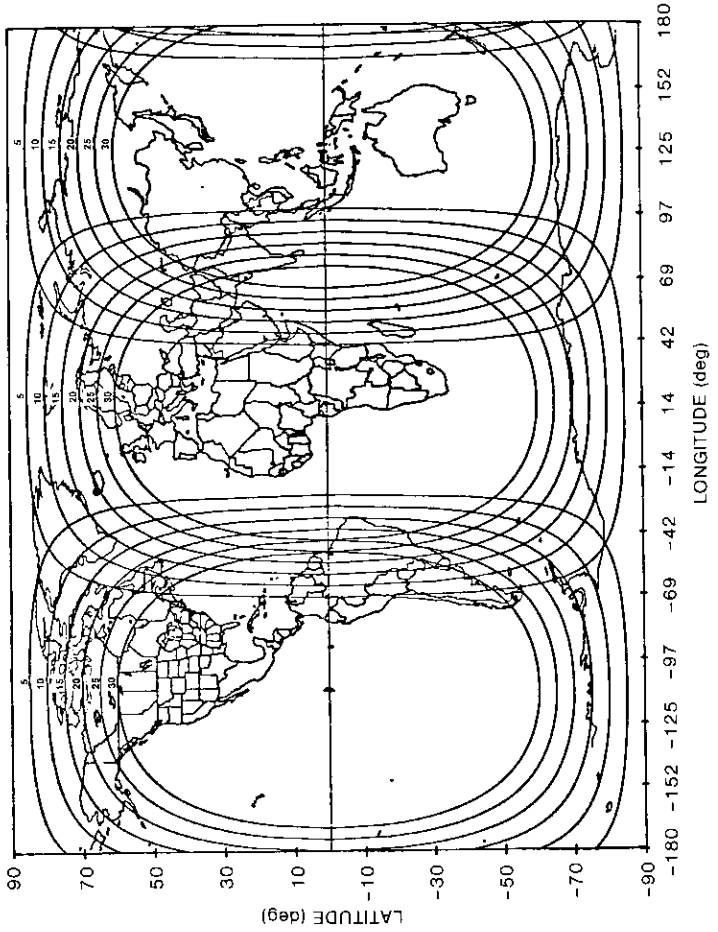

Figure 7. *Extended Coverage With Three ISL Satellites at 15°, 125°, and 250°E, Shown by Contours of Constant Elevation Angle*

where N_n is the number of antennas needed at the earth stations in non-ISL systems, and N_i is the number of antennas needed at the earth stations in ISL systems.

When satellites serve separate common coverage areas, the ISL advantage factor can be shown by

$$M_E = 1 + \frac{\theta_s}{\Delta\theta} \tag{2}$$

where θ_s is the total orbital arc length used, and $\Delta\theta$ is the orbital arc spacing between adjacent satellites. Arc spacing $\Delta\theta$ ranges from 2° to 3°, in accordance with recent Federal Communications Commission (FCC) licensing policy [14].

The total number of earth stations in the ISL *vs* non-ISL network systems is a difficult parameter to quantify because it depends on the systems architecture and traffic model. For example, if each of the multiple isolated satellites provides subdivided coverage, the corresponding ISL network will eliminate only the double-hop relay earth stations. In this case, M_E is given by

$$M_E = 1 + \frac{1}{N_{ES}} \sum_{i=1}^{N_s - 1} N_{Ri} \tag{3}$$

where N_s = number of isolated satellites
N_{ES} = total number of earth stations in the ISL network system
N_{Ri} = number of relay stations for double-hopping between adjacent, ith, and $(i + 1)$-th coverages.

Equation (2) provides the upper bound of M_E as a limiting case of ISL applications.

Potential ISL applications

Systems characteristics were evaluated for various categories of ISLs ranging from a very short separation (<0.1° between collocated satellites) to a 120° separation between ITU regional satellites. Based on these systems characteristics, figure-of-merit factors for ISLs were defined and derived in order to rank candidate ISL applications.

Selection of an ISL system involves a broad range of issues, including technical, operational, and economic considerations, and regulatory bounds. Because operational, economic, and regulatory aspects are difficult to define in the early study of ISL systems applications, technical considerations were focused in deriving an overall figure of merit for an ISL system.

Overall ISL figure of merit

An overall figure of merit (M) for an ISL system, with reference to a corresponding non-ISL system, can be expressed as

$$M = M_\theta \cdot M_B \cdot M_T \cdot M_E \quad . \tag{4}$$

Table 3 gives the figure-of-merit factors for ISL applications to CONUS for two East- and West-half CONUS coverage satellites, as well as for four-time-zone-coverage satellites employing ISLs.

TABLE 3. CONUS ISL FIGURE-OF-MERIT FACTORS AND OTHER CONSIDERATIONS

FACTORS	CONUS ISL APPLICATIONS	
	TWO (EAST/WEST-HALF) COVERAGES	FOUR-TIME-ZONE COVERAGE
Orbital Arc Expansion		
C-Band	1.68	1.89
K_u-Band	1.86	2.29
K_a-Band	11.80	18.80
Bandwidth Utilization Improvement	1.35	1.64
Time Delay	1.3–1.4 (1.35 avg)	1.3–1.4 (1.35 avg)
Earth Station Antenna Reduction	2 max	4 max
Total Figure of Merit		
C-Band	6.12	16.74
K_u-Band	6.78	20.28
K_a-Band	43.00	166.50
Other Considerations		
• Up/Down-Link Capacity/Satellite	Exceeding 1,000 × 2 transponders	Not exceeding 500 × 2 transponders
• Satellite Spare	1	1 (minimum)
• Operational Complexity	Moderate	Increased

Selected ISL network architectures

Six ISL applications were selected for further investigation. They are as follows:

1. CONUS, Four-Zone-Coverage Domestic Services
2. U.S./North America–Europe
   (a) CONUS–Europe
   (b) North America–Europe
3. CONUS–International
   (a) CONUS–Pacific Ocean Region (POR)
   (b) CONUS–Atlantic Ocean Region (AOR)
4. ITU Region 1–International
   (a) Region 1–AOR
   (b) Region 1–Indian Ocean Region (IOR)
5. ITU Regions 1, 2, and 3
   (a) Region 1–Region 2
   (b) Region 2–Region 3
   (c) Region 3–Region 1
6. Intercluster ISL for CONUS

These applications were selected based primarily on their potential high impact on satellite communications, as well as on traffic concentrations. The following subsection discusses their network architectures and payload configurations, which were initially summarized in Reference 15.

Network architectures and payload configurations

The space segment and ISL capacity requirements for each of the selected applications were derived from the available FSS traffic models, such as the following:

- a NASA-supplied U.S. domestic traffic model for the year 2000 [16], [17];
- the INTELSAT traffic database [18];
- the FCC's Space World Administrative Radio Conference (WARC) 1985 traffic forecast [19]; and
- other models [20]–[22].

A generalized traffic grouping program was used to quantify ISL traffic models for various applications. Based on the models, ISL capacity requirements were determined for applications to U.S. domestic, regional, international, and ITU regional group ISLs. (See Appendix A for a more detailed discussion.)

For each candidate ISL application, two system architectures were derived (one using ISL, the other non-ISL) based on the following assumptions:

- Satellite-addressable traffic models for the year 2001.
- ISL capacity for 100-percent capture of traffic.

- 4,500 half-voice circuits per 36-MHz transponder bandwidth, employing 32-kbit/s rate speech encoding with digital speech interpolation and quadrature phase-shift keying/time-division multiple-access (QPSK/TDMA) transmission.
- Space hardware technology available at the end of 1990 for ISL implementation.
- ISL and non-ISL systems providing the same services.

Both microwave (60-GHz) and optical (0.85-μm) ISL implementation approaches were evaluated for payload sizing and cost.

NETWORK ARCHITECTURES

Table 4 presents a summary of the selected ISL network architectures, including the ISL range, ISL traffic requirement, and satellite orbital locations. Figure 8 is a simplified representation of ISL and non-ISL satellite constellations for each of these applications.

TABLE 4. SELECTED ISL NETWORK ARCHITECTURES

APPLICATION NUMBER	ISL APPLICATION	ISL RANGE (NOMINAL)	ISL PAYLOAD CAPACITY (Mbit/s)	ORBITAL LOCATIONS
1	CONUS Four-Zone Coverage	30°	7,600; 10,300; 20,500	49° to 143°W
2	U.S./North America–Europe			
2a	CONUS–Europe	50°	618	58°W, 8°W
2b	North America–Europe	50°	677	58°W, 8°W
3	CONUS–International			
3a	CONUS–POR	50°	317	131°W, 177°E
3b	CONUS–AOR	30°	1,220	58°W, 24.5°W
4	ITU Region 1–International			
4a	Region 1–AOR	70°	845	15°E, 53°W
4b	Region 1–IOR	70°	200	15°E, 81°E
5	ITU Regions 1, 2, and 3			
5a	Region 1–Region 2	125°	1,430	15°E, 110°W
5b	Region 2–Region 3	125°	360	110°W, 125°E
5c	Region 3–Region 1	110°	576	125°E, 15°E
6	Intercluster ISL for CONUS	0.1°	50 to 10,300 (Configuration-dependent)	98° to 103°W

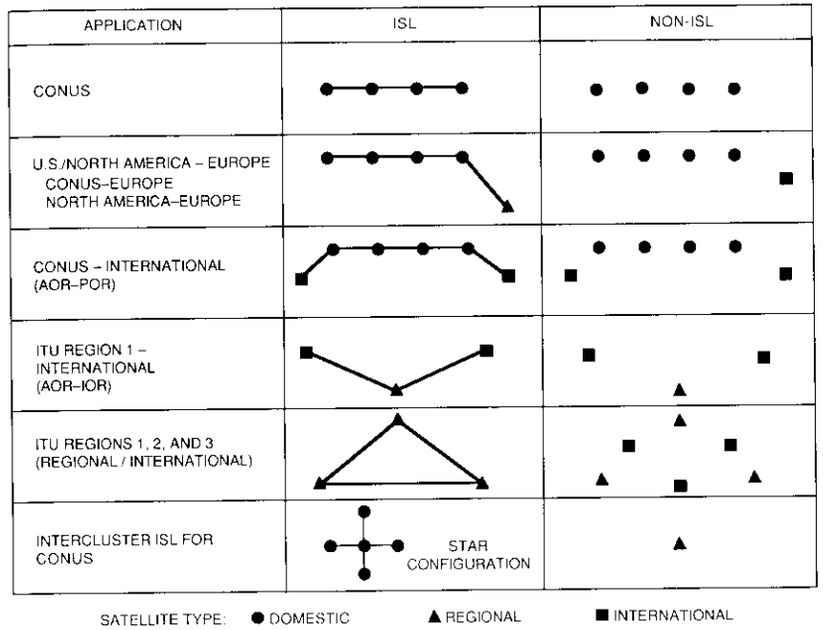

Figure 8. *ISL vs Non-ISL Satellite Constellations*

The CONUS ISL application for the four-time-zone-coverage satellite (Figure 9) provides a significant expansion of the useful orbital arc. CONUS satellites, under a 30° elevation angle criterion for K_a-band services, can be placed anywhere within the following arc segments:

CONUS TIME-ZONE SATELLITES	ORBITAL LOCATION
Pacific	49° to 99°W
Mountain	66° to 119°W
Central	86° to 128°W
Eastern	97° to 143°W

In comparison, the corresponding non-ISL CONUS coverage satellites for K_a-band services must be placed in a slot between 98° and 103° (*i.e.*, the useful orbital arc length is only 5°).

Figure 10 shows the ITU regional three-satellite system network architecture with ISLs. The CONUS ISL and non-ISL system architectures are shown in Figure 11. Each zone satellite employs extensive frequency reuses, with a number of spot beams in the C-, K_u-, and K_a-bands. The up- and down-link

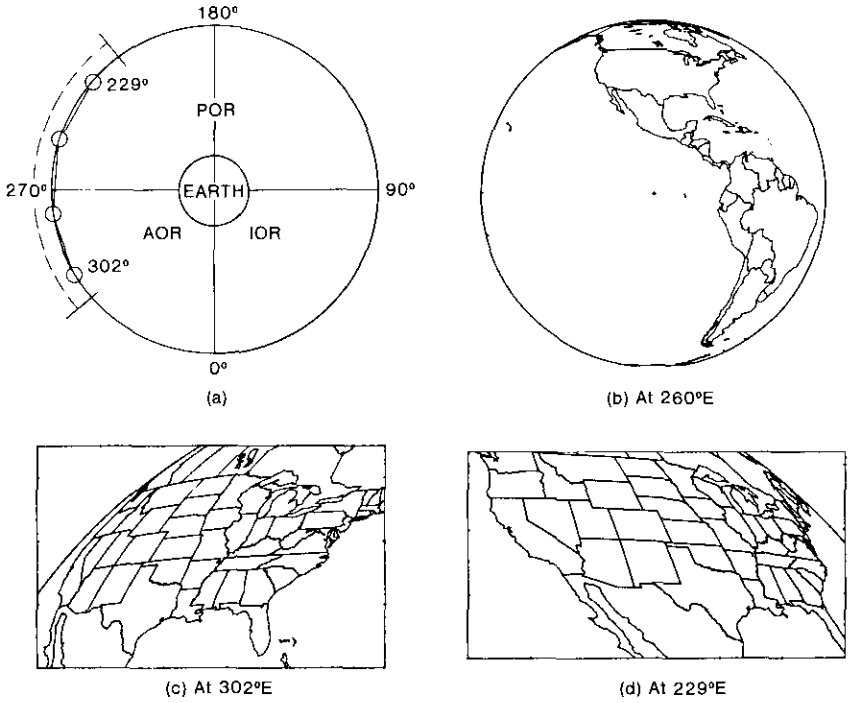

Figure 9. *ISL Application 1 for CONUS*

capacity requirement ranges from 125 transponders for the Mountain time zone satellite, to 1,145 transponders for the Eastern time zone satellite.

Figure 11 also shows two different non-ISL systems architectures: a double-hop network (architecture 1) and a multiple colocated earth station network (architecture 2). Traffic interconnectivity in the double-hop network can be provided at a central switching/processing station.

The multiple-hop network configurations were taken as representative non-ISL system architectures for the other ISL applications (nos. 2 through 5 in Table 4), except for inter-cluster ISL. Multiple colocated partitioned satellites without ISLs, or a large "super" satellite, were considered as the corresponding non-ISL system of the intercluster ISL.

PAYLOAD CONFIGURATIONS

ISL payload configurations and spacecraft size were determined for each network architecture. Microwave (60-GHz) and optical (0.85-μm) implementations of the ISL payload were evaluated for mass and power requirements.

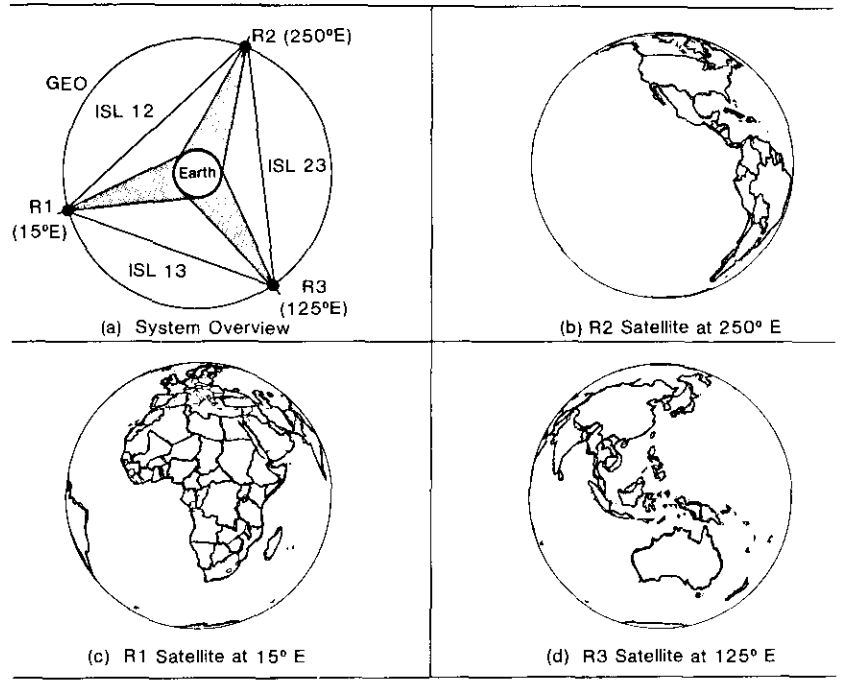

Figure 10. *Three-ITU-Regional ISL Satellite System*

Table 5 lists the basic ISL system parameters. A conservative optical receiver sensitivity of -76 dBW at 1-Gbit/s direct detection [quaternary pulse-position modulation (QPPM)] was used, with low-noise silicon avalanche photodiodes (APDs) and GaAs metal semiconductor field-effect transistor (MESFET) front-end amplifiers. The state-of-the-art highest receiver sensitivity reported in the literature is about 5 dB higher than this design value [23]. A system margin of about 6 dB was included in the link design to account for optical power losses due to various imperfections in pointing and tracking performance, point-ahead angle compensation, and optical transmit and receive circuit losses [24].

For a given ISL distance and transmission rate, ISL payload design involved a tradeoff between aperture size and transmit power. Figure 12 is an example of the tradeoffs in the optical ISL payload design for a 0.85-μm diode laser. Figure 13 shows a simplified optical ISL payload block diagram.

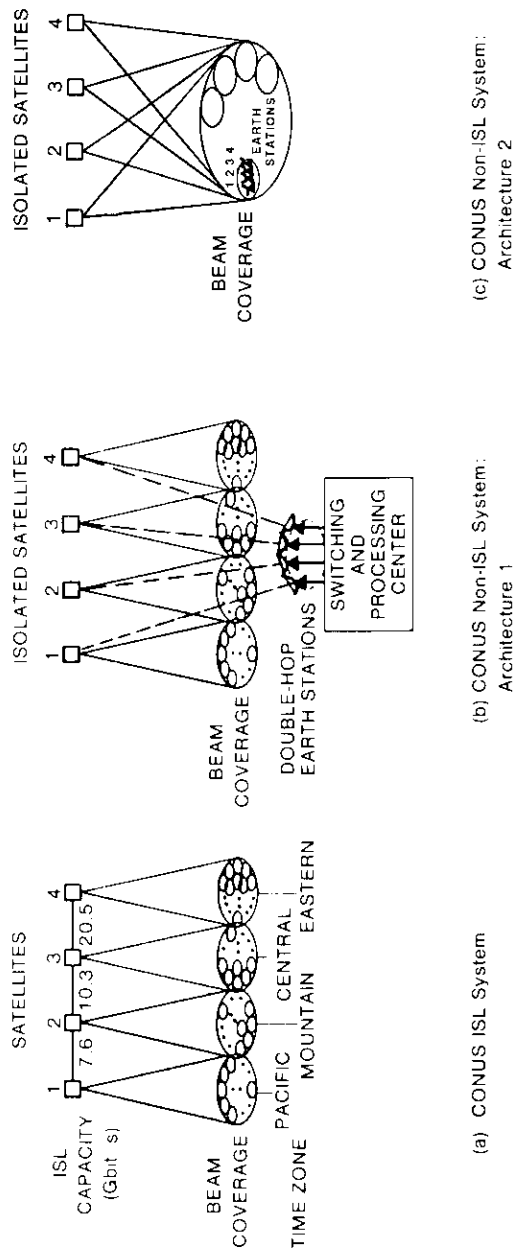

Figure 11. *CONUS ISL and Non-ISL System Architectures*

TABLE 5. CHARACTERISTICS OF MICROWAVE (60-GHz) AND OPTICAL (0.85-μm) ISLs

PARAMETER	MICROWAVE	OPTICAL
ISL Distance	Per selected application	Per selected application
Bit Error Rate	$\leq 10^{-7}$	$\leq 10^{-7}$
Modulation	Uncoded QPSK	Diode laser QPPM, uncoded, direct-detection receive system
Antenna Aperture Size	≤2 m	≤60 cm
Transmit Power	10–75 W	100–300 mW
Receive Characteristics	Noise figure = 8 dB (HEMT device)	Optical receiver sensitivity = −76 dBW at 1-Gbit/s rate

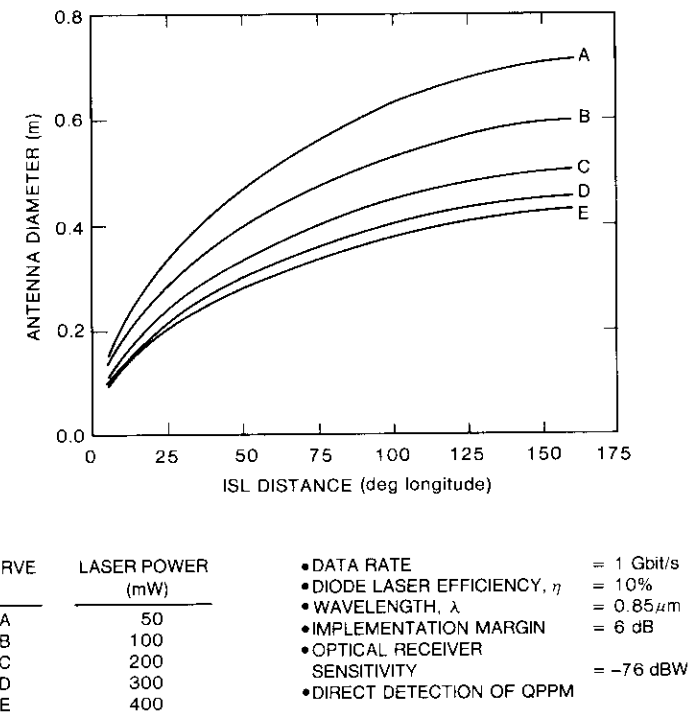

Figure 12. *Optical ISL Payload Design: Parameter Tradeoffs*

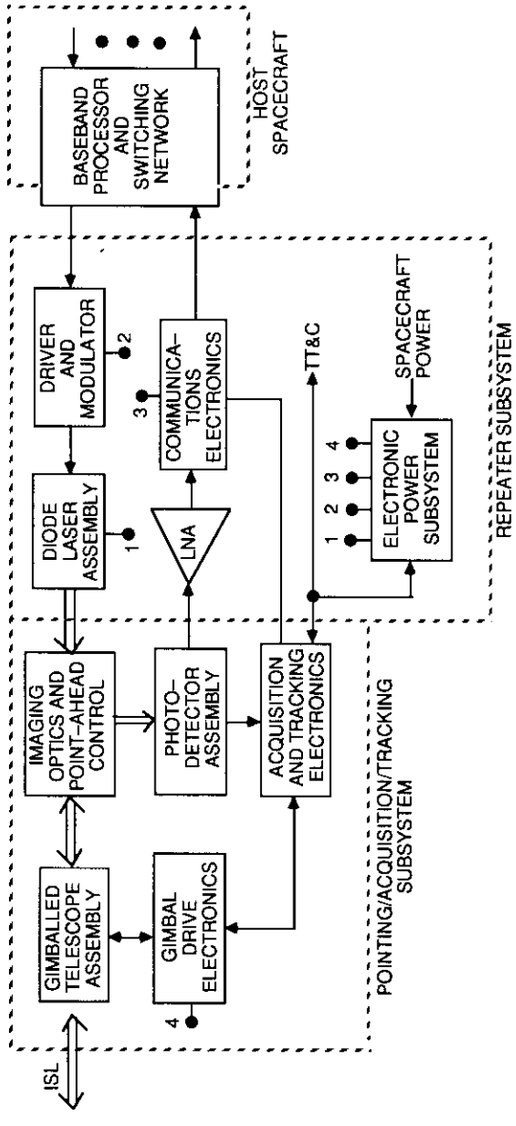

Figure 13. *Optical ISL Payload Block Diagram*

Tables 6 and 7 present the resulting terminal design and sizing of optical and microwave ISL payloads, respectively, for the selected ISL applications (see Table 4). A payload sizing algorithm for ISL was developed using available data to estimate mass and power requirements. The statistical algorithms were derived using multiregression techniques, based on databases assembled from 10 commercial spacecraft programs and other ongoing programs.

Antenna, repeater, and high-power amplifier (HPA) characteristics were used as input parameters for the microwave ISL payload sizing [25], [26]. The input parameters to the optical ISL payload sizing model were as follows:

- optical aperture diameter in meters,
- laser output power in watts,
- data rate in Mbit/s, and
- diode laser efficiency, η, in percent.

Appendix B summarizes the optical ISL payload sizing algorithms.

TABLE 6. OPTICAL ISL PAYLOAD TERMINAL SIZING FOR SELECTED APPLICATIONS

APPLICATION NUMBER	ISL APPLICATION	OPTICAL ISL PAYLOAD SIZING*		
		APERTURE (m)	DC POWER (W)	MASS (kg)
1a	CONUS	0.51	110.9	107.6
1b	CONUS	0.54	127.9	119.1
1c	CONUS	0.65	191.5	158.4
2a	CONUS–Europe	0.34	65.7	67.4
2b	North America–Europe	0.35	66.2	68.8
3	CONUS–International			
3a	CONUS–POR	0.29	62.8	58.4
3b	CONUS–AOR	0.32	68.8	63.9
4	ITU Region 1–International			
4a	Region 1–AOR	0.43	68.9	84.5
4b	Region 1–IOR	0.30	62.4	60.1
5	ITU Regions 1, 2, and 3			
5a	Region 1–Region 2	0.62	76.3	128.7
5b	Region 2–Region 3	0.44	66.0	84.4
5c	Region 3–Region 1	0.47	68.0	92.3
6	Intercluster ISL for CONUS	0.1–0.3	57.2–118.9	23.6–34.9

* For 100-mW laser output with 10-percent efficiency at a 0.85-μm wavelength.

TABLE 7. 60-GHz ISL PAYLOAD (MASS AND POWER REQUIREMENTS PER ISL TERMINAL)

APPLICATION NUMBER	MASS (kg)			POWER (W)	
	REPEATER	ELECTRONIC POWER CONDITIONER	PAYLOAD*	REPEATER	PAYLOAD**
1a	27.1	18.9	80.6	192.6	220.5
1b	28.5	24.2	87.3	257.1	285.0
1c	43.1	44.5	121.2	500.5	528.4
2a	18.9	5.0	58.5	26.1	54.0
2b	19.1	5.1	58.8	27.5	55.4
3a	18.4	4.4	57.3	18.9	46.8
3b	19.6	6.2	60.4	40.4	68.3
4a	19.4	5.5	59.4	31.6	59.5
4b	18.1	4.2	56.9	16.1	44.0
5a	19.9	6.6	61.1	45.4	73.4
5b	18.4	4.5	57.5	19.8	47.8
5c	18.9	4.9	58.4	25.1	53.0

*Antenna (2 m) subsystem mass = 34.6 kg.
**Antenna tracking/driver power = 28 W.

Cost analysis and benefit evaluation

Cost models have been developed for both optical and microwave ISL implementations [26]. The cost model for optical ISL payloads (near 0.85 μm) is given in Appendix B. The models provide nonrecurring and recurring cost estimates for the following subsystems:

- Fully gimballed antenna
- Repeater and electronic power subsystem
- Bus or support subsystem
- Management/engineering function

Table 8 provides the ISL payload terminal cost estimates in 1986 dollars for each application. On average, the cost of optical ISL payloads is about 7.5 percent higher than that of microwave ISL payloads.

The host spacecraft cost was derived from the statistical figure of merit of the space segment, which is defined as the on-station cost per 36-MHz equivalent transponder per year. Figure 14 represents the space segment figure of merit as a function of the number of transponders per spacecraft. Platform payloads (PL1 and PL2 in the figure) correspond to advanced payload design technology [27], [28].

TABLE 8. ISL PAYLOAD TERMINAL COST ESTIMATES* ($M, 1986)

APPLICATION NUMBER	APPLICATION	OPTICAL ISL			MICROWAVE ISL		
		NONRECURRING	RECURRING	TOTAL	NONRECURRING	RECURRING	TOTAL
1a	CONUS	16.519	6.536	23.055	16.815	5.078	21.893
1b	CONUS	17.785	7.137	24.922	17.866	5.511	23.377
1c	CONUS	21.914	9.101	31.015	—	—	—
2a	CONUS–Europe	11.713	4.229	15.942	12.885	3.798	16.683
2b	North America–Europe	11.906	4.324	16.230	12.948	3.814	16.762
3a	CONUS–POR	10.473	3.615	14.088	12.651	3.739	16.390
3b	CONUS–AOR	11.191	3.961	15.152	13.261	3.897	17.158
4a	Region 1–AOR	13.968	5.349	19.317	13.066	3.845	16.911
4b	Region 1–IOR	10.723	3.742	14.465	12.552	3.714	16.266
5a	Region 1–Region 2	19.289	7.993	27.282	13.392	3.933	17.325
5b	Region 2–Region 3	13.978	5.361	19.339	12.678	3.746	16.424
5c	Region 3–Region 1	14.963	5.848	20.811	12.858	3.791	16.649

* Program management costs are not included.

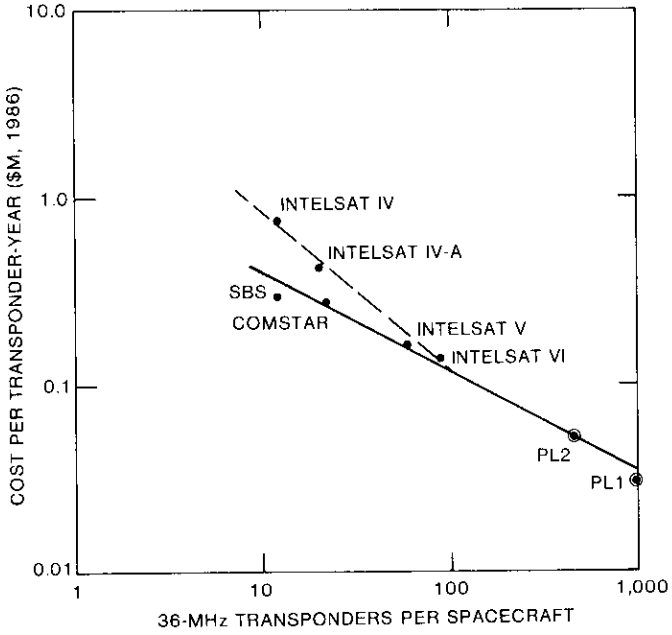

Figure 14. *Figure of Merit of Space Segment Cost*

ISL and corresponding non-ISL systems for each application were compared in terms of add-on systems costs. The ISL payload and its launch costs constitute the add-on systems cost of an ISL network, while a double-hop network includes a transponder double charge, as well as the relay station cost.

The total systems add-on cost of the CONUS ISLs for four-zone-coverage satellites is about $207 million. The corresponding non-ISL systems add-on costs are shown parametrically in Figures 15a and 15b for architectures 1 and 2, respectively.

For architecture 1, the 36-MHz equivalent transponder cost per year was assumed to be $0.112 million (nominal). The cost of a K_a-band relay station was estimated at $6 million per station, plus $3.6 million for operation and maintenance (O&M) for 12 years. The cost break-even point of the ISL is at about $0.01 million per transponder-year for the nominal estimate given in Figure 15a. In the worst case, if the relay station cost is reduced by 50 percent from the nominal and the ISL payload cost is increased by 25 percent, the break-even point becomes approximately $0.02 million per transponder-year.

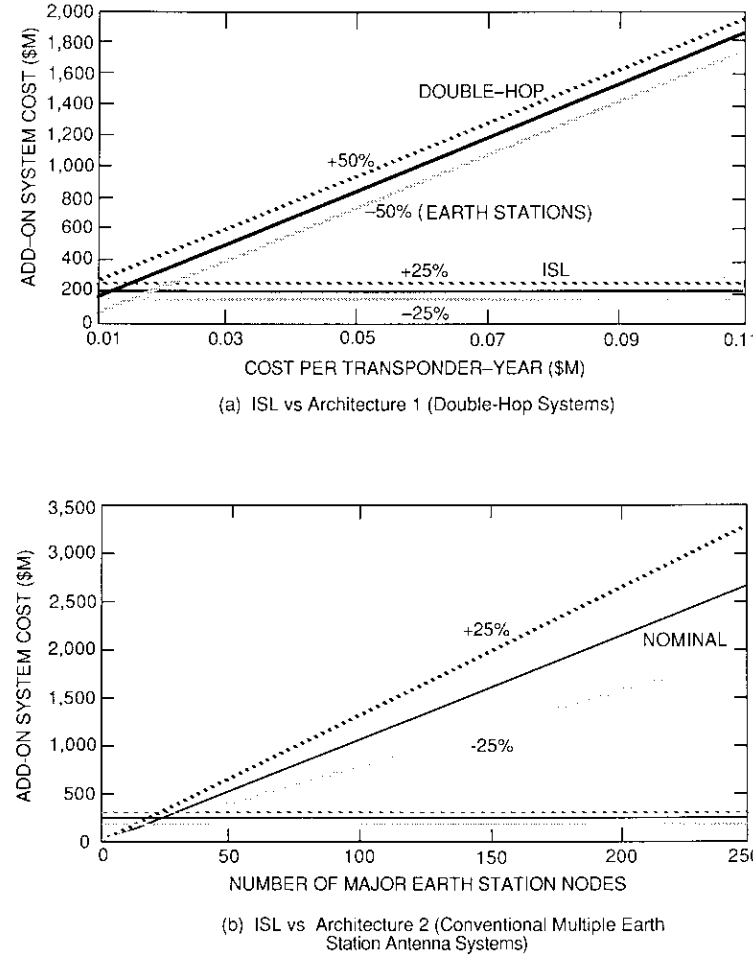

Figure 15. *Incremental Systems Cost ($M, 1986)*

In Figure 15b, the total add-on system cost for the ISL is compared with that for conventional multiple colocated earth station antennas. A single torus-antenna earth station at a cost of $10.5 million (including a 12-year O&M cost) was used instead of multiple antennas because of its cost effectiveness. The cost break-even point corresponds to 20 (± 7) major nodes for a ± 25-percent tolerance in the cost estimate.

Table 9 summarizes the total add-on systems cost for each selected application. The ISL systems cost effectiveness was defined as the add-on systems cost ratio of the corresponding non-ISL system to that of the ISL system. Figure 16 shows the ISL systems cost advantage ratio for each application.

TABLE 9. TOTAL SYSTEM INCREMENTAL COST COMPARISON ($M, 1986)

APPLICATION NUMBER	ISL APPLICATIONS	ISL SYSTEM	NON-ISL SYSTEM[a]	NON-ISL/ ISL COST RATIO
1	CONUS, Four-Zone Coverage	207.1	2,067.6[b] 304.5–5,250[c]	10.0 1.5–25
2a	CONUS–Europe	29.2	46.1	1.6
2b	North America–Europe	29.8	48.371	1.7
3a	CONUS–POR	25.615	25.2	1.0
3b	CONUS-AOR	27.656	68.531	2.5
4a	Region 1–AOR	35.688	54.688	1.6
4b	Region 1–IOR	26.344	20.761	0.8
5a	Region 1–Region 2	51.034	76.057	1.5
5b	Region 2–Region 3	35.736	26.809	0.7
5c	Region 3–Region 1	38.571	34.873	0.9

[a]Space segment cost at $0.112 million per 36-MHz transponder per year for 12 years.
[b]Architecture 1.
[c]Architecture 2 for 29 to 500 earth stations.

A large-space-segment approach provides N-fold orbital capacity utilization and a higher degree of frequency reuse with a large number of smaller spot beams. Also, significant cost advantages are expected due to the high ratio of payload to spacecraft housekeeping requirements.

ISLs interconnecting colocated ($\leq 0.1°$) satellites can be used to provide the functional equivalent of a large satellite. Each satellite functions as part of the large spacecraft through frequency band divisions or time divisions (*i.e.*, portions). Colocated partitioned satellites without ISLs also provide the functional equivalent of a large satellite to earth stations within the coverage area, provided that adequate stationkeeping can be maintained.

Table 10 presents a comparison of intercluster ISL satellites, colocated satellites without ISLs, and a single large platform payload concept. Intercluster ISLs ($\leq 0.1°$) do not provide significant advantage over the partitioned small satellites.

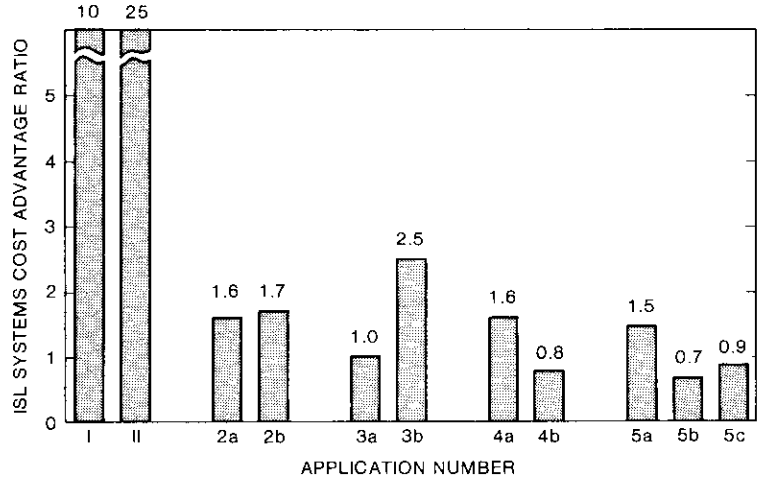

Figure 16. *ISL Systems Incremental Cost Advantage Ratio With Respect to Non-ISL Systems*

TABLE 10. COMPARISON OF INTERCLUSTER ISLs, COLOCATED SATELLITES, AND PLATFORMS

PARAMETERS	INTERCLUSTER ISLs	COLOCATED SATELLITES	SINGLE LARGE PLATFORM PAYLOAD
Satellite Traffic Cross-Strapping	ISL	Ground station	On-board switching network
TT&C and Stationkeeping	Complex	Difficult	Simple
Technology Involved	ISL payload	Existing bus and spacecraft technology	New platform payload
Launch Vehicle Limitation	None	None	Yes (space assembly may be needed)
Introduction	Phased time introduction	Phased time introduction	Future space segment
Initial Investment	Moderate	Small	Large
Growth Flexibility	Only planned buildup	Gradual buildup	No flexibility
Cost Benefit	Small	Small	Large
Application	Mid-term	Near-term	Year 2000

Further into the future, completely new satellite systems may evolve that fully utilize ISL systems to provide the following:

- increased coverage of world land masses (by about 15 percent) for K_a-band services employing domestic and regional satellites;
- an integrated space segment for domestic, regional, and global services; and
- global satellite coverage for integrated services digital networks (ISDNs).

ISL cross-linking of regional/domestic satellites will provide new global satellite network architectures. The existing three-ocean-region INTELSAT system for global coverage could be replaced by three ITU regional satellite systems employing ISLs.

Conclusions

Potential applications of ISLs to domestic, regional, and global satellite communications services have been identified through a comprehensive investigation of fundamental systems characteristics and the advantages of ISLs, and through use of satellite-addressable traffic models.

An ISL becomes cost-effective for a given application when the intersatellite traffic requirement is sufficiently large, exceeding a capacity of about eight 36-MHz equivalent transponders. ISL applications for U.S. domestic services could provide the largest systems cost benefit. For example, CONUS ISLs interconnecting four-time-zone-coverage satellites have a definite cost advantage over non-ISL satellite systems.

Other less cost-effective potential applications of ISLs include CONUS-to-Europe and North America-to-Europe, CONUS-to-AOR international communications, ITU Region 1-to-AOR international communications, and ITU Region 1-to-Region 2. Intercluster ISLs provide no significant systems advantage over partitioned small satellites without ISLs.

Acknowledgments

This paper is based on work performed under NASA Lewis Research Center Contract No. NAS3-24884 with the Communications Satellite Corporation.

The authors wish to thank J. Ramler and E. F. Miller of NASA Lewis Research Center for their helpful comments and encouragement during this study effort. I. Brelian and N. Srinivas of COMSAT contributed to the development of ISL traffic models and payload cost models, respectively. Finally, the authors thank the reviewers who provided helpful suggestions for the revision of this paper.

References

[1] W. W. Ward, D. M. Snider, and R. F. Bauer, "A Review of Seven Years of Orbital Service by the LES-8/9 EHF Intersatellite Links," IEEE International Conference on Communications, Boston, Massachusetts, June 1983, *Conf. Rec.*, Vol. 3, pp. 1171–1180.

[2] D. K. Sachdev and T. Chidambaram, "Intersatellite Links for International Communications," IEEE International Conference on Communications, Denver, Colorado, June 1981, *Conf. Rec.*, Vol. 4, pp. 70.2.1–70.2.6.

[3] G. R. Welti and Y. S. Lee, "Study of Intersatellite Links," Task 6, Final Report of Planning Assistance for the 30/20 GHz Program, NASA Contract NAS3-22905, November 1981. NASA Contract Report No. CR-182250.

[4] Y. S. Lee and R. E. Eaves, "Implementation Issues of Intersatellite Links for Future INTELSAT Requirements," IEEE International Conference on Communications, Boston, Massachusetts, June 1983, *Conf. Rec.*, Vol. 3, pp. 1189–1195.

[5] K. Bhasin, ed., "Optical Technologies for Communication Satellite Applications," *Proceedings of the International Society for Optical Engineering*, Vol. 616 (1986) and Vol. 756 (1987).

[6] COMSAT Laboratories, "Optical Intersatellite Link Technology," Final Report to COMSAT Intelsat Satellite Services Engineering under Project Support Authorization STA-5, December 1986. COMSAT Data Catalog No. 86DC133.

[7] COMSAT Laboratories, "TDAS Laser Intersatellite Communications Study," Final Report to Ball Aerospace Systems Division under NASA/Goddard Space Flight Center Contract NAS5-29128, July 1986. (Incorporated in NASA Contract Report No. CR-183419, "Tracking and Data Acquisition System Laser Intersatellite Communications Study," Final Report by Ball Aerospace Systems Division, Boulder, Colorado, August 1986.)

[8] D. S. Ponchak and R. L. Spence, "Application of Intersatellite Links to Domestic Satellite Systems," AIAA 11th Communications Satellite Systems Conference, San Diego, California, March 1986, *A Collection of Technical Papers*, pp. 29–38.

[9] ITU, *Radio Regulations*, 1982 ed., Geneva.

[10] N. Shacham *et al.*, "Speech Transport in Packet-Radio Networks With Mobile Nodes." *IEEE Journal on Selected Areas in Communications*, Vol. SAC-1, No. 6, December 1983, pp. 1084–1097.

[11] A. Gatfield, "Error Control on Satellite Channels Using ARQ Techniques," *COMSAT Technical Review*, Vol. 6, No. 1, Spring 1976, p. 179–188.

[12] R. R. Lovell and C. L. Cuccia, "Global Interconnectivity in the Next Two Decades—A Scenario," AIAA 11th Communications Satellite Systems Conference, San Diego, California, March 1986, *A Collection of Technical Papers*, pp. 39–49.

[13] J. E. Board, "Concept for a Worldwide Satellite Integrated Services Digital Network," AIAA 11th Communications Satellite Systems Conference, San Diego, California, March 1986, *A Collection of Technical Papers*, pp. 92–100.

[14] FCC Report and Order, "Licensing of Space Stations in the Domestic Fixed-Satellite Service and Related Revisions of Part 25 of the Rules and Regulations," CC Docket No. 81-704, released August 16, 1983.

[15] Y. S. Lee, "Cost-Effective Intersatellite Link Applications to the Fixed Satellite Services," AIAA 12th International Communications Satellite Systems Conference, Arlington, Virginia, March 1988, *A Collection of Technical Papers*, pp. 167–173, AIAA Paper No. 88-0770.

[16] S. Stevenson, W. Poley, and J. Salzman, "Demand for Satellite-Provided Domestic Communications Services to the Year 2000," NASA Technical Memorandum 86894, November 1984. NTIS No. N85-15099.

[17] W. Poley *et al.*, A Comparison of Domestic Satellite Communications Forecasts to the Year 2000," NASA Technical Memorandum 83516, October 1983. NTIS No. N84-10405.

[18] INTELSAT, "The INTELSAT Traffic Data Base Resulting From the 1984 Global Traffic Meeting," August 13, 1984.

[19] FCC WARC-85 Advisory Committee, "First Report on the Advisory Committee for the ITU's World Administrative Radio Conference on the Use of the Geostationary Satellite Orbit and the Planning of the Space Services Utilizing It," December 1983.

[20] J. E. Hollansworth, J. A. Salzman, and J. R. Ramler, "Telecommunications Forecast for ITU Region 2 to the Year 1995," NASA Technical Memorandum 87077, August 1985. NTIS No. N85-34150.

[21] G. Smith, G. Berreta, and P. Hansell, "Geostationary Orbit Capacity in Relation to Services Expansion and Technology Development," AIAA 9th Communications Satellite Systems Conference, San Diego, California, March 1982, *A Collection of Technical Papers*, pp. 495–503.

[22] W. R. Schnicke, J. B. Binckes, and D. H. Lewis, "Transponder Supply/Demand Analysis for the Geostationary Orbit," *COMSAT Technical Review*, Vol. 14, No. 2, Fall 1984, pp. 339–368.

[23] T. V. Muoi, "Extremely Sensitive Receiver for Laser Communications," Conference on Lasers and Electro-Optics, Baltimore, Maryland, April–May 1987, *Digest*, pp. 302–304.

[24] R. G. Marshalek, "Optical Communications Link Design for the Tracking and Data Acquisition System," *Proceedings of the International Society for Optical Engineering*, Vol. 756, 1987, pp. 100–109.

[25] P. Foldes, R. Meier, and T. Hill, "ISL Tracking Antenna Concepts," IEEE International Conference on Communications, Denver, Colorado, June 1981, *Conf. Rec.*, pp. 70.5.1–70.5.5.

[26] COMSAT, "Intersatellite Link (ISL) Application to Commercial Communications Satellites," NASA CR-179598, Final Report (2 vols.) to NASA Lewis Research Center under Contract NAS3-24884, January 1987. Vol. 1: Executive Summary, NTIS No. N87-19552; Vol. 2: Technical Report, NTIS No. N87-19553.

[27] Ford Aerospace and Communications Corporation, "Communication Platform Payload Definition (CPPD) Study," Final Report (3 vols.) to NASA Lewis Research Center under Contract NAS3-24235, March 1986. Vol. 1: Executive Summary, NTIS No. N86-27403; Vol. 2: Technical Report, NTIS No. N86-27404; Vol. 3: Addendum, NTIS No. N86-20705.

[28] RCA Astro-Electronics, "Communications Platform Payload Definition Study," Final Report (4 parts) to NASA Lewis Research Center under Contract NAS3-24236, July 1986. Executive Summary, NTIS No. N86-27407; Vol. 1: Executive Summary—Final Report 6/84-7/85, NTIS No. N86-27403; Vol. 2: Technical Report 6/84-7/85, NTIS No. N86-27404; Vol. 3: Addendum, NTIS No. N86-27405.

Appendix A. ISL traffic models

CONUS ISL traffic model

A 316 × 316 traffic matrix was derived by NASA using the criterion that FSS traffic requirements between two nodes 400 miles or more apart are satellite-addressable. Table A-1 presents a summary of NASA's total CONUS satellite-addressable traffic forecast. The traffic is expressed in numbers of equivalent half-voice circuits (HVCs) and the corresponding number of 36-MHz equivalent transponders. The transponder demand for the year 2000 is about 1,738 transponders, which shows an annual traffic growth rate of 7.6 percent from the year 1990.

TABLE A-1. TOTAL CONUS SATELLITE-ADDRESSABLE TRAFFIC

TIME FRAME	TOTAL NO. OF TRANSPONDERS*	EQUIVALENT HVCs**	REMARKS
Year 1990	835.8	2,340,240	2,800 HVC/transponder
Year 2000	1,737.2	7,817,400	4,500 HVC/transponder

*Based on an annual growth rate of 7.6 percent. Excluding Standard Metropolitan Statistical Area (SMSA) traffic less than 400 miles, a reduction factor of 0.8 was applied to voice, videoconferencing, and data.

**8,371,200 HVCs for the year 2001 (with 7.1-percent annual growth).

Detailed analysis of the CONUS traffic matrix resulted in the ISL capacity requirements for two half-CONUS coverages (Figure A-1) and four time-zone coverages (Figure A-2).

Regional and global ISL traffic models

International and regional/non-U.S. domestic traffic data were used to derive basic ISL traffic models for various regional/international FSS applications.

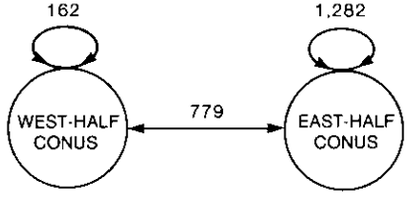

(a) Transponder Requirement

FROM	TO	
	WEST CONUS	EAST CONUS
WEST CONUS	728,410	1,751,460
EAST CONUS	1,751,460	5,768,914
TOTAL	10,000,252	

(b) Traffic Matrix (number of equivalent half-voice circuits)

Figure A-1. *East- and West-Half CONUS Coverage Transponder Requirement and Traffic Model*

INTERNATIONAL SATELLITE TRAFFIC MODEL

The INTELSAT traffic database contains data for international FSS traffic based on estimated requirements for the next 5 years, as well as a projected forecast for the following 10 years. This 15-year traffic forecast reflects the best estimates of international carriers and INTELSAT Signatories.

The 1984 INTELSAT traffic database was used to develop international ISL traffic models. The 1986 INTELSAT forecast foresees somewhat higher traffic growth in both the POR and IOR. However, the traffic forecast for the AOR is somewhat lower.

The data on telephone traffic in the three operating modes [FDM/FM, single-channel-per-carrier (SCPC), and companded FM] were collected and processed as part of the traffic grouping analysis. The traffic matrices of various geographical groupings of countries were also derived. The 1995 and 1998 traffic models of international FSS communications were used as the basis for developing regional and international ISL traffic models.

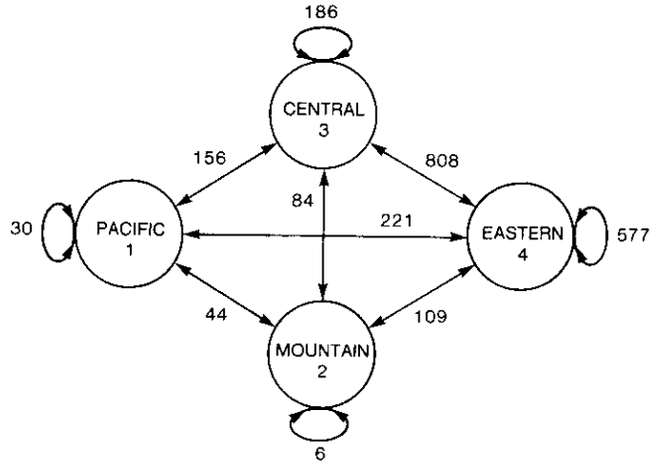

(a) Transponder Requirement

FROM	TO			
	PACIFIC	MOUNTAIN	CENTRAL	EASTERN
PACIFIC	134,346	99,335	355,445	497,504
MOUNTAIN	99,335	27,214	189,134	244,621
CENTRAL	355,445	189,134	836,138	1,818,191
EASTERN	497,504	244,621	1,818,191	2,594,094
TOTAL	10,000,252			

(b) Traffic Matrix (number of equivalent half-voice circuits)

Figure A-2. *Four-Time-Zone CONUS Coverage Transponder Requirement and Traffic Model*

SEVEN-GROUP REGIONAL TRAFFIC MODEL

ISL traffic models based on geographical region were derived from the 1984 INTELSAT traffic database, with additional modifications for the following considerations:

- Ten percent was added to the telephony traffic volume to account for TV broadcasting, videoconferencing, and other data traffic in international satellite communications.
- An 8-percent annual growth rate was used to extrapolate the traffic forecast to the year 2001.

- Domestic satellite traffic requirements were derived from various sources and incorporated into the intraregional group traffic.

Table A-2 shows the worldwide satellite traffic model for seven geographical groups for the year 2001. Intraregional traffic is shown by the diagonal elements of the traffic matrix. The off-diagonal elements represent interregional ISL traffic for a seven-group regional satellite network implementation.

The data in Table A-2 indicate a very small volume of traffic between South America and South Pacific countries, South America and Africa, South Pacific and Mideast countries, and South Pacific and Africa. This is a consequence of the double-hop requirement in the existing non-ISL satellite system. Interregional ISLs can provide full connectivity among these groups, introducing new services and more users in these regions.

Figure A-3 represents the 36-MHz equivalent transponder requirements of the seven-group regional ISL system. Intraregional traffic is clearly dominant. Although interregional ISL traffic is only 3.1 percent of the total traffic requirement, the existence of the ISL may encourage the use of new or improved services by more users. A large segment of the ISL traffic requirement is for the regional satellites between North America and Europe, and between Europe and Asia.

ITU REGIONAL TRAFFIC MODEL

The seven regional traffic matrices were reduced further to obtain an ITU regional traffic model for the year 2001 (Table A-3). It should be noted that the traffic requirements of Communist-bloc countries were not available for this study and were not included in the traffic model.

The ISL transponder requirements for 4,500 HVCs per 36-MHz transponder are as follows:

INTERREGIONAL ISL	NUMBER OF ISL TRANSPONDERS (2-WAY CAPACITY)
Region 2–Region 1	29.5
Region 2–Region 3	10
Region 1–Region 3	16

Figure A-4 shows the intraregional and interregional ISL transponder requirements.

TABLE A-2. SEVEN-GROUP REGIONAL SATELLITE TRAFFIC MODEL FOR THE YEAR 2001*

FROM	TO: NORTH AMERICA	SOUTH AMERICA	ASIA	SOUTH PACIFIC	EUROPE	MIDEAST	AFRICA	SUBTOTAL
North America	9,102,703	18,424	15,782	5,020	42,358	8,084	3,695	9,196,066
South America	18,424	188,097	1,329	112	11,262	723	222	220,169
Asia	15,782	1,329	546,966	3,709	20,430	6,047	746	595,039
South Pacific	5,020	112	3,709	37,161	7,882	318	479	54,681
Europe	42,358	11,262	20,430	7,882	792,046	17,212	14,077	905,267
Mideast	8,084	723	6,047	318	17,212	202,337	503	235,224
Africa	3,695	222	746	479	14,077	503	305,920	325,642
Total	11,532,088 (HVCs)							

* The total traffic model for the year 1998 was extrapolated to the year 2001, assuming an 8-percent annual growth rate.

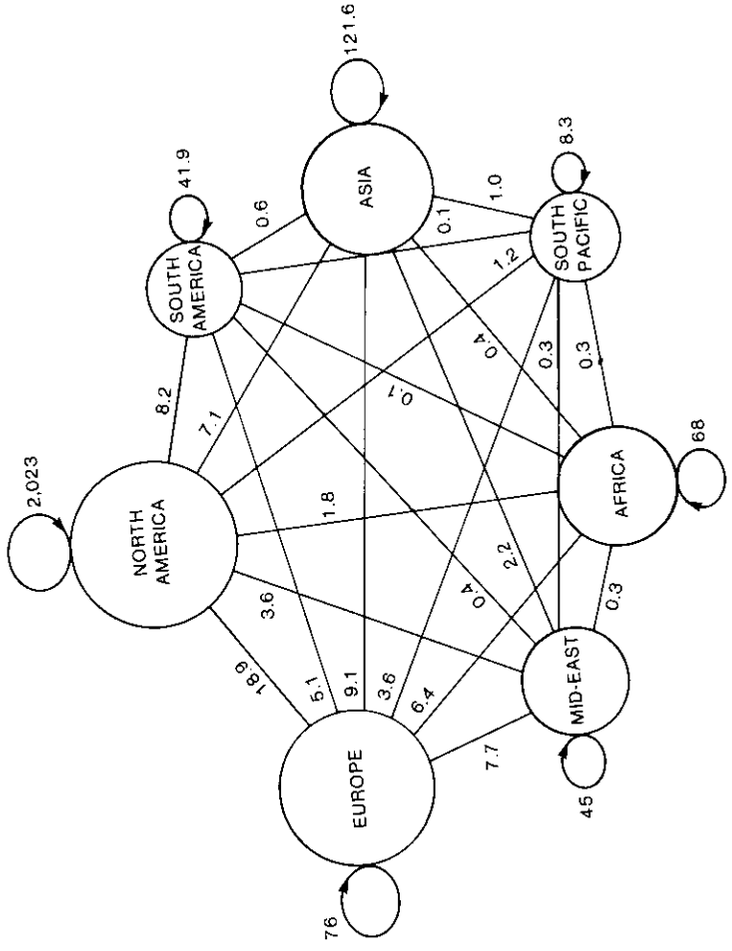

Figure A-3. *Seven-Group Regional ISL Transponder Requirement for the Year 2001*

TABLE A-3. THREE ITU REGIONAL* TRAFFIC MODEL FOR THE YEAR 2001

	To		
From	Region 1	Region 2	Region 3
Region 1	1,363,887	66,344	35,902
Region 2	66,344	9,327,648	22,243
Region 3	35,902	22,243	591,575
Total	11,532,088 (HVC)		

*Region 1: Europe, Mideast, Africa.
Region 2: North America, South America.
Region 3: Asia, South Pacific.

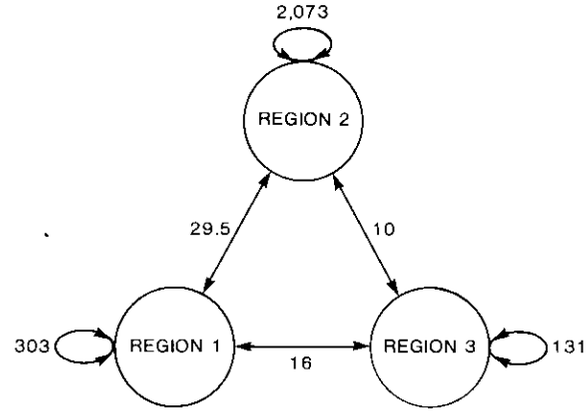

Figure A-4. *ITU Regional Transponder Requirement for the Year 2001*

Appendix B. ISL payload sizing and cost estimating models

ISL payload sizing and cost models were developed using available flight hardware data, based on the models described in References B-1 through B-3. The input parameters are determined from the ISL link design. The mass and power estimates for the major subsystems are used for the cost-estimating equations. The cost model provides both nonrecurring and recurring costs of the ISL payload.

Table B-1 presents the mass and power estimating equations for an optical (0.85-μm diode laser) ISL payload. The pointing, acquisition, and tracking subsystem consists of a lightweight (beryllium) gimballed telescope and control electronics assembly. The optical ISL payload cost model is summarized in Table B-2.

It should be noted that the equations relating payload mass to mirror aperture diameter, and optical antenna subsystem recurring cost to mirror aperture diameter, were obtained by a regression fitting to three data points in each case, as these were the only data available to the authors at the time of the study reported in Reference B-3. The opto-electronics were assumed to be sufficiently similar to microwave electronics that similar equations were used.

References

[B-1] G. R. Welti and Y. S. Lee, "Study of Intersatellite Links," Task 6, Final Report of Planning Assistance for the 30/20 GHz Program, NASA Contract NAS3-22905, November 1981. NASA Contract Report No. CR-182250.

[B-2] COMSAT, "Spacecraft Cost Model Study," Final Report to INTELSAT under Contract INTEL-290, October 1984.

[B-3] COMSAT, "Intersatellite Link (ISL) Application to Commercial Communications Satellites," NASA CR-179598, Final Report (2 vols.) to NASA Lewis Research Center under Contract NAS3-24884, January 1987. Vol. 1: Executive Summary, NTIS No. N87-19552; Vol. 2: Technical Report, NTIS No. N87-19553.

TABLE B-1. OPTICAL ISL PAYLOAD MASS (kg) AND POWER (W) ESTIMATING EQUATIONS

Primary Optics and Acquisition/Tracking Subsystem Mass (kg)

- Gimballed Telescope Mass*
  $M_{GT} = 1.747 + 216.1\ D^{1.8}$
  where D is the aperture size in meters.
- Control Electronics Mass
  $M_{CE} = 8.2$
- Total Mass
  $M_{GTC} = M_{GT} + M_{CE}$

Repeater Mass (including electronic power conditioners)
$M_{REPS} = 12.331 + 15.314\ PL^{1.3} + 0.0833\ P_{TOT}$
where PL is the laser optical output power in watts,
and P_{TOT} is ISL payload power total.

Thermal/Structural Mass
$M_{TS} = 0.1\ P_{TOT}$

ISL Payload Dry Mass Total
$M_{ISL} = M_{GTC} + M_{REPS} + M_{TS}$

Tracking/Gimbal Drive Power (W)
$P_{TR} = 39.66 + 20.3\ D^{1.3}$
where D is the aperture diameter in meters.

Laser Diode Power
$P_{LP} = 1.25 + 2 \times 10^2\ PL/EF$
where EF is the diode laser efficiency in percent.

Repeater Power

- Transmitter and Control Electronics
  $P_{TX} = 11.8 + 5 \times 10^{-3}\ R_b$
  where R_b is the data rate in Mbit/s.
- Receiver Electronics
  $P_{RX} = 2.1 + 1 \times 10^{-3}\ R_b$
- $P_{REP} = P_{TX} + P_{RX}$

ISL Payload Power Total
$P_{TOT} = P_{TR} + P_{LP} + P_{REP}$

* This equation was derived using regression analysis on three data points provided in Reference B-3.

TABLE B-2. OPTICAL (0.85-μm) ISL PAYLOAD COST MODEL ($M, 1986)

Optical Antenna Subsystem Cost
- Recurring Cost
  $CA_R = 0.847 + 13.06\ D^{1.5}$
  where D is the optical aperture size in meters.
- Nonrecurring Cost
  $CA_{NR} = 2\ CA_R$

Repeater Subsystem Cost
- Recurring Cost
  $CR_R = 0.0132\ M_{REPS}^{1.3}$
- Nonrecurring Cost
  $CR_{NR} = 0.6886\ M_{REPS}^{0.65}$

Thermal Control/Structural Cost
- Recurring Cost
  $CT_R = 0.0187\ M_{TS}^{0.95}$
- Nonrecurring Cost
  $CT_{NR} = 0.0034\ M_{TS}^{1.5}$

Optical ISL Payload Cost
- Recurring Cost
  $CPL_R = CA_R + CR_R + CT_R$
- Nonrecurring Cost
  $CPL_{NR} = CA_{NR} + CR_{NR} + CT_{NR}$

Upper Bound of Program Management Cost
- Recurring Cost
  $PG_R = 0.444\ CPL_R$
- Nonrecurring Cost
  $PG_{NR} = 0.449\ CPL_{NR}$

Young S. Lee received a B.S. and M.S. in electronics engineering from Seoul National University, Korea, and an S.M. and Degree of Electrical Engineer from the Massachusetts Institute of Technology. Since joining COMSAT in 1969, he has held positions as Member of the Technical Staff in the Microwave Laboratory, Staff Scientist in the Optical Communications Laboratory, and Senior Staff Scientist in the COMSAT Technical Services Division. Mr. Lee has made significant contributions in the areas of microwave integrated circuits and on-board regenerative repeater technologies for

advanced digital satellite systems. He also participated in a number of spaceflight programs, such as INTELSAT VI, COMSTAR Beacon, and ATS-F, and served as Project Manager of contract programs, including a NASA/Lewis Intersatellite Link Applications Study program. He is currently a Senior Scientist in COMSAT Systems Division, with responsibility for planning, analysis, and design of various satellite-based telecommunications systems. Mr. Lee is a Senior Member of IEEE and a Member of the Optical Society of America.

Ali E. Atia received a B.S.E.E. from Ain Shams University, Cairo, Egypt, and an M.S.E.E. and Ph.D. from the University of California at Berkeley. Prior to joining COMSAT in 1969, he held various research and teaching positions at both universities. As a Senior Scientist in the Microwave Laboratory at COMSAT Laboratories, Dr. Atia has made original contributions to satellite transponder and antenna technologies, most notably the development of dual-mode microwave filter technology, which is now the standard of the industry for satellite transponder channelization and many earth station applications. He also made significant contributions to several satellite programs, including INTELSAT IV-A, V, V-A, and VI, ARABSAT, and AUSSAT. He was responsible for the design, implementation, qualification, and testing of major subsystems in COMSAT's NASA ATS-F propagation experiment and the COMSTAR K_a-Band Beacon Experiment. He is currently Senior Director of Communications Engineering in the COMSAT Systems Division, responsible for all communications systems design, integration, implementation, and testing under contracts with various Government and commerical customers. Dr. Atia is a Fellow of IEEE, and Associate Fellow of AIAA, and a Member of Sigma Xi.

Denise S. Ponchak received her B.E.E. in 1983 and her M.S.E.E. in 1988 from Cleveland State University. She joined NASA Lewis Research Center in July 1983 as a member of the Space Communications Division. From 1983 to 1986 she was engaged in the analysis of future satellite systems for domestic and global applications. Subsequently, she has been involved in developing computer tools for international planning and management of the frequency spectrum for satellite systems.

Index: Communication satellites, geosynchronous orbit, intersatellite link, transmission, optical communication

Comparison of optical technologies for intersatellite link payloads*

Part I. Mass, prime power, and volume estimates

R. G. MARSHALEK

(Manuscript received September 3, 1987)

Abstract

Six optical technologies are compared with respect to the mass, prime power, and volume (MPV) requirements of an intersatellite link (ISL) communications payload for a full-duplex interconnection between two geostationary spacecraft. The communications subsystems of the ISL payloads are based on CO_2, Nd:YAG, InGaAsP, and GaAlAs laser sources utilizing either direct-detection or heterodyne-detection receivers, as appropriate. The MPV estimates include both the communications subsystem and the pointing, acquisition, and tracking subsystem of the ISL payloads for transmission of three wideband transponders (each 72-MHz-wide analog or 120-Mbit/s digital). The estimates use antenna diameters obtained from a consistent analysis of the communications performance of the six systems. Results indicate a preference for the GaAlAs systems for both analog and digital traffic. (Reliability issues are discussed in Part II of this paper.)

Introduction

The use of intersatellite links (ISLs) in future telecommunications systems could enhance the connectivity and coverage of the global network, reduce

*This two-part paper is based on work performed at COMSAT Laboratories under the sponsorship of COMSAT Intelsat Satellite Services Engineering.

signal propagation delay and tropospheric impairments as compared with a multihop interconnection or an interconnection that uses lower elevation angles, and conserve allocated spectral resources [1],[2]. Of particular interest with regard to these system improvements are ISLs between geostationary satellites serving users in separate geographical regions. For such interregional ISLs, the bandwidth and distance requirements are rather large (typically, several hundred megahertz over a 42,000-km range), and implementation of optical technologies [3]–[10] becomes an attractive option.

In an earlier paper [11], the communications performance of six potential optical technologies for an interregional ISL were analyzed to determine the antenna diameter requirements for both analog and digital traffic. The technologies analyzed were as follows:

- carbon dioxide laser system with heterodyne detection,
- neodymium-doped laser system with direct detection,
- InGaAsP laser system with a neodymium-doped power amplifier and direct detection,
- GaAlAs laser system with direct detection,
- GaAlAs laser system with wavelength-division multiplexing (WDM) and direct detection, and
- GaAlAs laser system with heterodyne detection.

This analysis indicated a preference for ISL systems based on the GaAlAs semiconductor diode laser because of its small size, high electrical-to-optical conversion efficiency, direct modulation capability, broad wavelength selectability, and potential for high reliability. Furthermore, the high level of research and development in the field of GaAlAs technology promises rapid advances in the state of the art of GaAlAs diode laser communications systems.

Additional factors of importance in technology selection for an optical ISL are the mass, prime power, and volume (MPV) requirements of the ISL payload. In this paper, these parameters are estimated for the six optical technologies noted above. The estimates include both the communications subsystem and the pointing, acquisition, and tracking (PAT) subsystem of the ISL payload, and use optical antenna diameter requirements obtained from a consistent analysis of ISL communications performance [12]. The results are combined with those from Reference 11 to select a preferred optical technology for near- and far-term applications for both analog and digital ISL traffic.

Review of communications performance tradeoffs

The six optical technologies noted above have been described, and the results of optical power budget calculations have been presented for analog and digital modulation formats compatible with the input signals likely to be found on board future INTELSAT satellites [11],[12]. In this comparison, a full-duplex link was considered between geostationary satellites separated by 42,000 km. The link capacity in each direction was three wideband transponders, each accommodating 120-Mbit/s baseband digital traffic (60-MHz signal bandwidth) or 72-MHz analog traffic consisting of 120-Mbit/s quadrature phase-shift keying (QPSK) modulation of a 4-GHz carrier.

Tables 1 and 2 summarize the antenna diameter requirements and assumed optical transmitter power levels for the six systems with transmission of the three baseband-digital or QPSK transponders, respectively. The modulation formats assumed in the calculations are described in Table 3. In these calculations, the baseband-digital traffic was received with a 10^{-9} bit error rate (BER), and the analog traffic was received with a 22.9-dB signal-to-noise ratio (*S/N*) at the receiver output. The BER requirement ensured that the digital optical ISL was a transparent part of the cascaded link consisting of the RF up- and down-links and the optical cross-link. The *S/N* requirement was selected so that the analog optical ISL degraded the total cascaded link *S/N* by only 1 dB.

TABLE 1. ANTENNA DIAMETER REQUIREMENTS FOR BASEBAND DIGITAL TRANSMISSION OF THREE WIDEBAND TRANSPONDERS (360-Mbit/s TOTAL THROUGHPUT) OVER A 42,000-km RANGE

SYSTEM	λ (μm)	MODULATION FORMAT*	AVERAGE TRANSMITTER POWER (mW)	ANTENNA DIAMETER (cm)
CO_2	10.6	OOK	3,000	18.4
Nd	0.532	PPBM	400	20.4
InGaAsP	1.064	OOK	300	29.8
GaAlAs	0.87	OOK	200	25.6
GaAlAs WDM	0.9	OOK	200**	25.5
GaAlAs Heterodyne	0.87	QFSK	50	23.4

*See Table 3 for definition of abbreviations.
**Optical power of each transmitter.

TABLE 2. ANTENNA DIAMETER REQUIREMENTS FOR TRANSMISSION OF THREE 72-MHz QPSK TRANSPONDERS OVER A 42,000-km RANGE

SYSTEM	λ (μm)	MODULATION FORMAT*	AVERAGE TRANSMITTER POWER (mW)	ANTENNA DIAMETER (cm)
CO_2	10.6	QPSK/FDM-FM-SC/AM	3,000	30.7
Nd	0.532	QPSK/FDM-FM-SC/IM	300*	36.6
InGaAsP	1.064	QPSK/FDM-FM-SC/IM	300	52.4
GaAlAs	0.87	QPSK/FDM-FM-SC/IM	200	43.9
GaAlAs WDM	0.9	QPSK-FM-SC/IM	200**	31.6
GaAlAs Heterodyne	0.87	QPSK/FDM/FM	50	22.5

*In continuous-wave (CW) operation.
**Optical power of each transmitter.

TABLE 3. MODULATION FORMATS FOR OPTICAL ISLS

ABBREVIATION	DESCRIPTION
OOK	On-off keying
PPBM	Pulse-polarization binary modulation.
QFSK	Quaternary frequency-shift keying.
QPSK/FDM-FM-SC/AM	Three QPSK subcarriers frequency-multiplexed and modulated on an FM carrier before amplitude modulation of the optical carrier.
QPSK/FDM-FM-SC/IM	Three QPSK subcarriers frequency-multiplexed and modulated on an FM carrier before intensity modulation of the optical carrier.
QPSK-FM-SC/IM	One QPSK subcarrier modulated on an FM carrier before intensity modulation of the optical carrier.
QPSK/FDM/FM	Three QPSK carriers frequency-multiplexed with direct frequency modulation of the optical carrier.

Mass, prime power, and volume estimates

The MPV requirements of the six ISL systems are estimated using the optical terminal block diagram shown in Figure 1. As indicated in the figure, the estimates include the communications and PAT subsystems (including the support electronics) and the optical telescope. The MPV requirements for the communications subsystem and optical telescope are strongly dependent upon the optical technology being considered, while those for the PAT subsystem are essentially fixed for each of the six technologies. Before estimates are generated for the six ISL systems, the mass and volume of the optical telescope are assessed as a function of primary mirror diameter.

Optical telescope mass and volume

The mass of the optical telescope is determined by the required primary mirror diameter and the telescope type (fully gimballed telescope or fixed telescope with an external gimballed flat mirror). Figure 2 gives the optical telescope mass as a function of primary mirror diameter for each telescope type, as extrapolated from estimates [13] at three specific antenna diameters. This figure is used in the next section, in conjunction with the antenna diameter requirements given in Tables 1 and 2, to estimate the mass of the optical telescopes for baseband-digital and QPSK-analog transmission in the six optical ISL systems. A fully gimballed telescope is assumed in these estimates, since this allows both east and west communications redundancy and provides excellent stray light rejection.

The optical telescope volume is determined by the diameters of its primary and secondary mirrors, and by the optical design which sets the focusing distances between them. The estimates given here assume an off-axis Cassegrain antenna design whose volume is a rectangular box of dimensions $(D + 2\text{ cm})$ by $(D + D/3 + 4\text{ cm})$ by $(2.5D)$, where D is the primary mirror diameter in centimeters. The $(D + 2\text{ cm})$ dimension, which is normal to the transmitted optical beam, is determined by the primary mirror diameter, with a small margin included for packaging. The $(D + D/3 + 4\text{ cm})$ dimension, which is also normal to the transmitted optical beam, is determined by the primary and secondary mirror diameters ($D_{sec} \sim D_{pr}/3$ assumed) and the selected off-axis design, which eliminates obscuration losses in the optical power budget. A small margin has again been included for packaging. Finally, the $(2.5D)$ dimension is determined by the optical telescope design, which sets the focal distances between the two telescope mirrors. These dimensions are consistent with those used in the telescope designs of Reference 14.

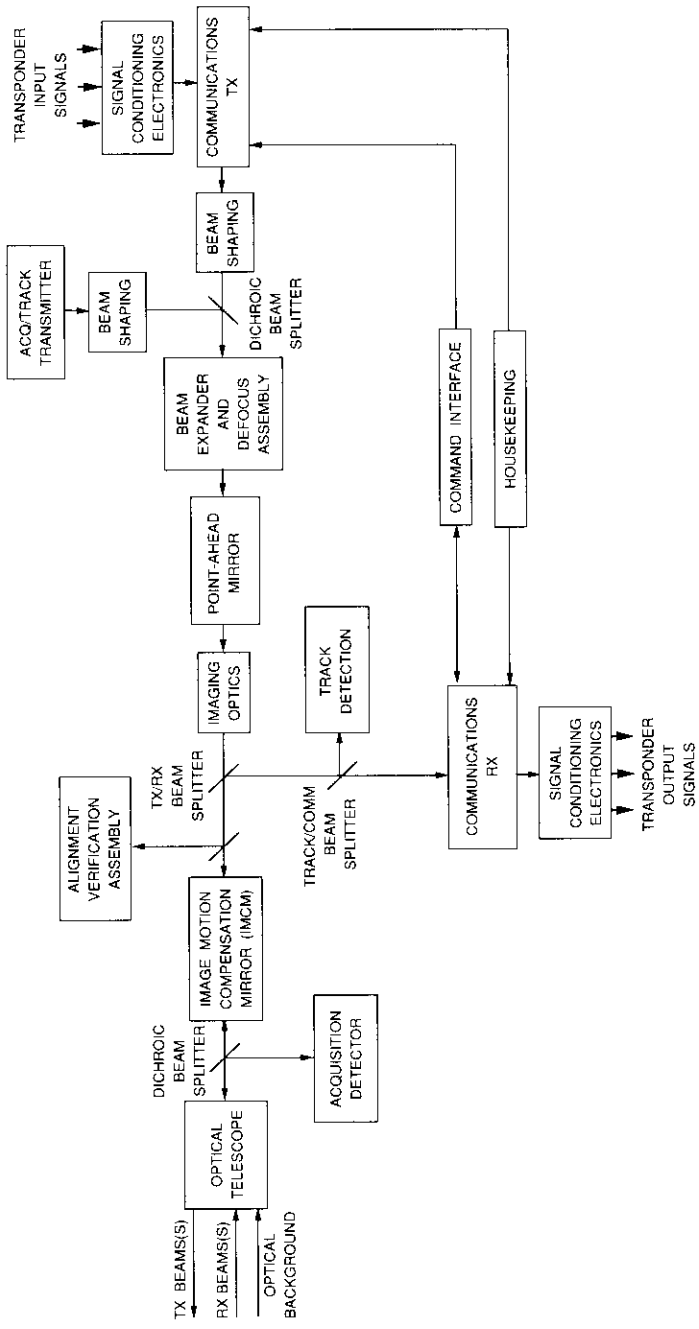

Figure 1. *Block Diagram of an Optical ISL Terminal*

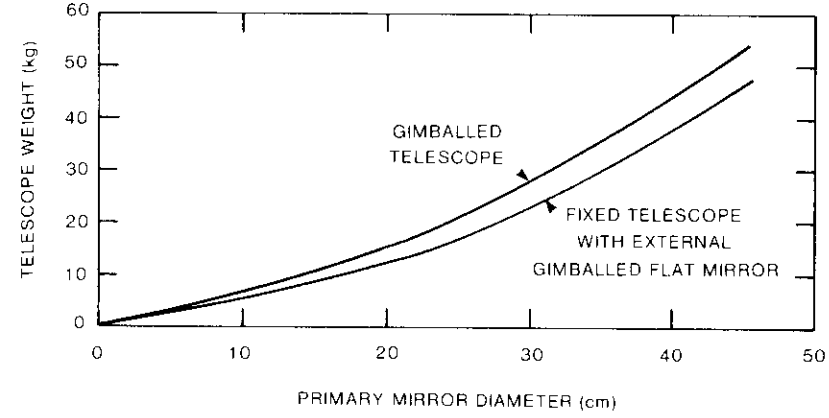

Figure 2. *Optical Telescope Mass* vs *Primary Mirror Diameter*

Mass, prime power, and volume estimates for the optical ISL terminals

In this subsection, appropriate engineering estimates of MPV are given for the six optical terminals, including a 10-percent margin to account for those needs not specifically addressed. The estimates do not include the redundant components required in order to achieve a 5- to 10-year lifetime with high reliability (~0.9). MPV estimates with redundancy can be obtained by using the discussions in a companion paper [15] and adding the appropriate system component values to the estimates given here. These estimates are made based on actual hardware data (components, subsystems, housing, etc.) as far as possible. The details of the estimation process are given below. It is expected that the statistics of engineering estimates will improve in the future as a result of new development and field trial/laboratory prototypes.

CO_2 LASER ISL TERMINAL

The MPV requirements of a CO_2 ISL terminal have been assessed by several researchers [3],[4],[7]. Based on many years of research and development, mainly at NASA [4] and more recently at the European Space Agency [7], fairly accurate estimates can be derived from the open literature. Table 4 gives MPV estimates for a CO_2 ISL terminal, and several of the entries in the table are further described below.

The communications subsystem consists of an RF-excited waveguide laser for the transmitter, and a local oscillator (LO) in the heterodyne receiver, with each laser requiring line- and frequency-stabilization circuitry. An external electro-optic (EO) modulator is used, requiring a well-stabilized

TABLE 4. MPV ESTIMATES FOR A CO_2 LASER ISL TERMINAL (WITHOUT REDUNDANCY)

ITEM	VOLUME (cm^3)	MASS (kg)	POWER (W)
Communications Transmitter • Transmitter Laser (4-W optical output at beginning of life) and Power Supply • Stabilization Electronics • Laser Gas Tank and Vacuum Valves	4,000	4.5	42.0
Modulator and Modulator Driver	1,000	1.8	12.5
Conductive Cooler for Transmitter Laser and Modulator	15,000	5.0	—
Communications Receiver • LO Laser (1-W optical output at beginning of life) and Power Supply • Stabilization Electronics • Photomixer and Auto-Alignment System • Communications Electronics, Including Regenerator and Clock Recovery Circuit	3,000	3.0	14.0
Added Requirements for QPSK-Analog Transmission With Bandwidth Expansion (normalized to baseband-digital requirements)	450	0.5	2.7
Detector Cooler	7,400	1.6	—
PAT Subsystem • Acquisition/Tracking Transmitter • Beacon Receiver Subsystem • IMCM Assembly • Beam Expander and Defocus Assembly • Point-Ahead Assembly	1,750	7.9	17.5
Gimballed Optical Telescope	—	—	25.0
• Gimbal Power Supply	—	2.0	—
• Baseband-Digital Transmission (18.4 cm)	26,750	12.5	—
• QPSK-Analog Transmission (30.7 cm)	113,250	29.0	—
Support Electronics • Signal Conditioning Electronics • Servo Electronics • Commands and Telemetry • Microprocessors	2,400	8.8	28.0
Power Conditioning Subsystem (efficiency = 80%)	2,000	7.0	—
• Digital			30.8
• Analog			31.3

TABLE 4. MPV ESTIMATES FOR A CO_2 LASER ISL TERMINAL (WITHOUT REDUNDANCY) (CONT'D)

ITEM		VOLUME (cm^3)	MASS (kg)	POWER (W)
Miscellaneous • Diplexer and Miscellaneous Optics • Support Structure and Spacecraft Interface • Cables and Connectors • Radiation Shielding • Passive Radiator		—	9.5	—
Thermal Control and Thermal Blankets		—	4.0	15.0
Subtotal	Digital	63,000	67.6	184.8
	Analog	150,250	84.6	188.0
10% Margin	Digital	6,330	6.8	18.5
	Analog	15,025	8.5	18.8
Total	Digital	69,630	74.4	203.3
	Analog	165,275	93.1	206.8
Prime Power Weight Burden at 0.15 kg/W	Digital	—	30.5	—
	Analog	—	31.0	—
Total Terminal Burden	Digital	69,600	104.9	203.3
	Analog	165,300	124.1	206.8

modulator crystal temperature to compensate for RF and optical absorption. The receiver contains a HgCdTe photovoltaic diode radiatively cooled to approximately 100 K, as well as an active control subsystem to align the LO and received signal beams to ensure high heterodyne conversion gain.

The compact heterodyne receiver package containing a tunable line- and frequency-stabilized LO laser and a photomixer is estimated to have dimensions of 25 × 15 × 7.5 cm^3. Adding the communications electronics increases the volume by about 10 percent. The radiative detector cooler is about 25 cm in diameter and 15 cm deep, and is capable of maintaining a small photomixer at a temperature of less than 110 K. This unit has been constructed and tested to flight acceptance levels and weighs 1.6 kg. A larger volume is required for the transmitter, since it contains a more powerful laser. An additional 500 cm^3 has been added to the transmitter volume

estimate for a laser gas tank and vacuum valves to provide gas refilling for transmitter and LO laser lifetime extension. The modulator and the modulator driver are each about 20 × 5 × 5 cm^3 and weigh about 1 kg and 0.8 kg, respectively. The conductive cooling system for the laser and the modulator occupies approximately 15,000 cm^3 and weighs 5 kg.

For the CO_2 waveguide laser, including its power supply, a mass of roughly 1 kg/W of optical output power has been given [7]. This value only holds above a certain threshold power, and can be used for the transmitter laser. The LO laser has about a 1-W output, but requires the same line- and frequency-stabilization hardware as the more powerful transmitter laser. For this reason it is safe to estimate a 2-kg mass for the LO laser and 4 kg for the transmitter laser, assuming beginning-of-life optical output powers of 1 and 4 W, respectively. Additional contributors to the mass of the communications transmitter are the laser stabilization electronics (0.2 kg) and the gas tank (0.3 kg). For the receiver, the additional contributors are the detector and associated electronics (0.3 kg), and the auto-alignment system (0.7 kg) which provides for proper alignment of the received and LO beams in the heterodyne receiver.

The electrical power consumers in the transceiver are the two lasers, the EO modulator, and the receiver. For the lasers, an efficiency of 10 percent is obtained with the present state of the art. Assuming 4-W unmodulated power for the transmitter and 1 W for the LO at the beginning of life gives prime power needs of 40 and 10 W, respectively. An additional 2 W is required per laser for stabilization. The power required for the modulation driver depends on the modulation format, but a value of 10 W is estimated for the information bandwidths considered here. For the EO modulator, a voltage of about 10 V is applied to the 50-Ω traveling wave structure to obtain a phase shift of ½ wavelength. Thus, an 80-percent-efficient modulator will consume about 2.5 W. Finally, about 2 W is consumed in the receiver by the detector, electronics, and clock recovery circuitry (1.5 W) and by the auto-alignment subsystem (0.5 W).

The PAT subsystem of the CO_2 ISL terminal (see Figure 1) consists of the acquisition/tracking transmitter (500 cm^3, 1.5 kg, 5 W), the beacon receiver subsystem (500 cm^3, 3 kg, 1 W), the image motion compensation mirror (IMCM) assembly (500 cm^3, 1.4 kg, 6 W), the beam expander and defocus assembly (1 kg, 0.5 W), and the point-ahead assembly (250 cm^3, 1 kg, 5 W). The support electronics for the ISL terminal consist of the signal conditioning electronics (250 cm^3, 1 kg, 7.5 W), the servo electronics (750 cm^3, 3 kg, 7.5 W), commands and telemetry (400 cm^3, 1.8 kg, 3 W), and microprocessors (1,000 cm^3, 3 kg, 10 W). The miscellaneous items in Table 4 include the transmit/receive diplexer and miscellaneous optics

(1.5 kg), the support structure and spacecraft interface (4 kg), various cables and connectors (2 kg), radiation shielding (1 kg), and a passive radiator (1 kg).

Nd:YAG LASER ISL TERMINAL

As with the CO_2 system, fairly accurate MPV estimates can be obtained for this system from the open literature [3],[5],[16],[17], and these are given in Table 5. The communications subsystem essentially contains three parts: a frequency-doubled GaAlAs diode-pumped Nd:YAG laser, an external EO modulator, and a direct-detection receiver. The laser includes the laser head, a cooling system of heat pipes, a power supply for the diode laser pump arrays, and a temperature-stabilized second harmonic generator unit. The external modulator consists of a multiplexing and signal processing circuit, a modulator driver, and the electro-optic crystal, which is oven-stabilized. Between the modulator and the laser is a lens system for beam matching. A lens system is also required at the output of the modulator for beam collimation. The receiver is composed of a narrowband optical filter, a focusing lens system, a silicon avalanche photodiode (APD) with a low-noise preamplifier, and signal processing circuitry.

The MPV of these components can be assessed from the characteristics of the individual elements. For this system, these estimates can be based on existing hardware developed for spaceflight use. The state-of-the-art Nd:YAG laser head is 38 cm long, has a cross section of about 100 cm^2, and weighs about 4.5 kg. It includes the frequency-doubling unit and the pump arrays. The power supplies for the pump arrays, laser, and modulator add about 4 kg. An additional 2,000 cm^3 is required for the transmitter power supplies and communications electronics. The heat-pipe cooling system adds about 16,000 cm^3 and 5 kg. With an end-of-life efficiency of 5 percent, assuming GaAlAs diode laser array pumping of the Nd:YAG crystal [18], a prime power of 8 W is required for the 400-mW laser. Another 5 W is needed for thermal stabilization of the frequency-doubling crystal and for laser control.

The EO modulator unit is estimated to have dimensions of 15 × 12 × 12 cm^3 and to weigh 4.5 kg. It requires a 10-W prime power driver and another 2.5 W for the oven. The modulator electronics add about 0.4 kg and require about 1 W of prime power.

The receiver can be compacted to a very small volume of about 500 cm^3 which weighs about 0.4 kg and requires 1.7 W of prime power, including the clock recovery circuitry. Two detectors are used in the receiver to accept the two orthogonally polarized components of the selected modulation scheme. Finally, the appropriate requirements of the PAT subsystem, support electronics, and miscellaneous items are assumed to be the same as for the CO_2 ISL terminal.

TABLE 5. MPV ESTIMATES FOR A Nd:YAG LASER ISL TERMINAL (WITHOUT REDUNDANCY)

ITEM	VOLUME (cm^3)	MASS (kg)	POWER (W)
Communications Transmitter • Transmitter Laser (400-mW optical output under mode-locked conditions) • Stabilization Electronics • Frequency-Doubling Unit • Power Supplies for Pump Arrays, Laser, and Modulator	5,800	8.5	13.0
Heat-Pipe Cooling System	16,000	5.0	—
Modulator (oven-stabilized) and Modulator Driver	2,160	4.9	13.5
Communications Receiver • Two Photodetectors Assumed • Regenerator and Clock Recovery Circuit Included	500	0.4	1.7
Added Requirements for QPSK-Analog Transmission With Bandwith Expansion (normalized to baseband-digital requirements)	450	0.5	27.7
PAT Subsystem • Acquisition/Tracking Transmitter • Beacon Receiver Subsystem • IMCM Assembly • Beam Expander and Defocus Assembly • Point-Ahead Assembly	1,750	7.9	17.5
Gimballed Optical Telescope	—	—	25.0
• Gimbal Power Supply	—	2.0	—
• Baseband-Digital Transmission (20.4 cm)	36,000	14.5	—
• QPSK-Analog Transmission (36.6 cm)	186,250	37.5	—
Support Electronics • Signal Conditioning Electronics • Servo Electronics • Commands and Telemetry • Microprocessors	2,400	8.8	28.0
Power Conditioning Subsystem (efficiency = 80%)	2,200	7.7	—
• Digital			22.7
• Analog			23.3
Miscellaneous • Diplexer and Miscellaneous Optics • Support Structure and Spacecraft Interface	—	9.5	—

TABLE 5. MPV ESTIMATES FOR A Nd:YAG LASER ISL TERMINAL (WITHOUT REDUNDANCY) (CONT'D)

ITEM		VOLUME (cm^3)	MASS (kg)	POWER (W)
• Cables and Connectors • Radiation Shielding • Passive Radiator				
Thermal Control and Thermal Blankets		—	4.0	15.0
Subtotal	Digital	66,810	73.2	136.4
	Analog	217,510	96.7	139.7
10% Margin	Digital	6,681	7.3	13.6
	Analog	21,751	9.7	14.0
Total	Digital	73,491	80.5	150.0
	Analog	239,261	106.4	153.7
Prime Power Weight Burden at 0.15 kg/W	Digital	—	22.5	—
	Analog	—	23.1	—
Total Terminal Burden	Digital	73,500	103.0	150.0
	Analog	239,300	129.5	153.7

InGaAsP LASER ISL TERMINAL

The communications subsystem for this terminal consists of a directly modulated InGaAsP diode laser transmitter, a Nd:YAG optical power amplifier, a direct-detection InGaAs APD receiver, and the associated electronics for various feedback controls, drive, and bias circuits. Table 6 summarizes the MPV estimates for an InGaAsP laser ISL terminal.

The volume and weight of the diode laser transmitter module are estimated to be 500 cm^3 and 0.5 kg, respectively, and a prime power requirement of 2.5 W is assumed. For beam matching to the power amplifier, an additional lens system is required. The Nd:YAG amplifier construction is assumed to be similar to that of the Nd:YAG laser in the previous system. A frequency-doubling crystal is not required in the amplifier; however, the lower estimated efficiency for the power amplifier as compared to the laser increases the needed optical pump power and crystal length. Therefore, it is assumed that the amplifier and its cooling system occupy roughly the same volume and weight as in the Nd:YAG laser. Because of the increased optical pump radiation, a 20-percent increase in prime power over the frequency-doubled Nd:YAG laser is assumed. The receiver MPV is estimated as 0.3 kg, 1.5 W, and 500 cm^3 (only one detector required).

TABLE 6. MPV ESTIMATES FOR AN InGaAsP LASER/Nd:YAG POWER AMPLIFIER ISL TERMINAL (WITHOUT REDUNDANCY)

ITEM	VOLUME (cm^3)	MASS (kg)	POWER (W)
Communications Transmitter • Transmitter Laser (40-mW optical output), Including Peltier Cooler, Stabilization Electronics, and Modulation Electronics	500	0.5	2.5
Nd:YAG Power Amplifier • Resonant Amplifier Assumed, Including Cooling System • Prime Power = 1.2 × Prime Power for Nd:YAG Laser	21,800	13.5	15.6
Communications Receiver • Regenerator and Clock Recovery Circuit Included	500	0.3	1.5
Added Requirements for QPSK-Analog Transmission With Bandwidth Expansion (normalized to baseband-digital requirements)	450	0.5	2.7
PAT Subsystem • Acquisition/Tracking Transmitter • Beacon Receiver Subsystem • IMCM Assembly • Beam Expander and Defocus Assembly • Point-Ahead Assembly	1,750	7.9	17.5
Gimballed Optical Telescope	—	—	25.0
• Gimbal Power Supply	—	2.0	—
• Baseband-Digital Transmission (29.8 cm)	103,750	27.0	—
• QPSK-Analog Transmission (52.4 cm)	526,500	69.0	—
Support Electronics • Signal Conditioning Electronics • Servo Electronics • Commands and Telemetry • Microprocessors	2,400	8.8	28.0
Power Conditioning Subsystem (efficiency = 80%)	2,200	7.8	—
• Digital			21.0
• Analog			21.6
Miscellaneous • Diplexer and Miscellaneous Optics • Support Structure and Spacecraft Interface	—	9.8	—

TABLE 6. MPV ESTIMATES FOR AN InGaAsP LASER/Nd:YAG POWER AMPLIFIER ISL TERMINAL (WITHOUT REDUNDANCY) (CONT'D)

ITEM		VOLUME (cm^3)	MASS (kg)	POWER (W)
• Cables and Connectors • Radiation Shielding • Passive Radiator				
Thermal Control and Thermal Blankets		—	4.0	15.0
Subtotal	Digital	132,900	81.6	126.1
	Analog	556,100	124.1	129.4
10% Margin	Digital	13,290	8.2	12.6
	Analog	55,610	12.4	12.9
Total	Digital	146,190	89.8	138.7
	Analog	611,710	136.5	142.3
Prime Power Weight Burden at 0.15 kg/W	Digital	—	20.8	—
	Analog		21.3	
Total Terminal Burden	Digital	146,200	110.6	138.7
	Analog	611,700	157.8	142.3

GaAlAs LASER/DIRECT-DETECTION ISL TERMINAL

Table 7 summarizes the MPV estimates for this terminal. The communications subsystem consists of a relatively simple transmitter and receiver. The transmitter includes two directly modulated GaAlAs diode lasers mounted on miniature Peltier coolers so that the beams have orthogonal polarizations. The outputs of the lasers are combined incoherently on one axis using a polarizing cube. The volume of this basic module is about 500 cm^3, when room for a driver circuit board and a supply for the cooler are included, and it is estimated to weigh 0.8 kg and require 4.5 W of prime power. The largest portion of the power requirement is for the high-speed driver and the Peltier cooler (which can also be used as a heater). The remainder is for feedback power and temperature stabilization circuitry, and laser bias.

The direct-detection receiver consists of a silicon APD and low-noise field-effect transistor (FET) preamplifier front end, a high-gain second-stage amplifier, and signal processing circuitry. It also includes the optics to focus the receive beam onto the detector. The volume and mass are estimated to be 500 cm^3 and 0.3 kg, respectively. The prime power depends on the complexity of the signal demodulation and processing functions and is estimated to be 1.5 W.

TABLE 7. MPV ESTIMATES FOR A GaAlAs LASER/DIRECT-DETECTION ISL TERMINAL (WITHOUT REDUNDANCY)

ITEM	VOLUME (cm^3)	MASS (kg)	POWER (W)
Communications Transmitter • Transmitter Laser (2 diode lasers at 100-mW optical output each), Including Peltier Coolers, Stabilization Electronics, Modulation Electronics, and Polarization Combining Optics	500	0.8	4.5
Communications Receiver • Regenerator and Clock Recovery Circuit Included	500	0.3	1.5
Added Requirements for QPSK-Analog Transmission With Bandwidth Expansion (normalized to baseband-digital requirements)	450	0.5	2.7
PAT Subsystem • Acquisition/Tracking Transmitter • Beacon Receiver Subsystem • IMCM Assembly • Beam Expander and Defocus Assembly • Point-Ahead Assembly	1,750	7.9	17.5
Gimballed Optical Telescope	—	—	25.0
• Gimbal Power Supply	—	2.0	—
• Baseband-Digital Transmission (25.6 cm)	67,000	20.5	—
• QPSK-Analog Transmission (43.9 cm)	315,000	51.0	—
Support Electronics • Signal Conditioning Electronics • Servo Electronics • Commands and Telemetry • Microprocessors	2,400	8.8	28.0
Power Conditioning Subsystem (efficiency = 80%)	1,500	5.5	—
• Digital			18.3
• Analog			18.8
Miscellaneous • Diplexer and Miscellaneous Optics • Support Structure and Spacecraft Interface • Cables and Connectors • Radiation Shielding • Passive Radiator	—	10.0	—
Thermal Control and Thermal Blankets	—	4.0	15.0

TABLE 7. MPV ESTIMATES FOR A GaAlAs LASER/DIRECT-DETECTION ISL TERMINAL (WITHOUT REDUNDANCY) (CONT'D)

ITEM		VOLUME (cm^3)	MASS (kg)	POWER (W)
Subtotal	Digital	73,650	59.8	109.8
	Analog	322,100	90.8	113.0
10% Margin	Digital	7,365	6.0	11.0
	Analog	32,210	9.1	11.3
Total	Digital	81,015	65.8	120.8
	Analog	354,310	99.9	124.3
Prime Power Weight Burden at 0.15 kg/W	Digital	—	18.1	—
	Analog	—	18.6	—
Total Terminal Burden	Digital	81,000	83.9	120.8
	Analog	354,300	118.5	124.3

GaAlAs LASER/WDM/DIRECT-DETECTION ISL TERMINAL

The communications subsystem for this terminal includes three directly modulated laser transmitters, operating at different wavelengths, which are optically multiplexed using dichroic filters. Each of the transmitters is designed in the same way as those used in the previous system. A major difference in this system compared to the others is that the three independent optical carriers each operate at the single-transponder rate (120-Mbit/s or 72-MHz bandwidth). This affects the mass and prime power requirements of the electronics used in the ISL terminal. However, the increased number of optical components somewhat offsets these advantages.

The receivers for the three optical carriers are also identical to the receiver used in the previous system. Therefore, MPV requirements for this terminal can be amended from previous estimates, and are given in Table 8.

GaAlAs LASER/HETERODYNE-DETECTION ISL TERMINAL

The MPV estimates for this terminal can be amended from those for the GaAlAs laser/direct-detection ISL terminal (Table 7) and are given in Table 9. The communications transmitter in this system is similar to the one used in the GaAlAs/direct-detection system, except that only one directly modulated diode laser of suitably narrow linewidth is used, as determined by the system data rate and the selected modulation/demodulation scheme.

An optical isolator is added to suppress backscattered light from feeding back into the transmitter laser, which would affect the laser oscillation

TABLE 8. MPV ESTIMATES FOR A GaAlAs LASER WDM/DIRECT-DETECTION ISL TERMINAL (WITHOUT REDUNDANCY)

ITEM	VOLUME (cm^3)	MASS (kg)	POWER (W)
Communications Transmitter • Transmitter Lasers (6 diode lasers at 100-mW optical output each), Including Peltier Coolers, Stabilization Electronics, Modulation Electronics, Polarization Combining Optics, and Optical Multiplexing Elements	1,800	2.7	12.0
Communications Receiver • Three Separate Optical Receivers With Optical Demultiplexing Elements • Regenerators and Clock Recovery Circuits Included	1,800	1.5	4.5
Added Requirements for QPSK-Analog Transmission With Bandwidth Expansion (normalized to baseband-digital requirements)	1,200	1.5	7.2
PAT Subsystem • Acquisition/Tracking Transmitter • Beacon Receiver Subsystem • IMCM Assembly • Beam Expander and Defocus Assembly • Point-Ahead Assembly	1,750	7.9	17.5
Gimballed Optical Telescope	—	—	25.0
• Gimbal Power Supply	—	2.0	—
• Baseband-Digital Transmission (25.5 cm)	66,250	20.5	—
• QPSK-Analog Transmission (31.6 cm)	122,000	29.5	—
Support Electronics • Signal Conditioning Electronics • Servo Electronics • Commands and Telemetry • Microprocessors	2,200	8.1	21.5
Power Conditioning Subsystem (efficiency = 80%)	1,500	5.6	—
• Digital			19.1
• Analog			20.5
Miscellaneous • Diplexer and Miscellaneous Optics • Support Structure and Spacecraft Interface • Cables and Connectors • Radiation Shielding • Passive Radiator	—	10.7	—

TABLE 8. MPV ESTIMATES FOR A GaAlAs LASER WDM/DIRECT-DETECTION ISL TERMINAL (WITHOUT REDUNDANCY) (CONT'D)

ITEM		VOLUME (cm^3)	MASS (kg)	POWER (W)
Thermal Control and Thermal Blankets		—	4.0	15.0
Subtotal	Digital	75,300	63.0	114.6
	Analog	132,250	73.5	123.2
10% Margin	Digital	7,530	6.3	11.5
	Analog	13,225	7.4	12.3
Total	Digital	82,830	69.3	126.1
	Analog	145,475	80.9	135.5
Prime Power Weight Burden at 0.15 kg/W	Digital	—	18.9	—
	Analog	—	20.3	—
Total Terminal Burden	Digital	82,800	88.2	126.1
	Analog	145,500	101.2	135.5

characteristics [19] and disrupt reliable communications in the system. Furthermore, the temperature and injection current of the transmitter laser must be extremely well stabilized ($\pm 10^{-3}$ K and $\pm$ 10 μA with the selected modulation/demodualtion scheme), which requires more sophisticated electronic circuitry than for the direct-detection system. Thus, the same MPV values given in Table 7 are used for the communications transmitter.

The communications receiver is substantially more complex than the one used in the direct-detection systems. It includes a highly stabilized LO laser, frequency tracking provisions, a balanced silicon PIN photomixer, passive optical components for combining the LO and received beams, and demodulation circuitry. Furthermore, owing to inaccuracies in the pointing and tracking subsystem, an active self-aligning system consisting of two optomechanical beam steerers, a beam splitter, a quadrant photodetector, and feedback electronics is required for the LO beam. A stable RF or microwave oscillator is also required as an IF frequency reference. These optical and electronic functions increase the MPV of the heterodyne receiver substantially over that of the direct-detection receiver. The heterodyne receiver MPV estimates of 1.3 kg, 5 W, and 2,000 cm^3 include the silicon photomixer and communications electronics (0.3 kg, 1.5 W), the LO laser with its power supply and stabilization electronics (0.5 kg, 2.5 W), and the auto-alignment subsystem (0.5 kg, 1 W).

TABLE 9. MPV ESTIMATES FOR A GaAlAs LASER/HETERODYNE-DETECTION ISL TERMINAL (WITHOUT REDUNDANCY)

ITEM	VOLUME (cm^3)	MASS (kg)	POWER (W)
Communications Transmitter • Transmitter Laser, Including Peltier Cooler, Stabilization Electronics, Modulation Electronics, and Optical Isolator	500	0.8	4.5
Communications Receiver • Photomixer and Communications Electronics, Including Regenerator and Clock Recovery Circuit • LO Laser, Including Power Supply, Peltier Cooler, and Stabilization Electronics • Auto-Alignment System	2,000	1.3	5.0
Added Requirements for QPSK-Analog Transmission With Bandwidth Expansion (normalized to baseband-digital requirements)	400	0.4	2.5
PAT Subsystem • Acquisition/Tracking Transmitter • Beacon Receiver Subsystem • IMCM Assembly • Beam Expander and Defocus Assembly • Point-Ahead Assembly	1,750	7.9	17.5
Gimballed Optical Telescope	—	—	25.0
• Gimbal Power Supply	—	2.0	—
• Baseband-Digital Transmission (23.4 cm)	52,500	18.0	—
• QPSK-Analog Transmission (22.5 cm)	47,000	16.8	—
Support Electronics • Signal Conditioning Electronics • Servo Electronics • Commands and Telemetry • Microprocessors	2,400	8.8	28.0
Power Conditioning Subsystem (efficiency = 80%)	1,500	5.6	—
• Digital			19.0
• Analog			19.5
Miscellaneous • Diplexer and Miscellaneous Optics • Support Structure and Spacecraft Interface • Cables and Connectors • Radiation Shielding • Passive Radiator	—	10.0	—

TABLE 9. MPV ESTIMATES FOR A GaAlAs LASER/HETERODYNE-DETECTION ISL TERMINAL (WITHOUT REDUNDANCY) (CONT'D)

ITEM		VOLUME (cm^3)	MASS (kg)	POWER (W)
Thermal Control and Thermal Blankets		—	4.0	15.0
Subtotal	Digital	60,650	58.4	114.0
	Analog	55,550	57.6	117.0
10% Margin	Digital	6,065	5.8	11.4
	Analog	5,555	5.8	11.7
Total	Digital	66,715	64.2	125.4
	Analog	61,105	63.4	128.7
Prime Power Weight Burden at 0.15 kg/W	Digital	—	18.8	—
	Analog	—	19.3	—
Total Terminal Burden	Digital	66,700	83.0	125.4
	Analog	61,100	82.7	128.7

Summary

Table 10 summarizes the results presented in Tables 4 through 9 and indicates the superiority of GaAlAs laser systems with respect to mass and prime power requirements. However, the volume requirements are not always the lowest because the antennas required for the assumed optical transmitter powers are slightly larger for GaAlAs systems. The difference in analog and digital modulation schemes is caused by the size difference of the gimballed telescope/mirror required to meet the specified optical power budget of the link. Because digital transmission of an optical signal is much more efficient than analog transmission, a digital link requires a smaller-diameter optical telescope [11], and thus reduced volume, mass, and prime power.

TABLE 10. SUMMARY OF MPV ESTIMATES FOR OPTICAL ISL TERMINALS (WITHOUT REDUNDANCY)

	MASS (kg)		POWER (W)		VOLUME (cm^3)	
SYSTEM	DIGITAL	ANALOG	DIGITAL	ANALOG	DIGITAL	ANALOG
CO_2	104.9	124.1	203.3	206.8	69,600	165,300
Nd:YAG	103.0	129.5	150.0	153.7	73,500	239,300
InGaAsP	110.6	157.8	138.7	142.3	146,200	611,700
GaAlAs	83.9	118.5	120.8	124.3	81,000	354,300
GaAlAs WDM	88.2	101.2	126.1	135.5	82,800	145,500
GaAlAs Heterodyne	83.0	82.7	125.4	128.7	66,700	61,100

The results in Table 10 further support the system preferences obtained from optical power budget calculations, together with a qualitative assessment of the system characteristics for the six optical technologies [11]. That is, for near-term (1988–1992) baseband-digital applications, a single-carrier, 360-Mbit/s GaAlAs laser system with a direct-detection, silicon APD receiver is preferred for each direction in the duplex link. The transmitter uses the combined output power of two orthogonally polarized lasers and a binary pulse position (OOK) modulation format. For near-term analog applications, WDM of three 72-MHz GaAlAs laser/direct-detection systems is preferred in each direction. Each link in the WDM system uses a polarization-combined transmitter and intensity modulation with an FM subcarrier.

For the far term (1992–1995), a single-carrier GaAlAs laser system with a heterodyne-detection, silicon-PIN-photodiode receiver is preferred for both baseband-digital and analog applications. The baseband-digital and analog links use QFSK modulation and direct optical FM, respectively. Use of the heterodyne system is contingent upon obtaining solutions to the difficult engineering problems associated with its implementation, including frequency stability in the transmitter and frequency tracking and spatial alignment in the receiver.

Acknowledgments

Helpful discussions with G. Koepf and R. Nelson of Ball Aerospace Systems Division, Colorado, and D. Paul of COMSAT Laboratories, are greatly appreciated.

References

[1] G. R. Welti, "Intersatellite Link for Multiple Access Telephony," IEEE Electronics and Aerospace Systems Convention (EASCON), Arlington, Virginia, September 1978, *Convention Record*, pp. 432–440.

[2] D. K. Sachdev and T. Chidambaram, "Intersatellite Links for International Communications," IEEE International Conference on Communications, Denver, Colorado, June 1981, *Conf. Rec.*, pp. 70.2.1–70.2.6.

[3] D. C. Forster *et al.*, "Wide-Band Laser Communications in Space," *IEEE Journal of Quantum Electronics*, Vol. QE-8, No. 2, February 1972, pp. 263–272.

[4] J. H. McElroy *et al.*, "CO_2 Laser Communication Systems for Near-Earth Space Applications," *Proc. IEEE*, Vol. 65, No. 2, February 1977, pp. 221–251.

[5] M. Ross *et al.*, "Space Optical Communications With the Nd:YAG Laser," *Proc. IEEE*, Vol. 66, No. 3, March 1978, pp. 319–344.

[6] M. Ross *et al.*, "Space Laser Communications Systems for the Eighties," AIAA 8th Communications Satellite Systems Conference, Orlando, Florida, April 1980, *Proc.*, pp. 739–745.

[7] E. Bonek and H. Lutz, "CO_2 Laser Communication Technology for Intersatellite Data Links," *ESA Journal*, Vol. 5, No. 2, 1981, pp. 83–98.

[8] V. W. S. Chan *et al.*, "Heterodyne Lasercom Systems Using GaAs Lasers for ISL Applications," IEEE International Conference on Communications, Boston, Massachusetts, June 1983, *Conf. Rec.*, pp. E1.5.1–E1.5.7.

[9] J. E. Kaufmann and L. L. Jeromin, "Optical Heterodyne Intersatellite Links Using Semiconductor Lasers," IEEE Global Telecommunications Conference, Atlanta, Georgia, November 1984, *Conf. Rec.*, pp. 28.4.1–28.4.8.

[10] L. Freeon and E. Sein, "Optical Intersatellite Data Links With Semi-Conductor Laser," 35th Congress of the International Astronautical Federation, Lausanne, Switzerland, October 1984, *Proc.*, Paper No. IAF-84-69.

[11] R. G. Marshalek and G. A. Koepf, "Comparison of Optical Technologies for Intersatellite Links," Optical Technologies for Communication Satellite Applications, *Proc. SPIE*, Vol. 616, January 1986, pp. 29–48. (A revision of this paper appears in *Optical Engineering*, Vol. 27, No. 8, August 1988, pp. 663–676.)

[12] COMSAT Laboratories, "Optical Intersatellite Link Technology," Final Report to COMSAT Intelsat Satellite Services Engineering under Project Support Authorization STA-5, December 1986. COMSAT Data Catalog No. 86DC133.

[13] COMSAT Laboratories, "The Study of Optical Intersatellite Links," Final Report to INTELSAT under Contract INTEL-384, August 1985. COMSAT Data Catalog No. 85DC132.

[14] Ball Aerospace Systems Division, "Tracking and Data Acquisition System Laser Intersatellite Communications Study," Final Report under NASA/Goddard Space Flight Center Contract NAS5-29128, August 1986. NASA Contract Report No. CR-183419.

[15] D. K. Paul, "Comparison of Optical Technologies for Intersatellite Link Payloads: Part II. Impact of Reliability Considerations on Technology Selection," *COMSAT Technical Review*, Vol. 18, No. 2, Fall 1988, pp. 215–238 (this issue).

[16] J. A. Maynard *et al.*, "Multi-Gigabit Laser Communications for Satellite Cross-Links," 4th International Conference on Digital Satellite Communications, Montreal, Canada, October 1978, *Proc.*, pp. 155–159.

[17] J. D. Wolf *et al.*, "Application of Nd:YAG Optical Communications Technology for Aircraft to Satellite Links," IEEE Electronics and Aerospace Systems Convention (EASCON), Arlington, Virginia, October 1979, *Convention Record*, pp. 286–294.

[18] D. Begley *et al.*, "Solid-State Cross-Link Systems and Technology," *International Journal of Satellite Communications*, Vol. 6, No. 2, April–June 1988, pp. 91–105.

[19] K. Petermann and G. Arnold, "Noise and Distortion Characteristics of Semiconductor Lasers in Optical Fiber Communication Systems," *IEEE Journal of Quantum Electronics*, Vol. QE-18, No. 4, April 1982, pp. 543–555.

Robert G. Marshalek received the B.E.S. and Ph.D. degrees from The Johns Hopkins University in 1976 and 1982, respectively, both in electrical engineering. From September 1976 to May 1981, he was a Research and Teaching Assistant at Johns Hopkins. He joined COMSAT Laboratories in October 1981 as a Member of the Technical Staff in the Optical Communications Department of the Microwave Technology Division, where he was involved in investigations of wavelength-division multiplexed optical links, the use of fiber optics in a digitally multiplexed earth station and fiber optic local area networks, and optical intersatellite link technology. He also contributed to the design and testing of modular hardware for prototype space optical links. Dr. Marshalek is currently a Principal Design Engineer with Ball Aerospace Systems Division, Boulder, Colorado. He is a member of IEEE, SPIE, Phi Beta Kappa, Tau Beta Pi, and Eta Kappa Nu.

Index: communication satellites, geosychronous orbit, intersatellite link, transmission, optical communication, reliability

Comparison of optical technologies for intersatellite link payloads*

Part II. Impact of reliability considerations on technology selection

D. K. PAUL

(Manuscript received September 3, 1987)

Abstract

The component and system reliabilities typical of six representative optical technologies deemed viable for an optical intersatellite link (ISL) between two geostationary satellites are examined, and the results are assessed in terms of their impact on the selection of an appropriate technology. The redundancy requirements are calculated in each case, assuming a system reliability of 0.9. Because high-power light sources are the weakest element in the link, optical ISL systems require switched redundancy of the laser transmitters. Communications subsystem reliabilities are based on CO_2, Nd:YAG, InGaAsP, and GaAlAs laser sources utilizing either direct- or heterodyne-detection receivers. The results favor GaAlAs semiconductor laser technology. Optical ISLs that employ a nonredundant transmitter design must use heterodyne detection and high-stability, narrow-linewidth, injection-locked diode lasers. However, because a heterodyne-detection optical ISL system is technically very complex, it is risky to implement in near-term space applications. A less complex direct-detection optical ISL requires one redundant laser transmitter in order to meet the specified system reliability. (The mass, prime power, and volume requirements for the six technologies are compared in Part I of this paper.)

*This two-part paper is based on work performed at COMSAT Laboratories under the sponsorship of COMSAT Intelsat Satellite Services Engineering.

Introduction

For satellite communications to remain competitive vis-à-vis the formidable challenge of fiber optic technology, future satellite communications planning must include development of advanced yet economical satellite designs, and implementation of intersatellite link (ISL) technology and intelligent networking concepts. Advanced, economical satellite design efforts are just emerging, and the understanding of ISL systems has matured considerably through the many system studies conducted in the last 6 years. These studies have largely focused on broader issues of technical feasibility, and no systematic investigation of overall system and component reliability has been reported. With the current research and development trend in space-qualifiable ISL hardware, it is appropriate that the reliability of ISL components and subsystems, and its impact on technology selection, be critically assessed.

A series of papers and reports [1]–[7] have addressed the various technical attributes of ISLs, such as optical power budget; mass, power, and volume (MPV); pointing, acquisition, and tracking (PAT); and RF/optical interface requirements. A framework for optical ISL systems comparison has been established by considering six candidate systems which use the following technologies: CO_2 laser, neodymium (Nd):YAG laser, InGaAsP laser/Nd-doped optical amplifier, GaAlAs laser, GaAlAs laser/wavelength-division multiplexer (WDM), and GaAlAs laser/heterodyne. However, the feasibility of a selected ISL technology within a given time frame must be subject to the critical test of system reliability requirements.

In this paper, reliability issues in optical ISLs are discussed for each candidate system at the subsystem and component levels, and the redundancy requirement for a specified system lifetime is determined. The results thus complement those of the above companion papers to enable judicious selection of an economical and appropriate optical technology. An overall perspective generic to the six candidate optical ISL systems is provided, and state-of-the-art capabilities are briefly reviewed. Reliability model and redundancy requirements are then presented for each system.

System reliability

Figure 1 shows a typical optical communications transceiver for the ISLs. It should be noted that the communications and PAT subsystems use the same optical telescope. The overall systems perspective given in Figure 2 identifies the following basic building blocks for the six candidate optical ISL systems:

a. *Optical Transmitter:* includes light-emitting sources; drive circuits; modulators; and power, frequency, and thermal stabilization circuitry.

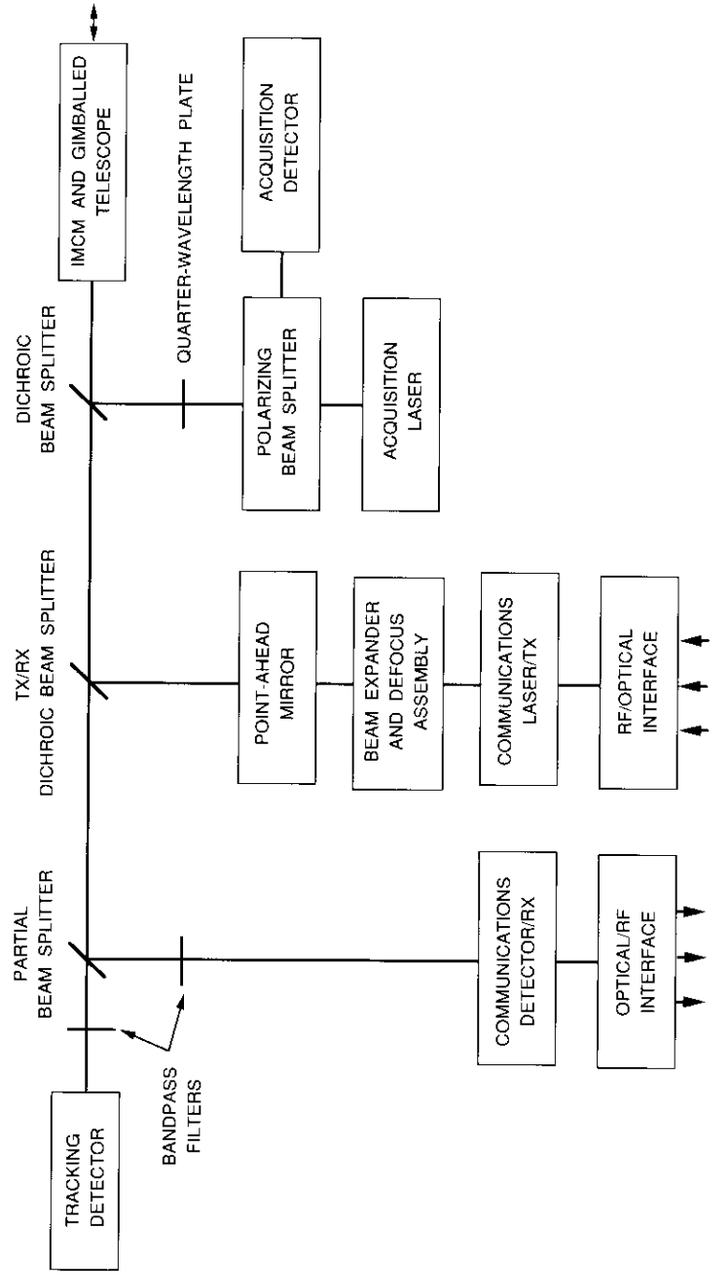

Figure 1. *Typical Communications Transceiver for an Optical ISL*

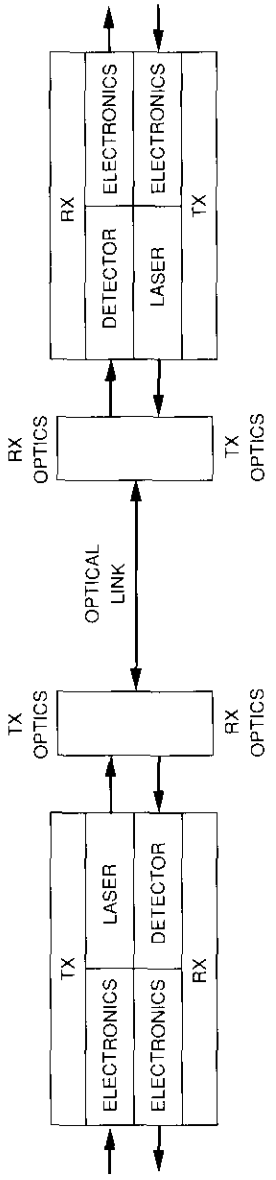

Figure 2. *Block Diagram of an Optical ISL Communications Subsystem*

b. *Optical Receiver:* includes photodetectors/mixers; amplifiers; equalizers; clock recovery; high-speed electronics; light-emitting sources for optical heterodyne detection; and power, frequency, and thermal stabilization circuitry.

c. *Optics:* includes optical filters, lenses, beam splitters, beam expanders/shapers, an image motion compensation mirror (IMCM), and a gimballed telescope.

d. *RF/Optical Interface:* for compatible interconnectivity between RF/microwave and optical signals.

The PAT subsystem does not require a high-power transmitter or a very sensitive receiver. Optical interfacing with RF/microwave signals is also not required. Consequently, the reliability and performance specifications of the PAT subsystem are not as complex as in the communications subsystem, and the design is simpler. However, the mechanical stability and other performance requirements for the gimballed mirror and servo-control mechanisms could be stringent [2],[4]. Both the optics and the RF/optical interfaces in the communications subsystem are generic to the six candidate optical ISL systems, and thus equally affect the performance and reliability of each system.

The communications subsystems representing the six candidate optical technologies are compared in Table 1. In spite of some generic similarity, the optical communications transceiver units and the architecture in each ISL system are distinctive enough to differentially affect overall systems reliability. An assessment of reliability for each of the six optical ISL systems follows.

State-of-the-art capabilities

This section presents the state-of-the-art operational characteristics and reliability performance of the various components and subsystems used in optical ISL systems. The goal is to assess both capabilities and limitations (including short- and long-term performance degradation) in order to select one of the six candidate technologies for deployment in the near future.

To appreciate the complex issues of systems reliability evaluation which involve, at the minimum, a critical examination of relevant technology, systems design and configuration, and deployment/test schedules, it is essential to identify those components and subsystems which are specific to the six optical ISL systems under consideration. This information can provide a list of the long-lead-time, critical technology hardware recommended for the optical terminals on board the satellites in an ISL. Also, a time line can be estimated for the laser communications hardware phase, which may require

TABLE 1. OPTICAL ISL COMMUNICATIONS SUBSYSTEMS CHARACTERISTICS

	LASER			MODULATOR			RECEIVER			
TECHNOLOGY	MATERIAL	PUMP	WAVELENGTH (μm)	MATERIAL	CONFIGURATION	FORMAT	DETECTOR	DETECTION PRINCIPLE	TECHNOLOGY STATUS	CRITICAL TECHNOLOGY AREA
CO_2	Gas	RF-discharge	9/10	Electro-optic crystal	External, bulk, or traveling-wave type	Intensity, polarization, frequency, phase	HgCdTe, photo-conductor	Coherent or incoherent heterodyne	Mature	• System reliability – especially RF-excited waveguide laser lifetime
Nd:YAG	Nd-doped crystal	GaAlAs diode laser arrays	1.064; (0.532 using SHG)	Electro-optic crystal	External, bulk	Intensity (pulsed), polarization	Silicon APD	Direct	Mature	• Pump efficiency • Duplex link
InGaAsP/Nd*	Quaternary III-V's	Current injection	1.064; 1.052; 1.08	III-V	Internal, directly modulated	Intensity (pulsed or subcarrier)	Germanium or InGaAsP APD	Direct	Very little work done	• Nd power amplifier • Duplex link
GaAlAs	Ternary III-V's	Current injection	0.81; 0.87	III-V	Internal, directly modulated	Intensity (pulsed or subcarrier)	Silicon APD	Direct	Most advanced	• System reliability—especially high-power diode laser, multilaser optical power-combiner
GaAlAs WDM	Ternary III-V's	Current injection	0.78 0.91	III-V	Internal, directly modulated	Intensity (pulsed or subcarrier)	Silicon APD	Direct	Advanced	• System reliability especially high-power diode laser, multilaser optical power-combiner
GaAlAs Heterodyne	Ternary III-V's	Current injection	0.81; 0.87	III-V	Internal, directly modulated	Frequency	Silicon PIN photo-detector	Incoherent heterodyne	Extensive R&D	• Stable, single-mode, narrow-linewidth laser • Complex receiver

* Uses power amplifier of Nd-doped crystal pumped by GaAlAs diode laser array.

further development and/or reliability certification before its implementation in practical systems.

For clarity of discussion, each of the six candidate optical ISL systems is critically assessed in terms of the two major subsystems: the optical transmitter and the optical receiver. For reasons given earlier, other components and subsystems such as optics, telescopes, and RF-optical interfaces, which are generic to all six optical ISL systems, are not considered in this evaluation.

System I: CO_2 laser heterodyne-detection link

OPTICAL TRANSMITTER

The optical transmitter in this system requires an RF-excited waveguide-type CO_2 gas laser emitting in the 9- and 10-μm wavelengths; an RF driver; external modulator and high-speed drive electronics; and control circuits for power, frequency, and temperature stabilization. The capabilities and reliability performance of these components are as follows:

a. *CO_2 Laser/Transmitter.* A power output of 4 to 5 W continuous-wave (CW) in a 10- to 15-cm discharge length of 50 to 100 mTorr gas mixture is typical. The best reported overall efficiency is 18 percent. Degradation is related to gas dissociation, contamination of optical surfaces, and leakage. Typical lifetime is in the range of 15,000 to 30,000 hours.

b. *RF Driver.* RF discharge of the gas mixture inside the dielectric waveguide provides the pump energy needed for the lasing action. Capacitive coupling reduces gas contamination and trapping caused by the metal electrodes used internally in DC-excited gas lasers.

c. *Modulator/High-Speed Driver.* External modulators fabricated on electro-optic (EO) materials such as GaAs and CdTe are efficient and reliable. They are preferred over internal modulators because of the internal heat dissipation, facet damage, and design complexity factors in the intracavity configuration of gas lasers. However, the major limitations of this technology are the large drive power, high thermal stability, and high-speed electronics required for the bulk modulators, as well as poor optical coupling.

d. *Stabilization Circuits.* This is a critical requirement for successful operation of the heterodyne-detection scheme employed in this system. Active control by feedback loops is essential to reduce link performance degradation and ease excessive complexity in heterodyne receiver design. Efficient circuit design and the use of integrated circuits (ICs) enhance systems reliability.

HETERODYNE-DETECTION OPTICAL RECEIVER

This receiver requires the same components as the optical transmitter. In addition, a fast HgCdTe photodetector/mixer and high-speed electronics for post-detection signal processing are needed. The following is a brief review of the performance of these components:

a. *CO_2 Laser Local Oscillator.* Although much less optical power (500 mW, CW) is needed in the local oscillator (LO), the requirements are far more stringent than in the optical transmitter. The tuning range must be much broader, with a very stable difference-frequency output at the photodetector mixer. This requires active tuning of the LO frequency to the received laser beam, which makes the heterodyne receiver design highly complex and prone to dynamic unreliability.

b. *Stabilization Circuits.* Typical short-term frequency stability should be better than 100 kHz. The stark cells and piezoelectric drives used for line and frequency stabilization feedback loops require high voltages, which are potential sources of systems failure.

c. *Photodetector/Mixer.* HgCdTe photodetectors must be cooled to below 130 K for low-noise, high-sensitivity operation. The technology of II-VI materials and devices is reasonably mature; however, the statistics on wide-bandwidth, high-reliability HgCdTe detectors are not as complete as those for the detectors used at near-infrared wavelengths. Selective screening/burn-in and controlled life-testing will be needed to space-qualify these components.

d. *High-Speed Electronics.* Silicon technology is mature and adequate for data rates ranging from high Mbit/s to low Gbit/s. State-of-the-art, high-reliability devices are commercially available for speeds up to 500 to 600 Mbit/s. To ensure a long system lifetime, extensive use of ICs and reliable packaging to reduce parasitics and leakage are recommended.

System 2: Nd:YAG laser direct-detection link

OPTICAL TRANSMITTER

The optical transmitter in this system requires a Nd:YAG laser emitting at 1.064-μm wavelength; a high-power optical source to pump the laser transmitter; a second-harmonic generator (SHG); external modulator and high-speed drive electronics; and stabilization circuits for power, frequency, and temperature control. The capabilities and reliability performance of these components are as follows:

a. *Nd:YAG Laser Transmitter.* A 300- to 400-mW mode-locked (or 300-mW CW) optical power is typically required for the INTELSAT ISLs. Nd:YAG laser cavities should be designed for high thermal stability and efficient optical pumping. Prevention of laser cavity distortion in operations having high repetition rate and large optical output power is particularly critical for single-mode lasers with diffraction-limited output beams. A lifetime of several thousand hours is possible when such lasers are carefully designed.

b. *Optical Pump Source.* An array of short-wavelength, high-power diode lasers (GaAlAs) is recommended as the most efficient pump source for the Nd:YAG laser cavity. However, this will require very high stability for both the wavelength and thermal control electronics (to ~0.5 nm of Nd:YAG emission) for a 90-percent peak absorption throughout the lifetime of the pump laser source. Active feedback control of pump laser output power is essential to avoid non-uniform heating of the Nd:YAG laser cavity. A total of sixty 50-mW CW lasers in three arrays, each array having 20 lasers, is required for pumping the laser transmitter recommended for the INTELSAT ISLs. For a redundant design, a three-array pump of 40 lasers each is recommended. A lifetime of 400,000 hours or better is estimated for each laser.

c. *Second-Harmonic Generator.* This optical ISL system uses a 0.532-μm wavelength, which is the second harmonic of the Nd:YAG laser fundamental emission at 1.064-μm wavelength. Nonlinear optical crystals are used to generate this second harmonic. The SHG efficiency, which is a quadratic function of the incident light intensity, can be very high. SHG crystals with acousto-optic transducers can be used for mode-locking. The critical requirements for reliable SHG operation are imposed by the need for optical alignment to phase-matching conditions and sensitive thermal control of the crystal.

d. *Modulator/High-Speed Driver.* Linear EO modulators (in bulk or integated-optic form) can operate at speeds up to several Gbit/s. The control of beam divergence in bulk modulators, and the static and thermal birefrigence due to RF heating in EO crystals, are critical for high-extinction-ratio, high-reliability devices. Thermal stabilization to less than 0.01°C of the operating temperature is needed. Modulator design and driver electronics should be compatible with the high-speed requirement of the system. The use of ICs is recommended.

e. *Stabilization Circuits.* This is a critical requirement for the link to remain operational. Active control by feedback loops is needed to correct for link performance degradation with aging and/or dynamic instability.

DIRECT-DETECTION OPTICAL RECEIVER

The direct-detection optical receiver in this system uses a high-speed, broad-bandwidth photodetector [silicon avalanche photodiode (APD)] and a suitable amplifier; high-speed electronics; and a demodulator for post-detection signal processing. The requirement for power, frequency, and temperature stabilization is not as critical as in the optical transmitter. The capabilities and reliability performance of these components are as follows:

a. *Photodetector.* Silicon APDs are recommended for their high sensitivity and low-noise performance. Both the material and device technologies are very mature. Wide-bandwidth, high-reliability photodetectors are commercially available for most applications. A typical lifetime of 100 million hours or higher (at room temperature) is predicted from accelerated life-test data; however, careful screening and burn-in will be required in order to select devices for long-lifetime optical ISLs.

b. *High-Speed Signal Processing Electronics.* The applicability of mature silicon technology to functions such as post-detection amplification, equalization, and threshold detection at the required high speed is already proven. Judicial use of ICs should enhance both the performance and reliability of the optical receiver subsystem.

c. *Demodulator.* Typical components in the demodulator include filters, delay line, and high-speed logic. The circuit design and its implementation must be compatible with the ISL system's high speed requirement and its use on board satellites.

System 3: InGaAsP laser/Nd-doped amplifier direct-detection link

OPTICAL TRANSMITTER

In contrast with ISL system 2 discussed above, system 3 utilizes the near-infrared emission of a semiconductor laser amplified by a Nd-doped cavity. The need for the SHG and the external modulator, and their complexities, can be avoided in this link by using InGaAsP laser transmitters and Nd-doped amplifiers operating at approximately 1-μm wavelength. Other components of the system 2 optical transmitter are required in this system, and a higher pump laser power is necessary. Also, because of the need to use the Nd-doped cavities as amplifiers (which are presently much less developed than the Nd:YAG lasers), additional complications are expected. The capabilities and reliability performance of these components are as follows:

a. *Nd-Doped Amplifier.* A resonant power amplifier design using a long crystal with high thermal stability and efficient optical pumping can provide a gain of approximately 10 dB. Prevention of laser cavity distortion under high repetition rate and large optical gain operating conditions is critical for the resonant amplifiers. This topic is currently being investigated, and little is known about the capability or reliability of Nd-doped amplifiers at this stage of development.

b. *Long-Wavelength Diode Laser/Transmitter.* InGaAsP lasers with 40- to 50-mW CW single spatial mode output at 1.08- and 1.064-μm wavelengths (for the two directions, east to west and west to east) are recommended for the laser transmitters. The lasers must have high-speed direct modulation capability. Quaternary III-V semiconductor technology is quite advanced due to fiber optic applications in long-haul terrestrial links. High-stability active feedback control circuits for power, wavelength, and temperature stabilization are essential for reliable operation of long-wavelength lasers. A typical lifetime is estimated to be 400,000 hours or more for state-of-the-art high-power lasers.

c. *High-Speed Modulation Driver/Electronics.* For high-speed direct modulation capability in semiconductor lasers, the design of the drive circuit must be compatible with the specified modulation drive and bias conditions, and with systems transmission parameters. Provision must also be made to compensate for any performance degradation due to aging or dynamic instabilities.

DIRECT-DETECTION OPTICAL RECEIVER

High-speed germanium or InGaAs APDs are used in this system. Other components such as the amplifier, high-speed electronics, and demodulator for post-detection signal processing are the same as in system 2. The long-wavelength photodetectors (both germanium and InGaAs APDs) are characterized by a mature technology and the commercial availability of high-reliability devices. Typical lifetime is estimated to be 100 million hours or better.

System 4: GaAlAs laser direct-detection link

OPTICAL TRANSMITTER

Directly modulated short-wavelength semiconductor lasers are recommended for the optical transmitter. As in system 3, the modulation driver and the high-speed electronics and stabilization circuits are also needed to ensure operation within the design specification. However, an important distinction results from the need to use very high power single-diode lasers in this link: the reliability assurance of diode lasers and the feedback stabilization of optical transmitter performance become very important.

Thermal stabilization to 0.01°C for a stable single-mode output, and simultaneous control of both the DC bias and modulation drive current to reduce aging-induced effects in diode lasers, are essential.

Typically, a short-wavelength, high-power diode laser system requires 200-mW CW lasers with a single spatial mode output at 810- and 870-nm wavelengths (for the two directions, east to west and west to east) and high-speed direct modulation capability. Because of extensive fiber optic applications, the technology of ternary III-V compounds has become very advanced. Since very high-power reliable lasers (above 50-mW CW output) are not commercially available, optical power combining of diode lasers is recommended. A proper reliability assurance scheme should mandate careful screening and accelerated life-testing of high-power diode lasers.

Thermal stabilization is critical in the optical transmitter because a large amount of heat is dissipated in the powerful lasers. Selection of low-threshold lasers, a suitable mounting arrangement, and thermoelectric cooling of the lasers are paramount considerations for long operation lifetime. Life-test data for 100-mW diode lasers are very limited. Available data indicate useful operation of these lasers to approximately 1,500 hours.

DIRECT-DETECTION OPTICAL RECEIVER

The optical receiver subsystem uses the same components as in system 2 (*e.g.*, high-speed silicon APDs, amplifier and high-speed electronics, and a demodulator for post-detection signal processing). For timing and clock recovery purposes, phase-locked-loop (PLL) or surface acoustic wave (SAW) filters are useful. Extensive use of ICs can enhance systems reliability.

System 5: GaAlAs laser WDM direct-detection link

OPTICAL TRANSMITTER

In this system, three short-wavelength diode lasers, each directly modulated at 120 Mbit/s, are wavelength-division multiplexed for a total throughput of 360 Mbit/s in the optical link. This combination of diode lasers relaxes the high-speed and high-power output capability of individual diode laser transmitters required in system 4. The optical transmitter uses the same components as in system 4, plus an optical multiplexer for wavelength-division combining of light beams of three different wavelengths. Stabilization of the lasers and the WDM device is critical for successful operation of the ISL system. Special features of the components used in this link are as follows:

a. *Short-Wavelength, High-Power Diode Laser.* Although the high power requirement of lasers can be relaxed somewhat in the WDM approach, it is prudent to provide an adequate link margin by recommending 200-mW CW laser transmitters with single spatial mode outputs at six wavelengths between 780- and 910-nm (with three wavelengths in each direction). Active feedback control schemes are needed to ensure reliable static and dynamic operation of the diode lasers. Due to the tight specifications for optical demultiplexers and interference filters, the selection of diode lasers and their stabilization schemes is most critical in high-density WDM links.

b. *WDM Optical Multiplexer.* All dielectric optical interference filters provide the multiplex/demultiplex function. For long-term reliable operation of the link, thermal and environmental effects on multiplexer/demultiplexer performance must be controlled. Quality control of the multilayer thin-film deposition process, suitable packaging to eliminate atmospheric and radiation effects, and thermal stabilization are required. Wavelength shift in the peak response, and polarization dependence at off-normal incidence, require that the devices be well aligned and extremely stable.

DIRECT-DETECTION OPTICAL RECEIVER

The direct-detection optical receivers (three in each direction) in this system use the same components as in system 2. In addition, an optical demultiplexer is required in order to separate the wavelengths of the received optical signal. Silicon APDs are fast, broad bandwidth, and responsive to the short-wavelength light emitted by the transmitters.

The most critical component is the optical demultiplexer, whose specification determines the requirements of the other major components and subsystems in the link. Considerations similar to those for the optical multiplexers used in the WDM optical transmitter apply. For high-density WDM applications where the wavelength channels must be closely spaced, the demultiplexer is designed for channels with extremely narrow spectral width and sharp cutoff behavior. The insertion loss should be low. These features are essential in order to separate the many wavelength channels of the WDM signal with minimal interchannel crosstalk in the broadband direct-detection optical receiver. Also, operation of the demultiplexer must be maintained within given tolerance limits. As a result, these components require much tighter specification, complex device fabrication, and stringent static and dynamic reliability testing.

System 6: GaAlAs laser heterodyne-detection link

OPTICAL TRANSMITTER

The basic components in this system are essentially the same as in system 5. However, the need to operate the link in a heterodyne-detection mode places severe restrictions on component selection and operational maintenance. Issues such as optical wavefront quality, transmit/receive beam isolation (via wavelength, polarization, etc.), and reduction of optical feedback to the lasers are addressed in the optomechanical and thermal designs. The special components used in this system, and their capability and reliability performance, are as follows:

a. *Short-Wavelength, High-Power Diode Laser/Transmitter.* Injection-locked GaAlAs lasers with 50-mW CW output power at 810- and 870-nm emission wavelengths (one for each direction) and quaternary frequency-shift keying (QFSK) modulation are recommended for the 360-Mbit/s or 240-MHz heterodyne-detection optical links. The lasers should be capable of high-speed, directly modulated, frequency-stabilized, single spatial mode output. Both external cavity-locked and distributed feedback (DFB) lasers are useful as transmitters. Linewidth-narrowing and frequency stability are the most critical requirements. The use of active feedback control schemes to stabilize optical output power, emission wavelength, frequency, and temperature can provide the required operational reliability, while the provision of diagnostic measurements of performance and reliable frequency standards can ensure long lifetime. Because of tight specifications for the stabilization schemes, diode laser selection is critical. Minimizing the effect of environment on heterodyne link performance is crucial for long-term reliable operation. Reliability data for frequency-stabilized, 50-mW-output CW diode lasers (DFB or cleaved-coupled-cavity) are not presently available. Operation to 400,000 hours or longer is predicted for conventional lasers with 50-mW CW output power.

Specific laser reliability issues are related to an extreme sensitivity to electrical transients, tolerance of the space launch environment (*e.g.*, thermal cycling, shock and vibration resistance, and radiation tolerance), screening of early failure modes, and drive conditions. Experience with conventional lasers has indicated that both high-temperature burn-in and several hundred hours of operation to stabilize the lasers will be required in order to achieve reliable performance of the transmitter. Narrow-linewidth lasers are usually more stable, and aging follows a logarithmic time-dependence typical of activated degradation processes.

Recently, under a U.S. Air Force program on LASERCOM, the MIT Lincoln Laboratory developed and tested a 220-Mbit/s QFSK-modulated optical heterodyne-detection ISL flight package weighing 200 lb and requiring 200 W of electrical power [7]. Typical system requirements included an ~0.8-μm Fabry-Perot laser with ~30-mW CW optical power, ~10-MHz linewidth, ~0.5- to 1-mW/mA L-I slope efficiency, ~30- to 50-mA threshold current, ~15- to 20-GHz tuning range for wavelength matching and frequency tracking, and a stable, reliable lifetime of ~50,000 hours.

b. *High-Speed Modulation Driver.* Accurate and controlled modulation of laser injection current to a few microamperes is required for FSK modulation of the 360-Mbit/s baseband digital input signal. High-speed *M*-ary FSK (MFSK) modulator design is complex because the FM transfer function of the laser [defined as the FM sensitivity (GHz/mA) *vs* modulation frequency (Hz) curve] requires a higher order equalization. Resistance/capacitance equalizer networks; silicon ICs; and fast rise-time, digital GaAs field-effect transistor (FET) differential current switches are adequate at this data rate.

INCOHERENT HETERODYNE-DETECTION OPTICAL RECEIVER

The optical receiver subsystem uses the same components as the optical transmitter discussed above. Also required are components such as a demodulator, matched filter, delay line, and high-speed logic used to recover the data from the photodetected signal. For the short-wavelength diode laser LO used in the heterodyne-detection optical receiver, considerations similar to those for the optical transmitter apply. In addition, the precise optical alignment required at the receiver to track the received optical beam dictates the need for a very stable, rigid mechanical structure. A self-aligning optical beam-steering mechanism for remote angular alignment and matching of the LO and signal beam profiles is essential for successful operation of the heterodyne-detection link.

Phase noise in broad-linewidth lasers affects both modulation and demodulation performance. A balanced receiver can reduce the intensity noise in the heterodyne receiver. Accurate tone spacing and chip combining at low data rates are recommended to minimize the demodulation degradation induced by laser frequency noise. To ensure generation of the very stable difference-frequency signal required in high-sensitivity heterodyne-detection schemes, active tuning of the LO frequency to the received laser beam will be needed. A broad tuning range in the LO, and use of appropriate stabilization schemes at the optical receiver, can ease the selection and/or operation criteria

of the optical transmitter subsystem. Compared to the direct-detection receiver, the design of a heterodyne-detection optical receiver is highly complex and prone to dynamic unreliability.

Summary of trends

Several important technology and reliability trends have been observed for the six candidate optical ISL systems [5],[6],[8],[9]. Although considerable progress is being made in developing optical components such as lasers and photodetectors, the light sources are still the weakest element in the link. In contrast, the signal processing electronics (*e.g.*, mux/demux, clock recovery, modulation driver, and low-noise amplifier) at the desired high speed of 300 to 400 Mbit/s will soon become commonplace, and improved packaging and increased use of ICs in future systems should enhance both performance and reliability.

The need for useful reliability statistics to build confidence in the predicted life-test data of the active devices in field operation is particularly overwhelming for those systems requiring a long lifetime. Careful screening of the devices by burn-in and accelerated life tests is essential for the state-of-the-art components and technology. Because the design of a heterodyne-detection optical ISL is far more complex and critical than that of a direct-detection link, very high performance and reliability of its components are mandated.

Reliability model and redundancy requirement

The inaccessibility of satellites and the high cost of repair, if ever possible from future space stations, make high standards of reliability essential for optical ISLs. A typical reliability of 0.9 per year for the ISL system [4] allows a failure rate of approximately 12,000 failures in time (FITs, defined as the number of failures in 10^9 hours) for the full system [5],[6]. This failure rate, in turn, sets the criteria for specification, selection, and redundancy requirements at the component and subsystem levels. High performance goals motivate the use of the most up-to-date technology. However, reliability standards should dominate component selection. These standards can only be met by implementing stringent life tests during component development and by adopting special quality assurance procedures, which often require the use of dedicated facilities.

The first-generation optical ISL design must be committed to using key components such as light sources and photodetectors, even before their reliability has been fully demonstrated. For such a system to have an adequate

lifetime, additional remotely switched redundant units are needed to provide reliability [6]. As will be shown later, a redundant configuration of optical transmitters can improve link reliability or relax the reliability required of the individual laser transmitters. Because of the increased power consumed in a redundant design, standby redundancy is preferable. Since degradation in semiconductor lasers is current-induced, a cold or softly driven diode laser is highly recommended [6]–[8].

Reliability calculations are based on the serial operations of N basic subsystems, as shown in Figure 2, where every major part of each subsystem is effectively a link in a long chain. The specific cases of 0 to Q redundancy in the light sources have been considered. For a series configuration of M components in a subsystem, all M components must be fully functional. The following three assumptions are made:

a. The system is considered to have failed when any one of the M components fails.

b. The failure probability of each component is independent of the remaining $(M - 1)$ components.

c. The probability that any component will fail in an interval, dt, given that it was operating at t, is $h^i(t)dt$, where $h^i(t)$ is the failure rate of the ith component.

The ISL system reliability may be expressed as [6]

$$R_{\mathrm{ISL}}(t) = \exp\left[-\sum_{i=1}^{N} H^i_{\mathrm{sub}}(t)\right] \tag{1}$$

where

$$H^i_{\mathrm{sub}}(t) = \int h^i_{\mathrm{sub}}(t)dt$$

is the failure distribution of the ith subsystem. The survivability of its M components will determine the subsystem failure distribution.

For a given N, system reliability is high when $H^i_{\mathrm{sub}}(t)$ is kept small. For systems using components that fail at constant rates, the system reliability is typically

$$R_{\mathrm{ISL}}(t) = \exp\{-[(\lambda_{\mathrm{LT}} + \lambda_{\mathrm{TE}}) + \lambda_{\mathrm{TO}} + \lambda_{\mathrm{RO}} + (\lambda_{\mathrm{PD}} + \lambda_{\mathrm{RE}})] \cdot t\} \tag{2}$$

where λ_{LT} = failure rate of the laser transmitter, which includes the laser chips and standby switch failures.

λ_{TE} = failure rate of the transmitter electronics, which includes circuitry for biasing, multiplexing, and modulation drive, and for wavelength, frequency, optical power, and thermal control.

λ_{TO} = failure rate of the transmit optics, which includes the beam collimator, expander and defocusing optics, point-ahead mirror, transmit/receive dichroic beam splitter (T/R DBS), transmit/acquisition (T/A) DBS, IMCM, and gimballed telescope.

λ_{RO} = failure rate of the receive optics, which includes the IMCM and gimballed telescope, T/A DBS, T/R DBS, receive/tracking partial beam splitter, bandpass filter, and beam-focusing optics.

λ_{PD} = failure rate of the photodetector.

λ_{RE} = failure rate of the receiver electronics, which includes the bias, low-noise preamplifier, amplifier/equalizer, automatic gain control (AGC), clock recovery, demodulator, and demutiplexing circuits.

Examination of the reliability data for optical ISL components [6],[7] listed in Table 2 indicates considerable variation in the mean time to failure (MTTF), ranging from a few thousand to a fraction of FITs, the laser being more prone to failure than the other components. This suggests that optical ISL system reliability will be determined primarily by the less reliable light sources, and redundancy of the lasers may be required to achieve the desired system reliability.

Assuming a series connection of 6 to 8 ICs in the transmit electronics (each rated at 25 FITs), λ_{TE} is typically 200 FITs. The receive electronics, with 10 to 12 ICs, similarly rates a failure (λ_{RE}) of 300 FITs. The transmit and receive optics failures (λ_{TO} and λ_{RO}), each comprising at least 8 to 10 optical elements rated at 25 FITs, are 250 FITs each. Thus $(\lambda_{TE} + \lambda_{RE} + \lambda_{TO} + \lambda_{RO}) = 1{,}000$ FITs.

Because operational stress is much lower in the photodetectors than in the high-power lasers, λ_{PD} is typically 100 FITs for the diode laser ISLs, and this value will be used in analyzing systems that employ such photodetectors. The ISL system reliability is then

$$R_{ISL}(t) = \exp\{-[(\lambda_{LT} + \lambda_{PD}) + 1{,}000] \cdot t\} \qquad (3)$$

TABLE 2. RELIABILITY OF RECOMMENDED COMPONENTS FOR OPTICAL ISLS

COMPONENTS	DEVICE TYPE	PERFORMANCE
Laser	Sealed-off CO_2 laser, RF-excited waveguide design	7,000 hr, tested ~100,000 FITs
	GaAlAs diode laser array-pumped Nd:YAG laser	10,000 hr, planned 100,000 FITs
	GaAlAs single-diode laser, 50-mW CW output power	400,000 hr (est.) <2,500 FITs
	InGaAsP single-diode laser, 50-mW CW output power	400,000 hr (est.) <2,500 FITs
Photodetectors	Cooled HgCdTe	<1,000 FITs
	Ge or InGaAs APD	~100 FITs
	Si APD	<100 FITs
	Si PIN photodiode	<10 FITs
High-Speed Electronics	Si FETs	0.1–10 FITs, typically
	Si ICs	10–100 FITs, typically
Optics	Optical filters/polarizers/ WDMs/lenses, etc.	Very high reliability
Switch for Redundant Design	Fiber optic switch (1 × 4), fiber-on-fiber loose-tube splice	Undegraded operation in >1 million switchings
	Electromechanical switch (1 × 2), rigid-reed type	Undegraded operation in >10,000 switchings

The redundancy requirement, as calculated here, assumes a system reliability of 0.9 and employs a switched redundancy of the laser transmitters. The nonredundant optical ISL system requires a failure rate of 10,000 FITs or lower for the laser source. Since state-of-the-art lasers are less reliable than other components, this choice is logical, and a redundant design for the laser sources must be incorporated.

Redundancy is generally provided by either a parallel or standby configuration. In the parallel configuration, all Q units operate simultaneously. An operable state is any state other than when all units have failed. To conserve on-board power consumption, standby redundancy is preferred. In the standby

configuration, only one component is on-line at a time. When that component fails, the standby component, which is connected through a switch, takes its place. This process continues until all $Q - 1$ units are exhausted. The following assumptions may be made for a standby redundant system:

- The system fails when all Q units have failed.
- The failure probability of each unit is independent of the other $Q - 1$ units.
- The equipment can only fail in the on-line position with a conditional probability of $\lambda_{LT}\, dt$, where λ_{LT} is the failure rate of the laser transitter.
- The switch, if imperfect (less than 100 percent reliable) is characterized by a failure rate of λ_{SW}.

The reliability of a Q-unit system ($Q - 1$ standby redundant units) with an imperfect switch that cannot fail until operated is expressed as [9]

$$R_{LT}^{stdby}(t) = \sum_{i=0}^{Q-1} \{[(\lambda_{LT} \cdot t)^i / i!] \cdot \exp[-(\lambda_{LT} + i \cdot \lambda_{SW}) \cdot t]\} \quad . \qquad (4)$$

The reliability of a standby redundant system with a perfect switch is always greater than that of a parallel redundant system. Under the condition of imperfect switching, there is an optimum value of $(\lambda_{SW}/\lambda_{LT})$ below which the standby configuration is preferable to the parallel configuration. In general, for $(\lambda_{LT} \cdot t) > 0.1$, λ_{SW} must be very small. Otherwise, the improvement in reliability may be offset by switch failures. In optical ISLs with 10-year lifetimes and typical laser failures, $\lambda_{SW} \leq 100$ FITs is acceptable for the standby redundant design. The fiber optic or similar switching device has an adequate reliability, which makes the standby redundant configuration very attractive.

For the 100-mW CW output power diode lasers recommended for use in direct-detection optical links, useful reliability data are almost nonexistent, and good statistics for FITs cannot be expected at this stage of development. A model of expected lifetime degradation with increasing optical power was used to estimate reliability at high power levels. For further details, see References 4 through 7.

Table 3 lists the required redundancy for the six optical ISL systems designed for a 10-year lifetime. A trend toward increased integration (preferably monolithic) and a dedicated manufacturing facility will be the key to the success of long-term optical ISLs.

TABLE 3. REDUNDANCY REQUIREMENT OF THE SIX CANDIDATE OPTICAL ISL SYSTEMS

System Number	Description: System	Description: Wavelength (μm)	Subsystem Failure Rate (FITs): Laser	Subsystem Failure Rate (FITs): Detector/LO	Subsystem Failure Rate (FITs): Electronics/Optics	System Reliability per Year: 1 Unit, 0 Redundant	System Reliability per Year: 2 Units, 1 Redundant	System Reliability per Year: 3 Units, 2 Redundant	System Reliability per Year: 4 Units, 3 Redundant
1	CO_2 Laser Heterodyne Detection	9/10	100,000	~100,000[a]	1,000	0.172	0.603	0.877	0.967
2	Nd:YAG Laser Direct Detection	0.532	100,000	100	1,000	0.412	0.778	0.939	—
3	InGaAsP Diode Laser/Nd:YAG Amplifier, Direct Detection	1.064	100,000	100	1,000	0.412	0.778	0.939	—
4[b]	GaAlAs Single-Diode Laser, Direct Detection	0.81; 0.87	15,000	100	1,000	0.868	0.991	—	—
5[c]	GaAlAs Diode Laser/WDM, Direct Detection	0.78–0.91	45,000	100	3,000	0.656	0.932	—	—
6[d]	GaAlAs Diode Laser/Injection-Locked, Heterodyne Detection	0.81; 0.87	2,500	~2,500[a]	3,000	0.933	—	—	—

[a] Penalty due to LO laser.
[b] Assumes laser power-combining of two 100-mW diode lasers.
[c] Laser transmitter in each channel rated same as in system 4.
[d] Assumes single-frequency operation. In practice, system-related laser failure may be an order of magnitude higher and require a redundant design.

Conclusions

Reliability issues in an optical ISL system have been discussed, and six candidate optical technologies have been assessed. A brief review of state-of-the-art capabilities formed the database used in determining the redundancy requirements of components and subsystems for each candidate ISL.

Several significant trends were noted. Because life-test data for high-power light sources are very limited, reliability statistics are poor for lasers, which are more susceptible to failure than other components used in optical ISLs. Carbon dioxide lasers have adequate optical power output; however, their lifetime is very short. Semiconductor lasers, on the other hand, have a reasonably long lifetime but a much lower power output capability, which requires power-combining of multiple-diode lasers in the optical transmitter package. Heat dissipation, alignment, and packaging considerations then become important.

Except for the system using diode lasers with heterodyne technology, a redundant design of the optical transmitter is required. For GaAlAs/direct-detection ISLs with or without WDM, a minimum of two units (*i.e.*, one redundant laser transmitter) are needed to meet the specified system reliability. High-stability, single-frequency operation is essential in diode laser heterodyne ISLs. Because systems-related dynamic laser failures may limit performance well before static failure occurs, a redundant design is required even for the heterodyne system.

Acknowledgments

The author wishes to acknowledge valuable discussions on optical ISLs with COMSAT colleagues K. Greene (presently with the Analytical Sciences Corporation, Virginia) and G. Koepf and R. Marshalek (presently with Ball Aerospace Systems Division, Colorado). Thanks are also due to K. Mizuishi, Hitachi Central Research Laboratories, Japan; M. Ettenberg, RCA David Sarnoff Research Center, U.S.; and G. Lengyel, Siemens A. G., West Germany, for helpful technical information on lifetest data/methodology and complexities of state-of-the-art, high-output-power diode lasers.

References

[1] See, for example, "Optical Technologies for Communication Satellite Applications," K. Bhasin, ed., *Proc. SPIE*, Vol. 616, January 1986, and Vol. 756, January 1987; also, "Optical Systems for Space Applications," H. Lutz and G. Otter, eds., *Proc. SPIE*, Vol. 810, September 1987, and "Free-Space Laser Communication Technologies," G. A. Koepf and D. L. Begley, eds., *Proc. SPIE*, Vol. 885, January 1988.

[2] R. Nelson, "Experimental Verification of the Pointing Distribution of an Intersatellite Optical Link," Free-Space Laser Communication Technologies, G. A. Koepf and D. L. Begley, eds., *Proc. SPIE*, Vol. 885, January 1988.

[3] R. G. Marshalek, "Comparison of Optical Technologies for Intersatellite Link Payloads: Part I. Mass, Prime Power, and Volume Estimates for Optical Intersatellite Link Payloads," *COMSAT Technical Review*, Vol. 18, No. 2, Fall 1988, pp. 191–214 (this issue).

[4] COMSAT Laboratories, "The Study of Optical Intersatellite Links," Final Report to INTELSAT under Contract INTEL-384, August 1985. COMSAT Data Catalog No. 85DC132.

[5] COMSAT Laboratories, "TDAS Laser Intersatellite Communications Study," Final Report to Ball Aerospace Systems Division under NASA/Goddard Space Flight Center Contract NAS5-29128, July 1986. (Incorporated in NASA Contract Report No. CR-183419, "Tracking and Data Acquisition System Laser Intersatellite Communications Study," Final Report by Ball Aerospace Systems Division, Boulder, Colorado, August 1986.)

[6] COMSAT Laboratories, "Optical Intersatellite Link Technology," Final Report to COMSAT Intelsat Satellite Services Engineering under Project Support Authorization STA-5, December 1986. COMSAT Data Catalog No. 86DC133.

[7] See, for example, "High Data Rate Atmospheric and Space Communications," R. Hauptman, ed., *Proc. SPIE*, Vol. 996, September 1988.

[8] D. K. Paul, "High-Power Semiconductor Diode Lasers—Reliability Data and Lifetest Methodology," Fiber Optics Reliability: Benign and Adverse Environments, D. K. Paul, ed., *Proc. SPIE*, Vol. 842, August 1987, pp. 86–94.

[9] See, for example, "Reliability Considerations in Fiber Optic Applications," D. K. Paul, ed., *Proc. SPIE*, Vol. 717, September 1986.

[10] I. Bazovsky, *Reliability Theory and Practice*, Englewood Cliffs, New Jersey: Prentice Hall, 1961.

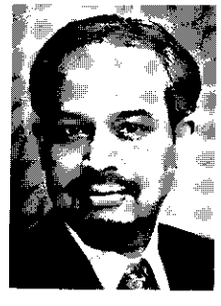

Dilip K. Paul received a B.S. with Honors in electronics and telecommunications engineering from Jadavpur University, India, in 1961; an M.S. in UHF and microwave engineering from the Indian Institute of Science (I.I.Sc.) in 1962; and a Ph.D. in electrical engineering from the University of Rhode Island in 1974. He joined COMSAT Laboratories in 1981, and is presently Manager of the Optical Communications Department where his R&D work includes integrated optics in ferroelectric and GaAs-based materials, and undersea, terrestrial, and space optical links. Prior to joining COMSAT, he held senior research/teaching faculty positions at the Indian Institute of Technology, Kanpur; I.I.Sc.; the University of Maryland; Harvard University; and

IBM's Thomas J. Watson Research Center. His research spans antenna beam shaping, optical waveguides, and thin-film materials and devices.

Dr. Paul holds two patents on display devices, and has authored numerous research publications. He was awarded the Institute of Electronics and Telecommunications Engineers (IETE) prize in 1967 for his work on optical waveguides, and is cited in Who's Who in Technology Today *and in Marquis International* Who's Who in Optical Sciences and Engineering *for contributions in the areas of thin-film technology and fiber optics. He is a Fellow of the IETE, and a member of the Society of Photo-Optical Instrumentation Engineers (SPIE), the Optical Society of America, and Sigma Xi. He is chairman of the SPIE communications working group for Fiber-Optic Components, Communications, and Sensors (FOCCAS).*

Index: coding, error control, communication satellites, earth stations

Reduced-complexity decoding of convolutional codes

F. HEMMATI

(Manuscript received February 22, 1988)

Abstract

A suboptimum method for soft-decision decoding of convolutional codes is introduced. The proposed method processes a few paths through the trellis diagram of the code, does not propagate error events, and is erasure-free. For long codes, the computations and memory requirements of the proposed algorithm are significantly less complex than those of the Viterbi algorithm. The performance of the reduced-complexity decoding algorithm in terms of bit error rate and probability of event errors is examined for quick-look-in codes of memory order 6 and 13.

Introduction

At the present time, some type of forward error correction (FEC) coding is being used in almost every commercial satellite communications system to improve the average energy-per-bit to noise-power-density ratio (E_b/N_o). Convolutional coding, with soft-decision Viterbi algorithm decoding, is an extremely powerful FEC technique. In particular, the memory order $m = 6$, 64-state convolutional code of rate 1/2 [1], or its punctured versions [2], has been considered for both fixed and mobile satellite services. At a bit error rate (BER) of 10^{-6}, the rate 1/2 code achieves about 5.5 dB of coding gain compared to uncoded binary phase-shift keying (BPSK) or quadrature PSK (QPSK) modulation over an additive white Gaussian noise (AWGN) channel.

The size and cost of earth stations can be significantly reduced by lowering the required E_b/N_o. Information theory promises the possibility of achieving this, at the cost of an unspecified number of computations per decoded information bit. For example, an additional 3 dB of coding gain over that provided by the 64-state code can be achieved by using an $m = 16$ code. If the Viterbi algorithm is used, the computational complexity and required memory for this code are more than 1,000 times larger than for the 64-state code. This prohibitive computational effort has ruled out consideration of the Viterbi algorithm for decoding of long convolutional codes.

Sequential decoding algorithms process a few paths, or states, in the tree diagram of the code for the majority of the time, and the number of computations per decoded bit is an unbounded random variable depending on m if the code rate is higher than the computational cutoff rate, R_{comp}. Problems inherent in sequential decoding algorithms include buffer overflow, which results in erasures and loss of the information sequence, and the excessive amount of required buffer memory.

Since the introduction of the Viterbi algorithm in 1967 [3], many attempts have been made to reduce its computational complexity while maintaining near-optimal BER performance. Earlier efforts focused on reducing the computational load by reducing the number of trellis states (or survivor paths) according to some specific rule [4]. The main drawback of these schemes is error propagation. That is, once the correct path is eliminated from the set of survivors, the decoder is unable to resynchronize itself to the correct state, even if the channel remains noiseless. This is particularly true for most of the good codes operating at high signal-to-noise ratio (S/N). At lower S/N, channel noise might accidentally force the decoder to the correct state.

Recently, new methods have been reported [5] for detecting the synchronization status of the decoder. If lack of synchronization is detected repeatedly, the decoder is reinitialized to an estimate of the correct state, which can be obtained from the received channel symbols.

Another decoding method with reduced complexity is syndrome decoding, which estimates the error sequence from the syndrome polynomial [6]–[8].

The reduced-complexity decoding (RCD) algorithm proposed in this paper is an erasure-free decoding method. For long codes, its computational complexity and memory requirements are significantly less than those of the Viterbi algorithm, whereas its asymptotic BER performance is equivalent to the BER performance of a maximum-likelihood decoder (MLD).

The RCD algorithm belongs to the class of suboptimum decoding methods proposed and analyzed in References 5, and 9 through 11, in which a small subset of paths is retained at each decoding cycle. However, rather than decoding the random sequence of equally likely received channel symbols,

the RCD algorithm computes and processes a syndrome sequence which is an encoded but noisy version of the channel noise [6]. The decoder output is an estimate of the channel errors, which is then used to correct errors in the received information sequence. The syndrome sequence is the all-zero sequence when the channel is noiseless; otherwise, it passes through a set of nonzero states. At the E_b/N_o values of interest, the generated syndrome is a biased (unequally likely) sequence of random symbols, and its distribution depends only on channel noise. This property can be used to realize a reduced-complexity decoder for convolutional codes, which, unlike a Viterbi algorithm, processes and retains a subset of the most likely paths in the trellis diagram of the code. Moreover, the RCD algorithm lends itself to a simple solution that avoids error propagation.

The structure and function of the syndrome former are described, followed by an explanation of the RCD algorithm and the error propagation problem. A method is then presented for finding path size, or the minimum number of paths that must be retained at each decoding cycle, so that, within the error correcting capability of the code, the correct path always remains in the set of retained paths. The usefulness and validity of the proposed decoding procedure and its analysis are confirmed by computer simulations.

Syndrome former

Figure 1 is a block diagram of an FEC coding system using the RCD algorithm. The receive end consists of a syndrome former and a reduced-complexity decoder. The structure and function of the syndrome former are presented in this section; details of the RCD algorithm are considered in the next section.

For simplicity of presentation, a quick-look-in (QLI) convolutional code of rate 1/2 [1], [12] and hard decision is considered. The advantages of using a QLI code for the proposed decoding method are given below. The presented decoding approach is readily applicable to soft-detected channel symbols, which yield about 2-dB extra coding gain compared to the hard-decision case. Figure 2 shows the configuration of the proposed coding system for soft-decision decoding, and is obtained from Figure 1 by replacing the modulo-2 adders in the syndrome former with real multipliers. Note that the output of the encoders in Figure 2 consists of $+1$ and -1 symbols, while the output of the encoders in Figure 1 consists of binary symbols 0 and 1. In Figure 2, E_1 and E_2 are real numbers representing noise in a Gaussian channel, and received waveforms R_1 and R_2 can be quantized to any desired precision.

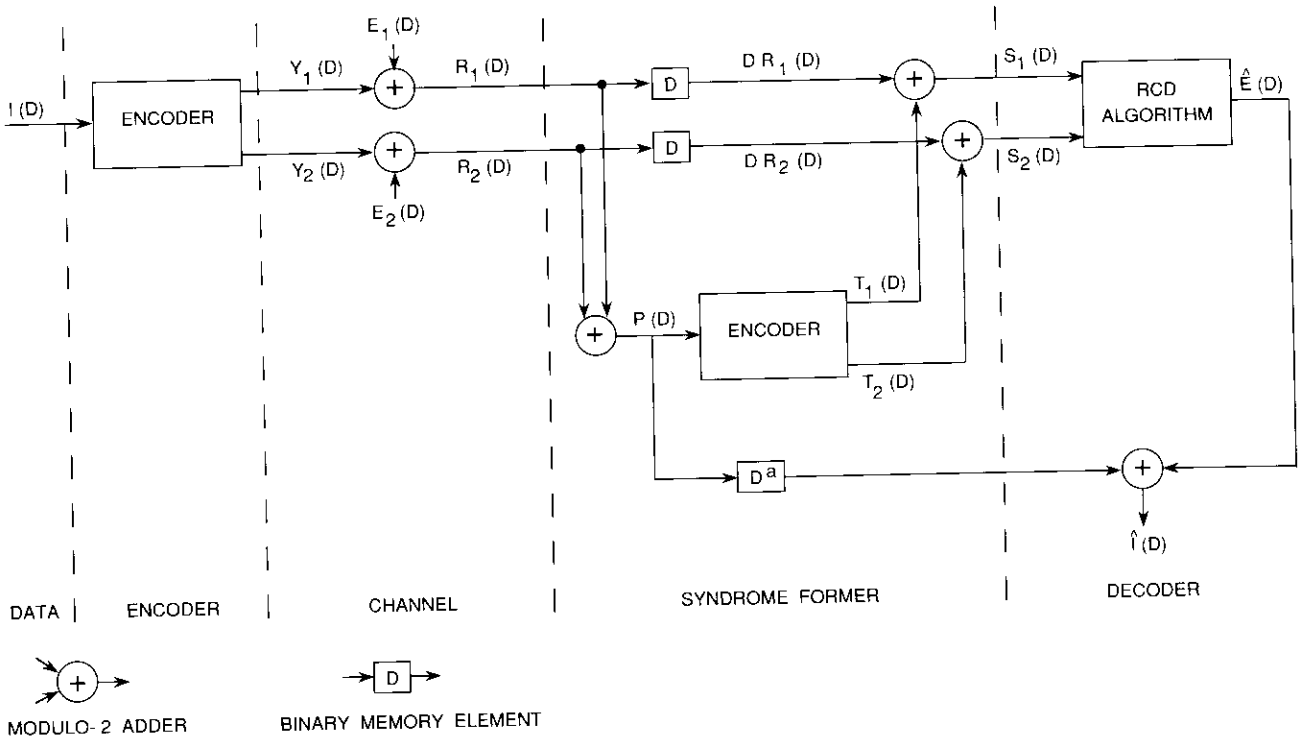

Figure 1. *Hard-Decision FEC Coding System Using the RCD Algorithmn*

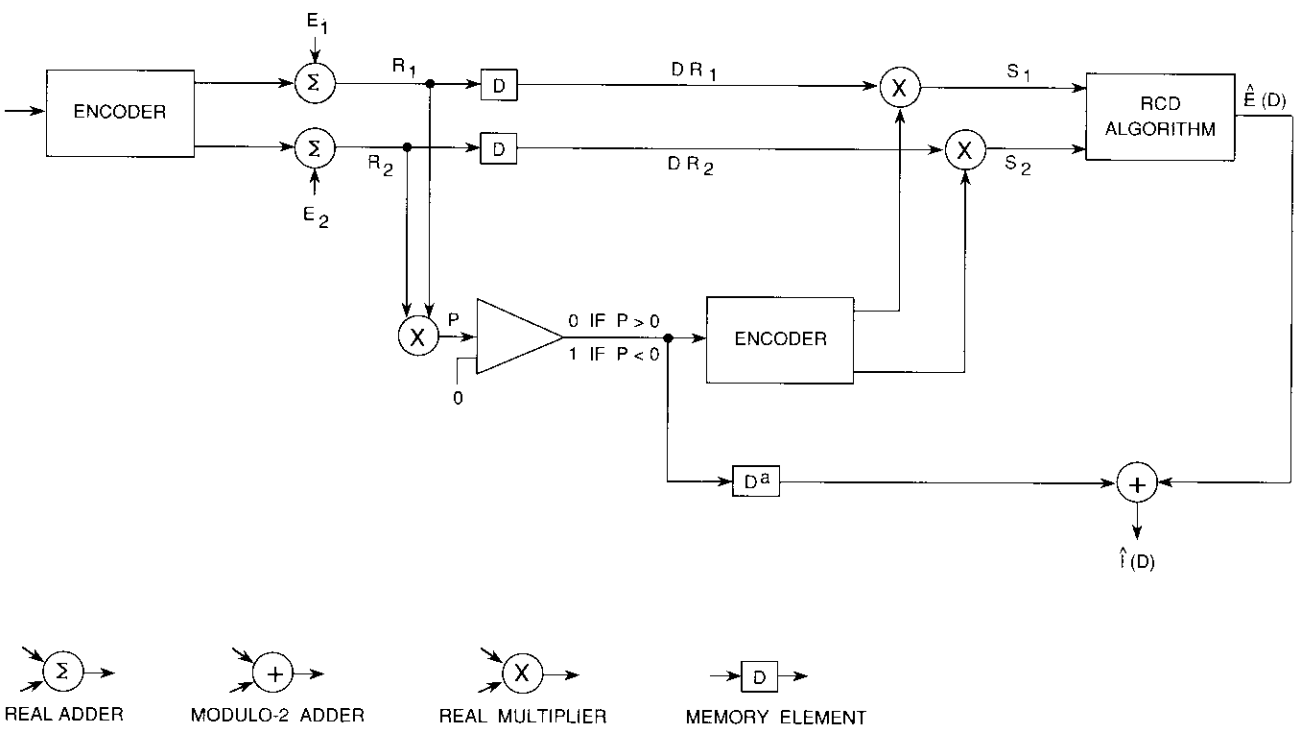

Figure 2. *Soft-Decision FEC Coding System Using the RCD Algorithm*

For the hard-decision case, let $I(D)$ be the polynomial representation of the information sequence encoded by a QLI convolutional code of rate 1/2 with generator polynomials $G_1(D)$ and $G_2(D)$. The transmitted sequence is generated by multiplexing

$$\begin{aligned} Y_1(D) &= I(D)G_1(D) \\ Y_2(D) &= I(D)G_2(D) \end{aligned} \tag{1}$$

where, for QLI codes, the encoder generator polynomials are related by

$$G_1(D) + G_2(D) = \mathrm{D} \quad . \tag{2}$$

The received sequence, after serial-to-parallel operation, is

$$\begin{aligned} R_1(D) &= Y_1(D) + E_1(D) \\ R_2(D) &= Y_2(D) + E_2(D) \end{aligned} \tag{3}$$

where $E_1(D)$ and $E_2(D)$ are D-transform representations of the channel noise sequence (*i.e.*, polynominals with coefficients 0 or 1), and + denotes a modulo-2 addition.

The main function of the RCD algorithm is to obtain an estimate $\hat{E}(D)$ of $E(D) = E_1(D) + E_2(D)$. To obtain $\hat{E}(D)$, let the sequence $P(D)$ be the sum of $R_1(D)$ and $R_2(D)$,

$$P(D) = R_1(D) + R_2(D) = DI(D) + E_1(D) + E_2(D) \tag{4}$$

and

$$\begin{aligned} T_1(D) &= P(D)G_1(D) = DI(D)G_1(D) + E(D)G_1(D) \\ T_2(D) &= P(D)G_2(D) = DI(D)G_2(D) + E(D)G_2(D) \quad . \end{aligned} \tag{5}$$

Then,

$$\begin{aligned} S_1(D) &= DR_1(D) + T_1(D) = E(D)G_1(D) + DE_1(D) \\ S_2(D) &= DR_2(D) + T_2(D) = E(D)G_2(D) + DE_2(D) \quad . \end{aligned} \tag{6}$$

From equation (4) it can be seen that the QLI property shown in equation (2) permits ready recovery of the information sequence $I(D)$ in the receiver, subject to the delay D and channel noise $E_1(D)$ and $E_2(D)$.

Note the analogy between equations (3) and (6), where $I(D)$ is analogous to $E(D)$. $I(D)$ is a random sequence of equally likely data symbols, but $E(D)$ is a random sequence of biased (unequally likely and more 0's than 1's) symbols, and its distribution depends only on channel noise. Using equations (3), $I(D)$ can be estimated by feeding $R_1(D)$ and $R_2(D)$ into a Viterbi decoder. By analogy, using equations (6), $E(D)$ can be estimated by feeding $S_1(D)$ and $S_2(D)$ into a Viterbi decoder. However, because of the properties of $E(D)$ discussed later, the number of states processed by the Viterbi algorithm can be reduced.

Lastly, the information sequence $I(D)$ is estimated by forming

$$P(D) + \hat{E}(D) = DI(D) + E(D) + \hat{E}(D) = D\hat{I}(D) \quad . \tag{7}$$

An advantage of using a QLI code in conjunction with a decoder that finds $\hat{E}(D)$ is that this approach results in a high-likelihood distribution for decoder states that have a low Hamming weight [13]. This follows from the fact that $E(D)$ passes through a state with Hamming weight of i if exactly i nonzero coefficients occur in a block of m consecutive terms of $E(D)$. Let ϵ be the probability that a coefficient of $E(D)$ is nonzero. Then, on a trellis path corresponding to $E(D)$, the likelihood for states of Hamming weight i and less is

$$L_i = \sum_{k=0}^{i} \binom{m}{k} (1 - \epsilon)^{m-i} \epsilon^i \quad .$$

For a QLI code, $E(D) = E_1(D) + E_2(D)$, and hence $\epsilon = 2p(1 - p)$, where p is the crossover probability for a binary symmetric channel.

Figure 3 shows the state-likelihood distribution, L_i, as a function of E_b/N_o for a QLI code of memory order 6. At an E_b/N_o of 4.5 dB ($p = 0.045$), $E(D)$ passes, more than 92 percent of the time, through the seven states of Hamming weight 1 or less. In other words, $E(D)$ passes through $7/64 = 11$ percent of the states more than 92 percent of the time. The remaining 57 states are expected to appear less than 8 percent of the time.

Figure 3 indicates that the likelihood of low-weight states approaches 1 as E_b/N_o increases. States with a large Hamming weight occur rarely. At an E_b/N_o of 4.5 dB, the probability of the all-one state is $(0.045)^6 = 8.3 \times 10^{-9}$, which is less than 2×10^{-6}, the estimated BER of the considered code if decoded by an MLD operating at this E_b/N_o. Therefore, it is not necessary to process all 2^m states of the code at every trellis step, as in the case of the Viterbi algorithm.

For a considered state-likelihood, $E(D)$ passes through a smaller fraction of total states as m increases. This can readily be shown by an example. Let $m = 13$ and $p = 0.045$. Then $L_2 \simeq 0.905$. That is, $E(D)$ is expected to pass more than 90 percent of the time through the $1 + \binom{13}{1} + \binom{13}{2} = 92$ states having Hamming weight of 2 or less. Hence, only $92/8192 \sim 1.1$ percent of the total number of states occurs more than 90 percent of the time. This must be compared to the $m = 6$ code for which 11 percent of the total number of states appears 92 percent of the time. Therefore, state-likelihood becomes more concentrated as m increases.

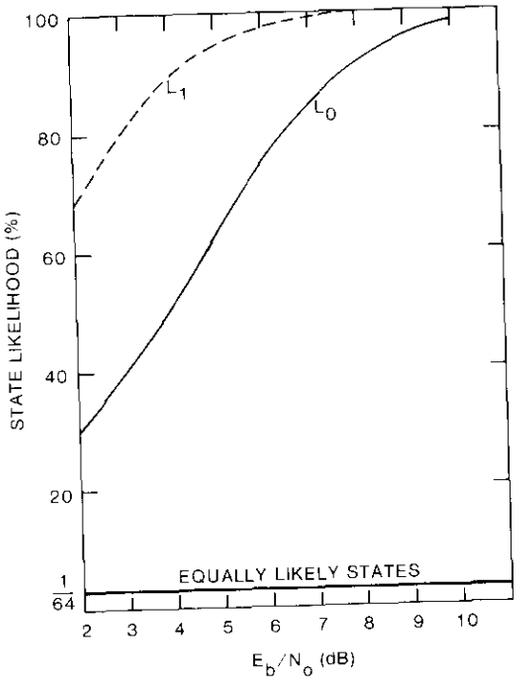

Figure 3. *State-Likelihood Distribution for a 64-State QLI code*

The high state-likelihood concentration obtainable for QLI codes allows a reduction in the complexity of the decoder. Long optimal codes do not enjoy the QLI property and do not generate a remarkable state-likelihood concentration [13]. Therefore, the RCD algorithm is unsuitable for decoding optimal codes.

The RCD algorithm

In each decoding cycle, the reduced-complexity decoder generates an estimate for one information bit. A decoding cycle consists of four main steps: extend, delete, sort, and traceback. Assume that at decoding cycle t, N paths, $N < 2^m$, terminating in N different encoder states have survived. The set of survived states $\{\underline{S}_i\}$ always includes the all-zero state, $\underline{S}_0$. Also, let $\{\Gamma_i\}$ denote both the set of survived paths and the set of corresponding path metrics.

A path extension consists of computing the new path metrics $\{\Gamma'_i\}$ and finding the set of next states $\{\underline{S}'_i\}$. $2N$ paths are generated at this step. The path with largest metric is deleted in the second decoding step if two paths

terminate in the same state. Ties are resolved randomly. The number of survivors at this step is $N' < 2N$. Next, the new path metrics $\{\Gamma'_i\}$ are sorted, and N survivor paths with the smallest path metrics are selected from the N' adversaries. The path terminating in $\underline{S}_0$ is always retained, even if its metric (Γ'_0) is out of the range of metrics for the set of N paths with the smallest metrics. This point is detailed in the next section, and is the only difference between the m-algorithm [9] and the RCD algorithm. Finally, in the traceback step, an estimate for one information bit is generated and the decoder goes back to the first step.

The most important parameter determining the complexity of the RCD algorithm is path size, N. For a given code, N is selected so that the probability, $P_{E,RCD}$, of event error for the RCD algorithm is approximately equal to the probability, $P_{E,MLD}$, of event error for an MLD.

$P_{E,RCD}$ approaches 0.5 if the correct path is deleted from the set of surviving paths. A later section details a procedure that finds the path size N so that, within the error-correcting capability of the code, the correct path is guaranteed to remain in the set of retained paths.

A path extension consists of two branch metric computations and two additions. Branch metrics are computed by finding the distance between the received BPSK channel symbols and the corresponding code symbols. The set of $2N$ updated path metrics is computed by adding the old path metrics to the corresponding branch metrics.

The process of deleting merged paths could become very time-consuming. The computational efforts required for this step and for the sorting step are roughly equivalent.

The computational complexity of sorting (in the third step) is a linear function of N [14]. However, "sorting" is not an adequate term for the function performed. It is not necessary to sort the N' numbers in an ordered form; any efficient algorithm that selects N smallest out of N' integers, in an ordered or nonordered form, is acceptable. Parallel algorithms [15],[16] are preferred for high-speed applications.

The traceback unit consists of a bank of shift registers of finite length, T, to store the history of surviving paths. These shift registers are usually about five to six times longer than the memory order of the code. An information bit can be decoded by tracing T steps back through the path having the smallest metric value, or by taking a majority vote among the oldest bits of the N paths. The overall computational complexity and memory requirements of the RCD algorithm depend on the specific algorithms used for path deletion and path selection, and on the system architecture. References 17 and 18 consider details for very large-scale integration (VLSI) implementation of the m-algorithm which can be adapted for implementation of the RCD algorithm.

Error propagation

A major problem of RCD-type algorithms is the error propagation property, as mentioned previously. However, the RCD algorithm presented in the previous section is a self-resynchronizing decoder, and no extra circuitry is needed to examine its synchronization status. [The decoder is in synchronization if both the syndrome sequences, $S_1(D)$ and $S_2(D)$, are zero for more than m consecutive bits.] In the range of moderate-to-high values of E_b/N_o, binary errors are rare, and the syndrome sequence is zero with a high probability. No infinite error propagation can occur because the RCD algorithm retains the path terminating in $\underline{S}_0$ at every decoding cycle. After an event error occurs, the metric for the path terminating in $\underline{S}_0$ begins to decrease, and the decoder resynchronizes itself if the channel remains noiseless for a sufficient number of decoding cycles. This is the most important advantage of the proposed decoding approach. Short codes resynchronize much faster than long codes because short noiseless periods are more likely to occur than long noiseless periods.

A procedure to compute path size

The probability of event error for the RCD algorithm, $P_{E,RCD}$, satisfies the inequality

$$P_{E,RCD} \leq P_{E,MLD} + \Pr(\text{correct path is not in } \{\Gamma_i\}) \tag{8}$$

where $P_{E,MLD}$ is the probability of event errors for an MLD. This term is an exponential function of the free distance of the code, d_f. A hard-decision MLD can correct channel errors up to a Hamming weight of $\lfloor d_f/2 \rfloor$, which occurred in about one constraint length of the code. The second term on the right-hand side of the equation is the probability that the correct path is eliminated from the set of surviving paths $\{\Gamma_i\}$, and is a function of the path size (N) and distance structure of the selected code.

For a specific code, the following search procedure finds the minimum number of paths that must be retained so that every possible error pattern of Hamming weight $\lfloor d_f/2 \rfloor$ or less can be corrected. The following notation is used:

N_i : An integer to initalize N.

$\underline{R}$: A binary sequence of length $2L$. The decimal equivalent of $\underline{R}$ is denoted by R. $L > m + 1$.

RCD* : A modified version of the RCD algorithm presented above, with the traceback step omitted. The decoder is not forced to retain the path terminating in the all-zero state $\underline{S}_0$; however, it examines the set of surviving paths $\{\Gamma_i\}$ at every decoding cycle for the existence of $\underline{S}_0$ in $\{\Gamma_i\}$.

The algorithm can now be presented as follows:

Step 0: Initialize $N = N_i$, $R = 0$.

Step 1: $R = R + 1$. If $R > 2^{2L}$, go to step 3. Otherwise, if $W_H(\underline{R}) > \lfloor d_f/2 \rfloor$, go to step 1. Otherwise,

Step 2: Decode $\underline{R}$ using RCD*. If $\underline{S}_0 \in \{\Gamma_i\}$ at every decoding cycle, go to step 1. Otherwise, $N = N + 1$ and go to step 2.

Step 3: $N = N + 1$. Stop.

In step 3, N is increased by 1, as the RCD algorithm keeps the path terminating in $\underline{S}_0$ at every decoding cycle.

If this procedure is used to find N for a code of moderate memory order, the number of computations is prohibitively large. Several simplifications are possible. For example, as mentioned above, the probability of more than six *consecutive* channel errors occurring in the range of E_b/N_o values of interest is less than the desired or achievable BER. Hence, it is not necessary to examine error patterns that have more than six consecutive 1's. Also, equivalent classes of error patterns can be identified, so that only a representative error pattern needs to be examined for each equivalent class [19].

Computer simulation results

Extensive computer simulations for the soft-decision case having the configuration depicted in Figure 2 were carried out to evaluate the BER and the probability of event error (P_E) of the RCD algorithm over an AWGN channel. The performance of two codes was examined. Code 1 has $m = 6$, 64 states, $d_f = 9$, and encoder subgenerators $(G_1, G_2) = (454, 654)$, in octal representation. Code 2 has $m = 13$, 8192 states, $d_f = 14$, and encoder subgenerators $(G_1, G_2) = (46716, 66716)$. A path size of $N = 20$ was obtained for code 1 by performing a nonexhaustive run of the search algorithm presented above. Similarly, $N = 94$ was obtained for code 2. Codes 1 and 2 are optimum in the sense of having maximum free distance in the

class of QLI codes. In general, the free distance of QLI codes is less than that for optimum convolutional codes of rate 1/2 [1]. Consequently, the QLI codes do not perform as well.

Figure 4 shows the performance curves for code 1 over an AWGN channel with infinite levels of soft quantization, $q = \infty$. BER curves are depicted for decoders with $N = 8$, 16, 20, and 64. The BER performance curve for the $N = 20$ decoder is within 0.1 dB of the BER performance for the 64-state MLD. P_E performance curves for $N = 20$ and 64 are also shown. Close inspection of the BER and P_E curves for code 1 reveals that the RCD algorithm is almost free of error propagation because the degradations in BER and P_E are equivalent in the range of E_b/N_o values of interest.

Figure 5 compares the BER and P_E for code 2 with the optimum 64-state convolutional code of rate 1/2 over an AWGN channel having eight levels of soft decision, $q = 8$. Regarding P_b, at a BER of 10^{-4}, code 2 gives about 0.4-dB additional coding gain over the 64-state code. The trend of the

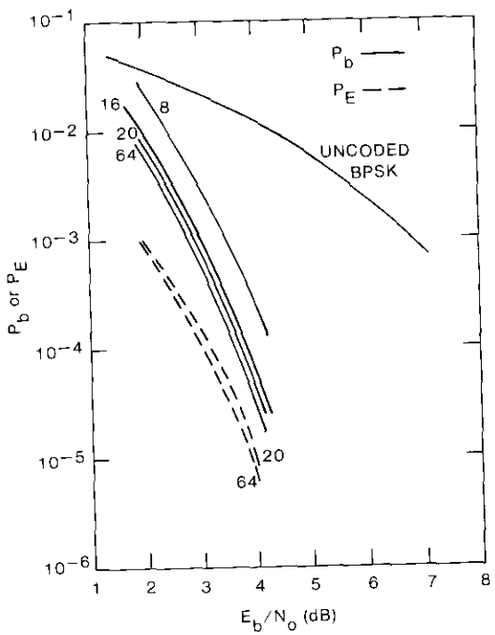

Figure 4. *Performance Curves for Code 1 With* q = ∞ *Over an AWGN Channel*

depicted BER curves indicates that an extra coding gain of more than 1 dB is achievable at a BER of 10^{-6}.

More important is the extra coding gain achievable for applications where P_E is the criterion for performance evaluation (*e.g.*, packetized data transmission). Figure 5 shows that, at a P_E of 10^{-4}, more than 0.7 dB of extra coding gain is achievable. A power advantage of more than 1 dB is expected at a P_E of 10^{-6}. Close inspection of the figure reveals that, while the curves for BER cross over at an E_b/N_o of about 2.5 dB, regarding P_E the power advantage for the $N = 94$ decoder remains positive even in the range of low E_b/N_o.

This confirms the earlier analysis. When the channel is noisy, long codes require more time than short codes to resynchronize to the correct state. As an example, computer simulation of code 2 shows that, at an E_b/N_o of 1.5 dB, the average number of bit errors per event error is about 45 bits, whereas this reduces to about 20 bits at an E_b/N_o of 3 dB.

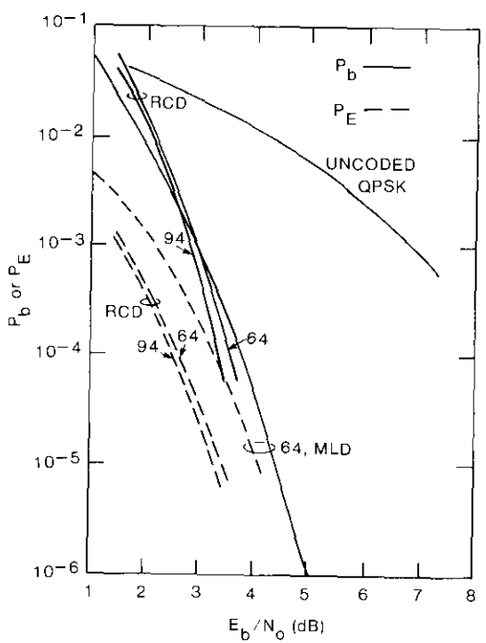

Figure 5. *Performance Curves for Code 2 and the Optimum 64-State Code of Rate 1/2 With* q = 8 *Over an AWGN Channel*

Figure 5 also shows performance curves for the RCD algorithm with a path size of 64. Although in the range of low E_b/N_o values the results are in agreement for decoders with $N = 64$ and 94, the performance of the $N = 64$ decoder is degraded more in the range of $E_b/N_o > 3$ dB. This is due to those error patterns that can be correctly decoded by the $N = 94$ decoder while remaining unresolvable by the $N = 64$ decoder.

Conclusions

The RCD algorithm presented in this paper is an efficient soft-decision technique for decoding convolutional codes. It also has the potential for application to signal-space coded modulation systems. The performance curves presented indicate that this suboptimum decoder can achieve a large coding gain with a computational complexity significantly lower than that required by the Viterbi algorithm.

References

[1] S. Lin and D. J. Costello, Jr., *Error Control Coding: Fundamentals and Applications*, Englewood Cliffs, New Jersey: Prentice-Hall, 1985.

[2] Y. Yasuda *et al.*, "High-Rate Punctured Convolutional Codes for Soft Decision Viterbi Decoding," *IEEE Transactions on Communications*, Vol. COM-32, No. 3, March 1984, pp. 315–319.

[3] A. J. Viterbi, "Error Bounds for Convolutional Codes and an Asymptotically Optimum Decoding Algorithm," *IEEE Transactions on Information Theory*, Vol. IT-13, No. 2, April 1967, pp. 260–269.

[4] F. Hemmati, "Convolutional Code Structure and the Performance of the Viterbi Algorithm," Ph.D. Dissertation, Illinois Institute of Technology, December 1977.

[5] C. F. Lin and J. B. Anderson, "M-Algorithm With Path Recovery for Convolutional Channel Codes," IEEE Global Telecommunications Conference, Houston, Texas, December 1986, *Digest*, pp. 5.5.1–5.5.5.

[6] J. P. M. Schalkwijk and A. J. Wink, "Syndrome Decoding of Binary Rate 1/2 Convolutional Codes," *IEEE Transactions on Communications*, Vol. COM-24, No. 9, September 1976, pp. 977–985.

[7] T. Truong and I. S. Reed, "Simplified Convolutional Codes," *NASA Technical Briefs*, Vol. 8, No. 4, July 1984.

[8] T. Truong and I. S. Reed, "Simplified Decoding of Convolutional Codes," *NASA Technical Briefs*, Vol. 10, No. 2, March 1986.

[9] J. B. Anderson, "A Stack Algorithm for Source Coding With a Fidelity Criterion," *IEEE Transactions on Information Theory*, Vol. IT-20, No. 2, March 1974, pp. 211–226.

[10] T. Aulin, "A New Trellis Decoding Algorithm: Analysis and Applications," Technical Report NR2, Chalmers University of Technology, Gothenburg, Sweden, December 1985.

[11] T. Hashimoto, "A List-Type Reduced-Constraint Generalization of the Viterbi Algorithm," *IEEE Transactions on Information Theory*, Vol. IT-33, No. 6, November 1987, pp. 866–876.

[12] J. L. Massey and D. J. Costello, Jr., "Nonsystematic Convolutional Codes for Sequential Decoding in Space Applications," *IEEE Transactions on Communications Technology*, Vol. COM-19, No. 10, October 1971, pp. 806–813.

[13] M. Tajima and H. Suzuki, "Viterbi Decoding Algorithm Using Likelihood Distribution," IEEE Global Telecommunications Conference, Houston, Texas, December 1986, *Digest*, pp. 5.6.1–5.6.6.

[14] D. E. Knuth, *The Art of Computer Programming, Vol. III: Sorting and Searching*, Reading, Massachusetts: Addison-Wesley, 1973.

[15] A. R. Siegel, "Mimimum Storage Sorting Networks," *IEEE Transactions on Computers*, Vol. C-34, No. 4, April 1985, pp. 355–361.

[16] J. Cooper and S. G. Akl, "Efficient Selection on a Binary Tree," *Information Processing Letters*, Vol. 23, No. 10, October 1986, pp. 123–126.

[17] S. Mohan and A. K. Sood, "A Multi-Processor Architecture for the (M, L)-Algorithm Suitable for VLSI Implementation," *IEEE Transactions on Communications*, Vol. COM-34, No. 12, December 1986, pp. 1218–1224.

[18] S. J. Simmons, "A Nonsorting VLSI Structure for Implementing the (M, L) Algorithm," *IEEE Journal on Special Areas in Communications*, Vol. SAC-6, No. 3, April 1988, pp. 538–546.

[19] C. F. Lin, "A Truncated Viterbi Algorithm Approach to Trellis Codes," Ph.D. Dissertation, Rensselaer Polytechnic Institute, Troy, New York, September 1986.

Farhad Hemmati received an M.S.E.E. and Ph.D. from the Illinois Institute of Technology in 1973 and 1977, respectively. Since joining COMSAT Laboratories in 1982, he has worked on coding techniques and various signal processing methods for satellite channels. He is currently a Staff Scientist in the Communications Research Department, where his primary interests are coding, spectrum, and multiple access.

Index: satellite antennas, digital systems, control data (computers)

Digital controller for high-speed multibeam antennas

T. HAMPSCH

(Manuscript received May 16, 1988)

Abstract

A digital controller that is used to drive high-speed beam-scanning and beam-hopping antenna arrays is described. In such arrays, the radiated beam direction is controlled electronically instead of mechanically, and the controller routes the appropriate switch-state data to each element in the array. A distributed controller architecture using low-power complementary metal-oxide semiconductor (CMOS) electronics was selected and optimized specifically for time-division multiple-access (TDMA) communications satellite applications. The use of local random-access memory to step through the semi-static TDMA switching cycle avoids the need for high-bandwidth data distribution. Details of the various units of this distributed architecture are presented, and current progress in breadboard development is discussed.

Introduction

An architecture has been developed to digitally control either a beam-scanning or beam-hopping antenna array. Both of these arrays are candidates for future highly flexible time-division multiple-access (TDMA) communications satellites, which require high-speed cyclic RF switching between multiple up- and down-link beams. The controller routes data to the various antenna elements in the array and provides the timing signals necessary to synchronize the RF switching for the entire array.

A beam-scanning antenna is a phased-array antenna in which the entire array of elements combine to form narrow pencil beams. The direction of

each beam is controlled by applying an appropriate phase shift at each element of the antenna. The various phase-shifted fields radiated by each antenna element add coherently to produce a narrow beam, and multiple beams can be formed by combining the outputs of multiple phase shifters at each element.

A beam-hopping antenna consists of an array of radiating elements feeding a reflector. In this system, a single element or a cluster of elements form one beam. The direction of each beam is determined by the location of the active antenna element(s) in the array. Multiple beams can be generated by enabling multiple elements, but in general only a small subset of the array elements are active at any one time. These beams are routed to the various radiating elements through a microwave switch matrix (MSM).

The control of both antenna systems is greatly simplified by digitally controlling the microwave components, phase shifters, and switches; that is, by entirely digital control. Although these two antennas have many differences on the system level, from the controller viewpoint they are nearly the same. Each system requires high-speed cyclic switching of RF components, and one phase shifter in the beam-scanning antenna is equivalent to one microwave switch in the beam-hopping antenna.

System requirements

The control architecture is strongly influenced by the satellite system performance specifications, as defined in a previous system study [1]. The specifications require that both the beam-scanning and beam-hopping antennas be implemented using this architecture. The scanning and hopping antennas can be operated together with one controller, or a hybrid scanning/hopping system can be implemented. Also, multiple simultaneous beams can be generated by each antenna. In principle, the number of simultaneous beams can be as large as 50; however in practice the number will be less due to RF power-divider and power-combiner losses, and amplifier backoff considerations. The array can contain a large number of radiating elements, up to several hundred.

The final and most important requirement is that the array will switch beams in a cyclic TDMA frame timing scheme. An INTELSAT VI TDMA timing frame is used as a baseline configuration, although the control architecture must be flexible enough to adapt to a different TDMA timing frame with only minor modifications. The INTELSAT VI timing requirements are a 2-ms TDMA frame period and a switching time resolution of 1 μs, with a switching transition time of 50 ns. The minimum dwell time in any state is 4 μs, and the maximum number of states in one frame is 64.

In addition to the above requirements, any electronics built for a geosynchronous satellite application must be small, lightweight, low-power, and radiation-hardened. Telemetry must be provided for verification of the controller configuration. Some form of redundancy or fault tolerance must also be included to bypass any single-point failure, and any on-board random-access memory (RAM) must have error detection and correction to recover from radiation-induced single-event upsets (SEUs).

Design description

Comparison of the beam-hopping and beam-scanning antennas reveals that the beam-scanning configuration is the more complex subsystem to control. The beam-hopping antenna uses an MSM to change beams, and each switch requires one bit for on/off control. Thus, one bit per antenna element per beam is required. The number of control bits can be reduced by column decoding of the control bits in the MSM.

The beam-scanning antenna employs a beam-forming matrix (BFM) consisting of phase shifters instead of switches. For example, use of a 5-bit phase shifter requires 5 control bits per antenna element per beam. Since the controller for the beam-hopping antenna can be built as a subset of the controller designed for the beam-scanning antenna, the controller for the scanning antenna is discussed first.

Beam-scanning controller

A rough calculation to determine the bit update rate for a realistic application will demonstrate the scope of the controller design problem. The number of antenna radiating elements needed for a 0.5° beamwidth is 700. The number of simultaneous beams that can easily be implemented is eight, and each beam requires one phase shifter behind each radiating element. If each phase shifter uses 5 control bits, then 28,000 bits must be updated for each antenna state change. Using the INTELSAT VI 4-μs minimum dwell time specification gives a maximum update rate of 7 Gbit/s. A brute-force solution to this problem would require the use of power-hungry emitter-coupled logic (ECL) and a large harness to distribute the data quickly to the antenna elements.

An alternative approach to the high-speed data distribution problem is to use fiber optic cable to route the data to the various antenna elements. Fiber optic cables are well suited for high-speed, point-to-point communications, but are difficult to use in a point-to-multipoint architecture because splicing the cables and attaching the fiber connectors is difficult and introduces significant signal loss. However, advances in fiber optic technology may make this approach feasible for a future phased-array antenna implementation.

The data distribution problem could be resolved more efficiently by taking advantage of the cyclic nature of a TDMA system, instead of designing for a general-purpose phased-array antenna. In a TDMA system, the antenna sequences through a number of beam-pointing directions, or antenna states, during a TDMA frame period. For example, the INTELSAT VI TDMA timing plan allows up to 64 states in each TDMA frame period. Because this sequence is repeated in each subsequent TDMA frame period, the antenna changes states cyclicly. The states can be modified or replaced, but at a rate much slower than the TDMA frame rate. The data distribution bottleneck can be relieved by storing the cyclic data for each antenna element locally in RAM. Then, the high-speed data transfers only occur over the short distances between the local control modules (LCMs) containing the RAM, and the BFM containing the phase shifters. The harnessing between elements is simplified by using a low-data-rate serial bus to send the state update data to each LCM. This architecture, which employs distributed control [2] in place of high-bandwidth data distribution, allows the use of low-power complementary metal-oxide semiconductor (CMOS) electronics instead of ECL.

To simplify the controller design for a large antenna array, and to enhance testability, the controller was made modular. The entire antenna array is built up from several subarrays, each with its own controller. The subarrays are synchronized by a higher level of control.

Figure 1 is a block diagram of the control architecture. The executive control unit (ECU) provides the highest level of control for the antenna system and is the source of data for the phase shifters or switches in the antenna array. In a satellite system, the ECU would reside partially in a ground-based computer and partially in the satellite telemetry and command subsystem. The ECU downloads antenna state data files containing phase shifter settings and dwell time information to the LCMs and to the data distribution and timing units (DDTUs).

An oscillator provides the TDMA timing signals, which are used to synchronize all the elements of the antenna array. The output of the oscillator consists of four clocks: a 2.5-MHz shift clock which is used within the LCMs for high-speed data clocking, a 1-MHz unit clock which determines the antenna state change boundaries, a 500-Hz frame clock which determines the TDMA frame boundary, and a 0.06-Hz master frame clock which determines the boundaries for changing from the on-line frame state table to the off-line frame state table. These clocks and their associated functions correspond to the TDMA clocks on board the INTELSAT VI satellite.

The DDTU routes data to various LCMs under its control, and routes telemetry from those LCMs back to the ECU. It also has a programmable dwell time

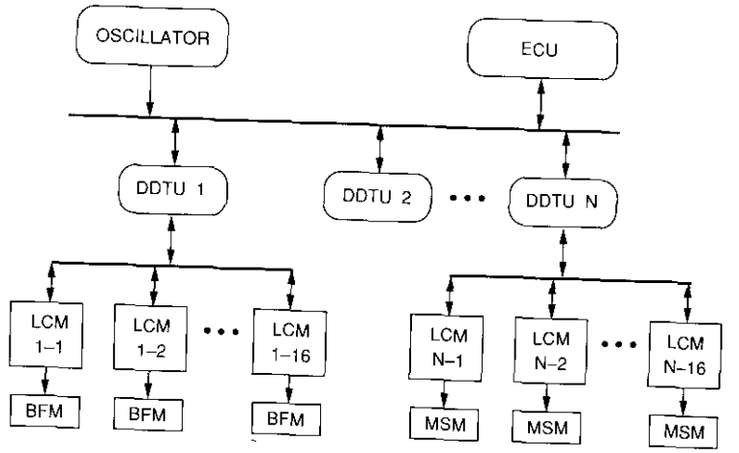

Figure 1. *Control Architecture*

counter which determines the amount of time spent in each state. The dwell time data for each state in the TDMA frame are sent to the DDTU RAM from the ECU and are cyclicly loaded into the programmable counter. Because of I/O bus loading, the maximum number of LCMs that one DDTU can control is 16. The maximum number of DDTUs that the ECU can control depends on the specific satellite telemetry and command bus used.

The LCM is an intelligent unit which is responsible for cycling through the on-line antenna state RAM table, maintaining an off-line antenna state RAM table for updates, and swapping on-line and off-line tables. To maintain local RAM, the LCM must perform error detection and correction on the data in the RAM, and send back telemetry to verify these data. Each LCM can control one 8 × 8 BFM board, which contains sixty-four 5-bit phase shifters and some additional control electronics for driving the phase shifters. Each BFM board can control a row of eight antenna elements, and 16 LCMs can control an 8 × 8 array of elements with dual polarization. Therefore, the natural subarray unit is 8 × 8. This subarray would be controlled by one DDTU and 16 LCMs.

The oscillator and the DDTU both reside within the satellite, while the LCMs and BFMs are mounted on the appropriate antenna subarray structure. The ECU, the oscillator, and the DDTU I/O to these units are specific to the satellite system. The remainder of the DDTU and all of the LCMs are generic, and will be the same for any of a wide variety of satellite systems that have TDMA timing requirements.

In general, the ECU and the oscillator will each have 2 for 1 redundancy (not shown). The redundancy for the DDTU depends on the number of DDTUs used (*i.e.*, the redundancy could be 2 for 1, 3 for 2, etc.). The redundancy configurations for the LCMs and the BFMs are more complex, and are described in a later section.

DATA DISTRIBUTION AND TIMING UNITS

The DDTU is responsible for controlling the timing and synchronization of the 16 LCMs under its control, and for inputting the commands and data from the ECU and formatting and forwarding them to the LCMs. It also formats and forwards telemetry from the LCMs to the ECU. The data distribution function of the DDTU eliminates the need for the ECU to drive a large number of LCMs directly, which in turn eliminates the problem of excessive I/O bus loading and facilitiates the implementation of a modular system. The timing function of the DDTU off-loads that function from the individual LCMs, resulting in a significant savings in power and weight.

The timing inputs from the oscillator are a 2.5-MHz shift clock, a 1-MHz unit clock, a 500-Hz frame clock, and a 0.06-Hz master frame clock. There are three timing outputs to the LCMs and BFMs: a gated shift clock used by the LCMs to preload the BFMs with the next state, a switchover pulse which causes the BFMs to change to the next state, and a swap command which instructs the LCMs to change from the on-line state table to the off-line state table. The swap command originates from the ECU, but is not forwarded to the LCMs until the beginning of the next master frame.

As shown in the block diagram of Figure 2, the DDTU comprises three major units: a microcontroller, a dwell time counter, and a timing unit. The microcontroller passes data from the ECU to the LCMs, and passes telemetry from the LCMs to the ECU. It also maintains the dwell time data in its RAM, and transfers these data to the programmable dwell time counter. Identical microcontrollers are used in the LCMs, and are described in detail in a later section.

The timing section of the DDTU is responsible for commanding the LCMs to switch from one state to the next. The ECU loads the dwell time data for each state in the TDMA frame into RAM in the microcontroller. The microcontroller then cyclicly loads these data into a programmable counter, in much the same way that the LCMs cyclicly load data into the BFM. On-line and off-line state tables are used, error detection and correction must be performed, and telemetry must be provided.

The programmable counter counts down for the specified dwell time and then sends a switchover pulse to the LCMs. This pulse causes the BFMs to

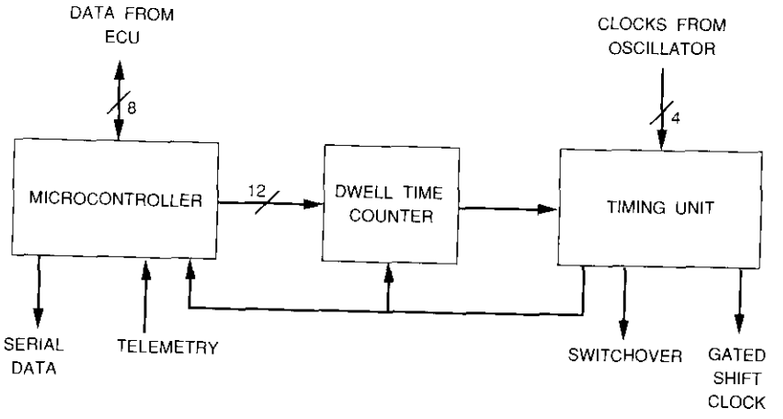

Figure 2. *Data Distribution and Timing Unit*

immediately change to the next state. The switchover pulse also loads the next dwell time data into the programmable counter. Soon after the switchover pulse is sent, the timing unit sends a gated shift clock to the LCMs which they use to preload the BFMs with the next state. This clock consists of a burst of 10 clock pulses sent at a rate of 2.5 MHz. In this way, the data can be serially preloaded into the BFM in 4 μs, the specified minimum dwell time.

The I/O portion of the DDTU, which communicates with the LCMs, is configured for dual-redundant buses for reliability. These buses can be cross-strapped with a redundant DDTU. The commands and data to the LCMs, and the telemetry from the LCMs, are sent over a full-duplex, 250-kbit/s serial bus. In addition, the shift clock and the switchover pulse are bused to the LCMs. The shift clock has a burst rate of 2.5 MHz, but the average rate is about 300 kHz. The switchover pulse is sent once for every 10 shift clock pulses, giving an average rate of 30 kHz. Each signal sent by the DDTU to the LCMs uses a differential RS-422 driver, which provides noise immunity and the ability to send the signals over a long distance. This capability is important, since the DDTU will reside within the satellite, while the LCMs will be an integral part of the antenna structure.

The interface to the ECU depends on the ECU design. For demonstration purposes, an IBM AT computer is used to implement the function of the ECU, and an 8-bit bidirectional bus is used to interface between the ECU and the DDTU.

LOCAL CONTROL MODULES

Figure 3 is a block diagram of the LCM. Each LCM can control eight simultaneous beams for a row of eight antenna elements. The LCM consists of four active microcontrollers and one redundant microcontroller. Each active microcontroller controls 16 of the phase shifters in the BFM.

The microcontrollers are the core of the LCM. They maintain the RAM that contains the TDMA frame data, and pass these data on to the BFMs, which consist of serial-to-parallel converters. The I/O section of the LCM converts the dual-redundant differential signals from the DDTU to the CMOS logic levels used by the LCM.

I/O Section. The LCM has three inputs from the DDTU (serial data, a gated shift clock, and a switchover pulse) and one output (telemetry). The serial data signal is an asynchronous serial communications link which inputs commands and antenna state data. The gated shift clock is a burst of 10 clock pulses at 2.5 MHz which is used to shift data from the LCM to the BFM. The switchover signal is passed directly on to the BFM to command a state change. The telemetry output is a serial asynchronous communications link which allows telemetry from the LCM to be sent to the ECU through the DDTU.

The LCM has 34 outputs to the BFM board: a gated shift clock, a switchover signal, and 32 data lines. Eight data bits from each of the four active microcontrollers form the 32 output data bits. The gated shift clock clocks a serial string of 10 bits on each of the 32 data lines, giving a burst data transfer rate from the LCM to the BFM of 320 bits in 4 μs, or 80 Mbit/s. The average data rate is much lower, about 10 Mbit/s or less.

Microcontroller. Each microcontroller (Figure 4) is a very large-scale integration (VLSI) circuit which consists of a core 8-bit microprocessor along with various peripherals and memory integrated onto a single chip. The core microprocessor (based on the popular Intel 8051 processor) has an 8-bit data bus and a 64K-byte address space, and runs at a maximum clock frequency of 16 MHz. An external 2K bytes of RAM is used to store the on-line and off-line state tables, and an internal 256 bytes of RAM is used to store temporary variables and to maintain a stack. The peripherals include the following:

- a universal asynchronous receiver transmitter (UART) for communication with the DDTU;
- a high-speed, 128-byte, first-in first-out (FIFO) buffer memory for outputting data to the BFM;

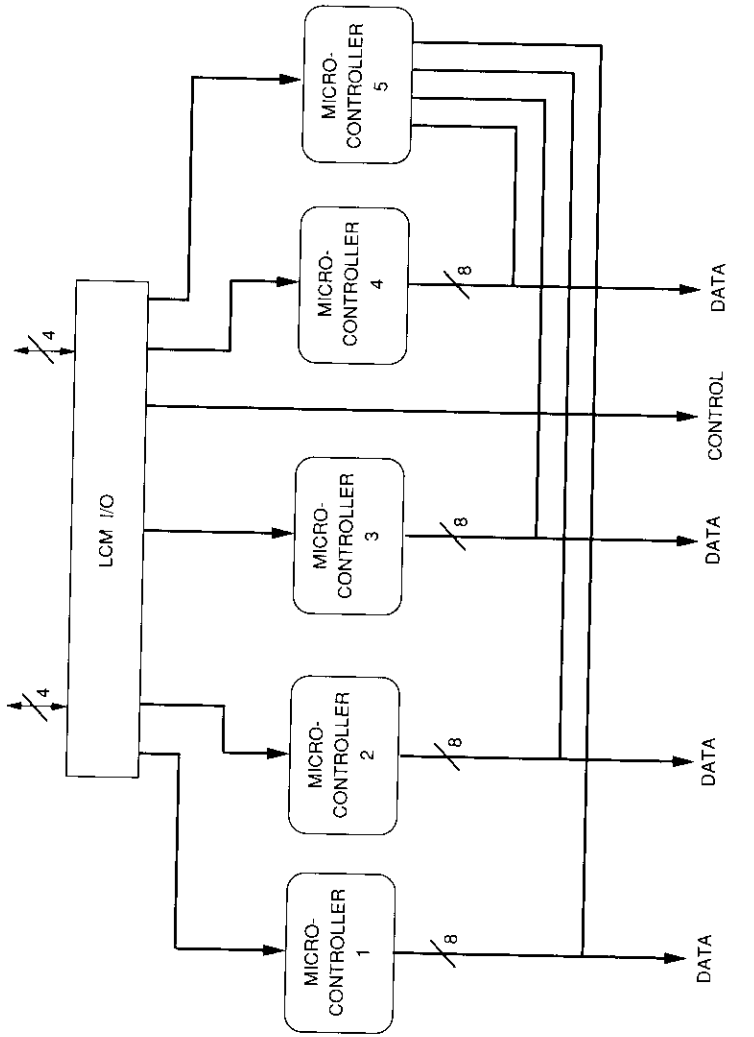

Figure 3. *Local Control Module*

- a counter to check TDMA frame synchronization;
- a timer used as a watchdog timer; and
- an I/O port to input the microcontroller address.

The heart of the microcontroller is an 8-bit microprocessor, together with program read-only memory (ROM).

The microprocessor handles the tasks of cycling through the on-line state table, formatting the new data received from the DDTU, sending telemetry to the DDTU, and performing error detection and correction for the RAM data. A direct memory access (DMA) controller works in conjunction with the microprocessor for high-speed data transfer from the external RAM to the FIFO buffer. Each DMA transfer takes one CPU cycle, or about 750 ns. The FIFO buffer has an 8-bit output which serially drives eight different monolithic microwave integrated circuit (MMIC) drivers. The gated shift clock from the DDTU clocks 10 bytes out of the FIFO buffer and into the BFM.

Each microcontroller is separately addressable by the DDTU. With five microcontrollers per LCM and a maximum of 16 LCMs for each DDTU, there are 80 different addresses for the microcontrollers. A microprocessor-based implementation of the LCM was selected to add flexibility to the design. Any changes in the system-level requirements can be accommodated by software changes in the microcontrollers.

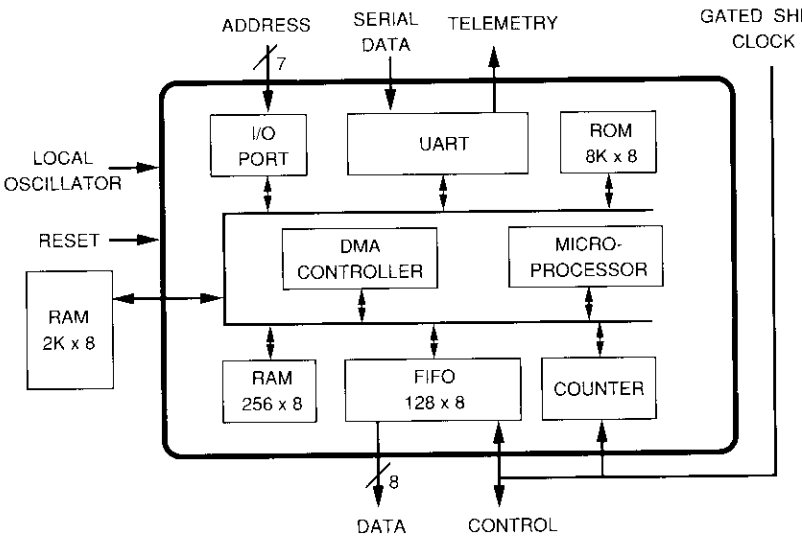

Figure 4. *Microcontroller*

Error Control. Error detection and correction (EDC) is implemented in software as a background task for each microcontroller. The EDC algorithm is a modified Hamming code which corrects all single-bit errors and detects all double-bit and some multibit errors. The EDC is performed on the antenna state data stored in the external RAM.

The internal RAM and registers are protected from SEUs through various software techniques, including software traps, a watchdog timer, and the multiple calculation and multiple storage of variables. Software implementation of EDC will save the additional power and area which a hardware implementation would consume. Some SEU-induced errors in the antenna state data may persist for a few hundred milliseconds; however, this temporary data corruption will have only a minor impact on overall antenna performance because of the inherent redundancy of a phased-array antenna. Greater care must be taken with EDC for the DDTU, since a single bit error in the DDTU will affect the entire antenna subarray under the control of the DDTU.

Redundancy. Redundancy for the LCM can be addressed by taking advantage of the graceful degradation failure mode of any large phased-array antenna. Failure of any one element in an array has only a small impact on overall antenna performance. Because the antenna has sufficient margin in the number of array elements, it will still provide the required gain and sidelobe suppression, even after multiple element failures. Partitioning the electronics in the LCM into four separate active sections means that the failure of any one component will affect only two antenna elements. This makes the LCM tolerant of a single-point failure.

The I/O section of the LCM is common to all five microcontrollers. However, because it is dual-redundant in order to handle the dual-redundant I/O buses, this section is single-point failure free. Additional reliability is incorporated by cross-strapping the microcontrollers in a 5 for 4 configuration. Other redundancy configurations (3 for 2, 2 for 1, etc.) are possible, depending on system requirements.

BEAM-FORMING MATRIX

Figure 5 is a block diagram of the control electronics in the BFM. The input control and data lines are first buffered and then level-shifted. The level shifters convert the CMOS logic levels of the LCM to the negative voltage levels needed by the variable phase shifters (VPS) and the MMIC drivers. The drivers consist of 10-bit serial shift registers with a 10-bit latch and 10-bit inverters. The inverters provide the complementary outputs needed by the VPS. Each MMIC driver provides the 20 control lines necessary to drive two 5-bit VPS.

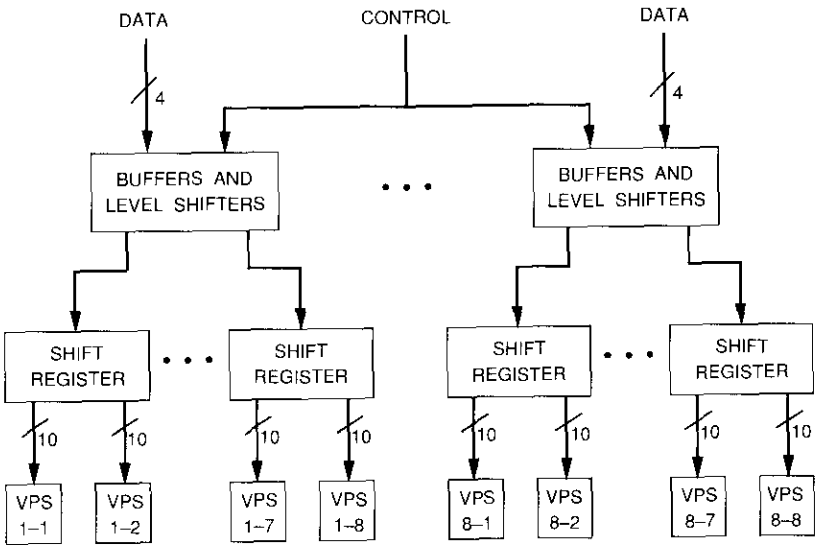

Figure 5. *Beam-Forming Matrix Board*

The BFM is configured so that any component failure will affect only one antenna element. Due to the graceful degradation of the antenna system as described above, it is not necessary to have redundant components within the BFM.

Beam-hopping controller

The controller for the beam-hopping antenna differs in some important respects from that for the beam-scanning antenna. A beam-hopping antenna has an MSM or a group of interconnected MSMs to control beam switching. Each MSM is controlled by one LCM, and the size of the MSM determines the size of the LCM. For example, an 8 × 8 MSM would require an LCM with one microcontroller and four MMIC drivers.

The MMIC drivers for the beam-hopping antenna have decoders in addition to the shift registers and latches. Decoders take advantage of the fact that no more than one beam is sent to an element at any one time. This reduces the number of control bits that must be stored in RAM. For example, a 3-to-8 decoder requires only 3 bits to turn on any one of eight switches. The beam-hopping antenna does not have graceful degradation; if one element is lost, then that beam direction is lost. Therefore active redundancy and cross-strapping are required at the MSM level.

Development status

A breadboard version of this controller architecture has been built and is currently undergoing test and evaluation. The ECU is implemented with an IBM AT computer running a BASIC program. The oscillator and timing signals were chosen to match the INTELSAT VI TDMA timing specifications.

Low-power, high-speed CMOS electronics are used almost exclusively in the design of both the DDTU and the LCM. The only exceptions are the transistor-transistor logic (TTL) differential drivers and receivers, which were used because equivalent CMOS parts are not currently available. Each LCM dissipates about 2 W and occupies 260 cm^2 on a printed-circuit board. Each DDTU dissipates about 4 W and occupies 160 cm^2. An 8 × 8 antenna subarray with dual polarization requires 16 LCMs and one DDTU, and will dissipate about 36 W.

All of the integrated circuits used, with the exception of the microcontroller, are available or soon will be available in radiation-hardened versions. In addition, RAM is also available in SEU-immune versions. The microcontroller can be built as a custom gate array using a radiation-hardened manufacturing process. At least one manufacturer has a library of macrocells for its radiation-hardened gate arrays, which include all the major components of the microcontroller, such as the 8051 microprocessor core, FIFO, UART, RAM, and ROM.

The software for the microcontrollers in the LCM and DDTU is written in assembly language to meet the stringent TDMA frame timing requirements. The lowest level of this controller architecture, the MMIC drivers, have been successfully tested with RF components, namely phase shifters and attenuators. Another version of an MMIC driver has been successfully tested with a prototype 4 × 4 MSM. The first application using the full controller architecture will be a proof-of-concept 2 × 8 beam-scanning antenna array with the capability for eight simultaneous beams. A controller for an 8 × 8 MSM is also scheduled to be built.

Summary

A modular, highly flexible control architecture has been developed for TDMA satellite antennas. This architecture is feasible for both beam-scanning and beam-hopping antenna systems. A breadboard version of the digital controller is under development, and plans are under way for both a beam-scanning and a beam-hopping application.

Acknowledgments

The author wishes to acknowledge A. Zaghloul, R. Gupta, and F. Assal for their guidance and helpful discussions. C. Arvin fabricated and tested breadboard hardware, and E. Hare developed the software for the ECU. The author also wishes to thank A. Ramos for his continuing support and encouragement.

References

[1] A. I. Zaghloul, F. T. Assal, and R. M. Sorbello, "Multibeam Active Phased Array System Configuration for Communications Satellites," IEEE Military Communications Conference, Washington, D.C., October 1987, *Conference Record*, Vol. 1, pp. 289–293.

[2] T. P. Waldron, S. K. Chin, and R. J. Naster, "Distributed Beamsteering Control of Phased Array Radars," *Microwave Journal*, Vol. 29, No. 9, September 1986, pp. 133–146.

Timothy Hampsch received a B.S.E.E. from Tufts University in 1981, and an M.S. in physics from the University of Maryland in 1986. Prior to joining COMSAT Laboratories in 1987 he was with Northrop Corporation, where he was involved in the design of electronics for inertial guidance systems and embedded navigation computers. Mr. Hampsch is currently a Member of the Technical Staff in the Applied Technologies Division at COMSAT, where he is responsible for the design of digital electronics for spacecraft and ground hardware. He is currently involved in system definition and hardware design for a satellite simulator. His research interests are in the fields of parallel processing and real-time computer systems. He is a member of IEEE and Tau Beta Pi.

Index: solid state devices, reliability, radiation effects, field-effect transistors (MOSFETs), geosynchronous orbit

Radiation-hardened deposited oxides

A. MEULENBERG

(Manuscript received August 2, 1988)

Abstract

Simple radiation-hardened, metal oxide semiconductor (MOS) structures have been fabricated using plasma-enhanced chemical vapor deposition (PECVD) techniques. By reducing both the mobility of radiation-induced charge in the oxide and the population of surface defects ($<10^{10}$ eV $^{-1}$cm^{-2}) in the Si-SiO_2 interface, the radiation hardness of such structures under bias is extended to beyond 10 Mrad. Mobility in the oxide of both thermally excited and radiation-induced charge carriers is reduced by using multiple dielectric layers to provide barriers which reduce charge transport. Plasma etching of the silicon wafers and doping of the oxide during deposition were employed to reduce the initial surface-state density and the probability of defect formation by radiation-induced charge. This technique is useful for a wide range of oxide thicknesses and was successfully tested at 50, 100–150, and 400 nm.

The ability to deposit useful oxides at low temperatures (<500°C), and the versatility of the PECVD process, may be important attributes in some very large-scale integration (VLSI) applications. Although field-effect transistors (FETs) have yet to be fabricated using these MOS structures, tests on MOS capacitors exposed to expected commercial processing conditions indicate appropriate behavior for both gate (thin) and field (thick) oxides.

Introduction

Each new generation of spacecraft has offered greater capacity and more complex on-board functions than previous generations, and has been designed for longer life expectancy in geostationary orbit. This evolution requires improved reliability of greater quantities of semiconductor devices. The

degradation of semiconductor devices due to the space radiation environment is one limitation on reliability. Despite a great deal of effort to alleviate this problem, radiation-induced degradation of electrical characteristics persists as a major limitation. Furthermore, requirements are becoming more severe as reduced shielding and enhanced radiation threats are envisioned.

The nature of radiation-induced degradation can be described in general terms as follows. Many semiconductor devices [*e.g.*, silicon metal-oxide semiconductor (MOS) transistors] require the use of an insulating oxide layer between the control electrode (gate) and the basic material of the device in order to reduce power dissipation from current flowing in the gate-control and bias circuits. This oxide layer also passivates the surface of the underlying semiconductor. (Unpassivated surfaces are less sensitive to changes in the gate voltage). Radiation absorbed in the insulator creates charge pairs which separate and migrate under the influence of an electric field resulting from an applied bias. These charges may become trapped in the insulator and alter the electric field in both the insulator and the semiconductor surface region. In addition, if the charges reach the interface with the semiconductor, they can cause population changes in the surface states at this interface. Both of these effects can have a profound impact on the operating characteristics of the device.

Demands for operation in higher frequency communications bands, higher speed operation of digital circuits, lower power dissipation, and higher component packing density require that smaller dimensions be used in microelectronic structures. In one sense, this trend has reduced the radiation effects problem because smaller lateral dimensions require the use of thinner insulating layers. Thin layers are inherently less susceptible to radiation damage because there is less volume to absorb radiation energy, and therefore fewer electron-hole pairs are generated for the same exposure. However, the problem of direct creation of surface states by radiation at higher levels exists independently of the thickness of the bulk oxide.

The presence of radiation-induced surface states, whether created by charge trapping or by direct radiation effects, reduces device operating speeds and degrades device control characteristics. Furthermore, material and fabrication requirements (*e.g.*, high-temperature processes, wafer surface defects, and particulate contamination) become more critical as the device dimensions shrink. Therefore, the requirements for useful oxides include low initial interface trap densities (D_{it}), low radiation-induced oxide charge (Q_{ot}), small changes in D_{it} with radiation, and high thermal stability both before and after irradiation.

An effort was begun in 1985 to harden an important class of electronic devices [MOS field-effect transistors (MOSFETs)] against the unshielded natural radiation environment at geostationary orbit. Unshielded radiation levels inside a spacecraft for this condition would exceed 1 Mrad for a 10-year mission. The goal was to provide a reliable MOS structure that was compatible with present silicon device technologies and that would survive a 100-krad radiation environment typical of mission requirements at the component level within a spacecraft. At many locations within a spacecraft, the structure, components, and component boxes provide sufficient shielding to reduce mission doses to below this level. After 1 year, the radiation goal was attained.

When the program was completed in 1987, with verification of structure stability and reliability, the radiation goals had been exceeded by two orders of magnitude. The approach used and the observations made provide an understanding of the final structures and processing presented here. The measurement techniques used to study the structures, as well as the representative data and the results of the program, are also presented.

Background

All commercial MOSFETs are currently manufactured using thermally grown oxides under the gates. Growth temperatures range from 900° to 1,200°C; however, extensive research has identified specific temperature ranges and processing steps as useful for radiation hardening of these oxides. When a technology is pushed to its limit, comparable results might be more easily obtained by using new technologies or a novel application of old technologies.

In this work, plasma-enhanced chemical vapor deposition (PECVD) was selected for preparing the oxide layers on silicon substrates. This approach permits low-temperature (~350°C) processing, the incorporation of dopant materials during deposition, and the use of an *in situ* etch and subsequent dielectric deposition without exposure of the sample to room conditions. An inherently radiation-hardened dielectric results from the high defect density that usually occurs in deposited layers (to increase charge trapping and thereby reduce charge separation).

Initially, single layers of 150-nm-thick PECVD SiO_2 were studied. These films, when optimized, exhibited the radiation hardness expected of high-defect-density layers; that is, less than 1-V shift in flatband voltage (V_{fb}) after a 10^5-rad exposure, where V_{fb} is that voltage required on the gate (metal of the MOS structure) to provide a zero field condition at the semiconductor surface and is related to the threshold voltage of a transistor. Although this hardness level was very good relative to other CVD oxides being developed at the time [1], an even more promising result from the initial effort was the very low value for the surface state (or interface) trap density ($D_{it} \simeq 3 \times 10^{10}$ eV $^{-1}$cm^{-2}) obtained by altering the etch and deposition parameters.

Still, these films exhibited two problems: a rather high V_{fb} (-6 to -10 V) and an unstable V_{fb} when subjected to elevated temperatures under bias. The V_{fb} could be controlled by surface doping of the silicon, but its thermal instability presented a reliability problem.

Because the etching step used in the procedure involved a gas (CF_4) containing fluorine, it was thought that the good characteristics observed might be due to inclusion of residual fluorine in the films. As a test of this hypothesis, films were deposited with a small percentage of CF_4 added to the gases used for deposition. Results from investigations in other laboratories have also shown the benefits of fluorine and chlorine (see, for example, References 2 and 3). The radiation hardness of the doped films was improved relative to undoped films; however, both the high V_{fb} and its temperature-related instability persisted.

The temperature instability indicated that many shallow traps existed in the oxide. An ideal layer would only contain a uniform distribution of uncharged, deep traps. This desired trap distribution was sought by depositing several thin layers of different insulators. The discontinuity in valence and conduction band levels that existed at the junction of these materials was expected to provide a high and continuous barrier to charge transport. Consequently, alternating layers of SiO_2 and Si_3N_4, with individual layer thicknesses ranging between 20 and 40 nm, were selected for study. This use of multiple layers had a marked effect on the radiation hardness of these films, and the resulting device stability was greatly improved relative to oxide-only layers when subjected to bias at elevated temperatures. Improvements obtained by using different multilayer structures have subsequently been reported by others [4].

Factors postulated to affect the electrical characteristics and radiation hardness of the MOS structures fabricated include impurities, layering in the dielectric, interdiffusion of elements, stress, and dielectric film thickness. The measurement techniques used to qualitatively and quantitatively characterize the doped PECVD dielectrics are discussed in later sections.

Device fabrication

Silicon wafers [2 × 2 cm, nominally 1 Ω-cm, *p*-type, <100> float zone (FZ) refined material] were selected and cleaned before insertion into a plasma deposition system. Also prior to sample insertion, the system was cleaned and a predeposition dielectric layer was applied to seal portions of the system that would be exposed to plasma or reaction products. The sample stage was heated and coated during this predeposition so that samples would only contact fresh dielectric. Samples were introduced into the chamber, which was then pumped down with a purge gas (helium) flowing. A 15-second etch (O_2 + CF_4) cleaned the native oxide from the silicon and etched the surface to some extent. The dielectric deposition process (N_2O + SiH_4 + CF_4 for oxide,* and NH_3 + SiH_4 for nitride) was initiated within 45 seconds after etch termination. Alternating layers of oxide and nitride were deposited in a 20-20-40-20-40-nm sequence (oxide first).

After removal from the system, the wafers were heat treated, using either rapid thermal anneal or a tube furnace, to stabilize and densify the dielectric layers when subsequent high-temperature steps were anticipated. Aluminum was then evaporated by resistive heating through a metal shadow mask to form the test capacitors. Subsequent heating at 450°C for 30 minutes markedly improved the electrical and radiation characteristics, particularly if no pre-aluminum-deposition, high-temperature heat treatments had taken place. The samples were then electrically characterized and tested under irradiation and combined thermal/bias conditions.

Device characterization

The means used to determine MOS capacitor properties included high-frequency (1-MHz) capacitance-voltage (C-V) measurements for quick checks, quasistatic C-V measurements to determine D_{it}, and Auger analysis to profile the elemental content of the layers exposed sequentially by ion milling. In addition, a number of tests were performed to characterize changes in MOS capacitor properties. These tests included high-temperature tests with and without aluminum contacts to determine the system thermal-mechanical and interface stability, radiation tests to quantify the strengths and weaknesses of the structure, and thermal/bias tests to provide an idea of operational limitations and some insight into device properties not easily measured by normal techniques.

The 1-MHz C-V measurement was a fast, easy means of characterizing the electrical properties of MOS structures and of recording changes introduced by radiation treatments, thermal treatments, and thermal/bias tests. V_{fb}, which was the parameter typically determined from this measurement, indicated the sign and quantity of charge trapped in the oxide layer and in the Si-SiO_2 interface.

The quasistatic technique was used to determine D_{it} initially, as well as after irradiation in a cobalt-60 gamma cell or thermal treatments. However, for low values of D_{it} ($\sim 10^{10}$ $eV^{-1}cm^{-2}$) the precision became poor. Devices

*For best results in the present structure, this fluorine source gas is only introduced into the first and last oxide layers.

measured at COMSAT with D_{it} values in the low 10^{10} $eV^{-1}cm^{-2}$ range were independently measured at the National Institute of Standards and Technololgy (NIST) and the Naval Research Laboratories (NRL) and found to have even lower values of D_{it} ($<10^{10}$ $eV^{-1}cm^{-2}$). Low initial values of D_{it} and low changes in D_{it} as a result of various tests were the goals for a good oxide structure.

Auger analysis was useful in confirming the layer thicknesses, their stoichiometry, and the interdiffusion of elements during various anneal steps. The buildup of nitrogen measured near the $Si\text{-}SiO_2$ interface may be an important observation. Because the Auger sensitivity was on the order of 1 to 5 percent of the total elemental content, most impurities (such as carbon and fluorine), while occasionally observed, were not quantitatively measured.

High-temperature tests were carried out to optimize anneal temperatures and times for the structures subsequent to deposition of aluminum contacts on the oxide layer. Tests at 400° to 500°C for 15 to 60 minutes gave an optimum at 450°C/30 min. Some SiO_2 layers with no metal contacts present were exposed to higher temperature in a tube furnance at up to 1,000°C for 30 minutes in dry N_2, or in a flash anneal chamber at up to 1,100°C for 15 seconds. Structural and electrical integrity under both sets of conditions, as determined by visual and C-V inspection, are important criteria in process control for both aluminum and polysilicon gate technologies.

Radiation tests were carried out in a cobalt-60 gamma cell with a nominal dose rate of 0.3 Mrad/hr. Wafer sections (up to three) typically containing twenty 3-mm^2 capacitors were placed face down on a vacuum chuck, and a negative bias was applied to their metalized back surfaces. This simple system gave confidence that electrical contact had been made to all of the otherwise isolated components. The resultant bias was equivalent to positive voltage on the aluminum side of the MOS capacitor, and the voltage levels were set to provide electric fields through the oxide in excess of 1 MV/cm. This level will generally give the worst-case radiation degradation. Voltage was removed when the devices were taken from the radiation field, and measurements were made as soon as possible thereafter, generally within an hour. When devices were stored in open-circuit condition for more than 24 hours between runs, they were remeasured before the next irradiation to test for recovery effects. Generally, radiation levels of 0.1, 0.5, 2 or 5, and 10 or 15 Mrad were selected for testing. Because the hardness of the multilayer structures was confirmed early in the testing, the 0.1-Mrad level was often bypassed in subsequent irradiations.

The thermal/bias tests were of two types: low-temperature ($\leq$125°C), long-term (~24 hr) tests to fulfill reliability requirements (*e.g.*, Mil. Std. 883); and higher temperature (300°C), short-term (15- to 250-min) tests to determine charge-trapping sites in levels unobservable by other techniques. The low-temperature tests were conducted with ± 1 MV/cm and zero-bias conditions, along with open-circuit samples. This approach also identified mobile charge in the oxide, such as ions incorporated during fabrication and carriers trapped during irradiation.

The 300°C test was conducted with a negative bias which drew holes and positive ions away from trap sites in the $Si\text{-}SiO_2$ interface. It also ejected electrons trapped in this region during the positive bias-radiation tests. This test has become common in the industry since the discovery of "rebound." This phenomenon, which is observed during recovery subsequent to irradiation, can exceed the initial radiation degradation [5]. It results from the different time constants for degradation and recovery of the trapped oxide and interface charges. In many radiation-hardened oxides, the two effects cancel during irradiation; however, after a recovery period they may differ significantly in magnitude. The final state, perhaps not reached for years at room temperature, could show strong radiation damage effects, even though none were revealed immediately after a heavy dose. The 300°C test with negative bias makes such effects apparent within an hour.

Results and discussion

The following data, while characteristic of the work carried out in the latter part of the program, are not necessarily representative of the full advantages that optimized structures could provide.

Radiation hardness

Figure 1 shows a family of curves indicating D_{it} at various radiation dose levels for the present technology. The change in D_{it} with irradiation was unusually low [3] for dielectric layers of this thickness (140 nm). The spread in results for several variations on the basic structure is depicted in Figure 2. The increase in D_{it} with dose (at 0.30 eV above the valence band edge, E_V) approached a linear relationship only in the region above 10 Mrad. However, the damage peak at 0.6 eV in Figure 1 approached the linear regime above 1 Mrad.

Many factors contributed to reducing the trapped oxide charge and interface trap density, both before and after irradiation. Some of these factors, such as predeposition etch time, inclusion of CF_4 during oxide deposition, total dielectric thickness, pre- and postmetalization anneals, and dielectric layering, were examined. All these factors had a significant impact, often at different radiation levels.

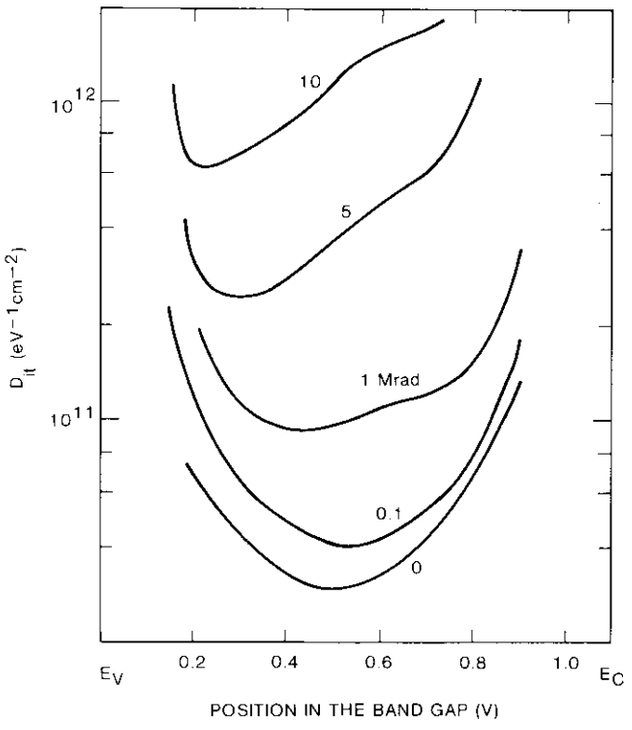

Figure 1. *Effects of Radiation on* D_{it} *for a 140-nm PECVD Oxide*

The effect of fluorine on the radiation hardness of the multilayer films can be seen by examining Figure 3. All three films were 140-nm thick and composed of five layers (20-nm SiO_2, 20-nm Si_3N_4, 40-nm SiO_2, 20-nm Si_3N_4, and 40-nm SiO_2), with the first SiO_2 layer adjacent to the silicon. Fluorine was introduced into different layers of the films, and all three samples were subjected to a 450°C/30-min anneal after application of the aluminum. The most significant feature revealed by Figure 3 is the radiation dose at which ΔV_{fb} exceeds 1 V. With fluorine incorporated into both the inside and outside (next to the aluminum) layers, ΔV_{fb} was less than 1 V up to 4 Mrad. The threshold dose was less with fluorine added to only the inside layer, and still less with no fluorine added at all.

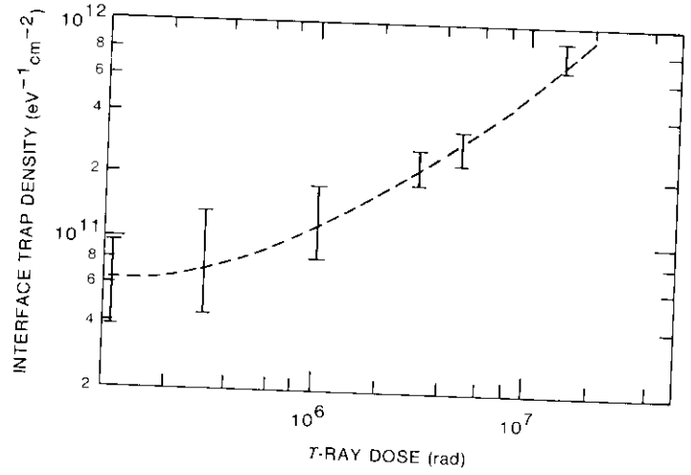

Figure 2. D_{it} *(at* E_V *+ 0.3 eV)* vs *Dose of MOS Capacitors for Several Runs With 140-nm Oxides*

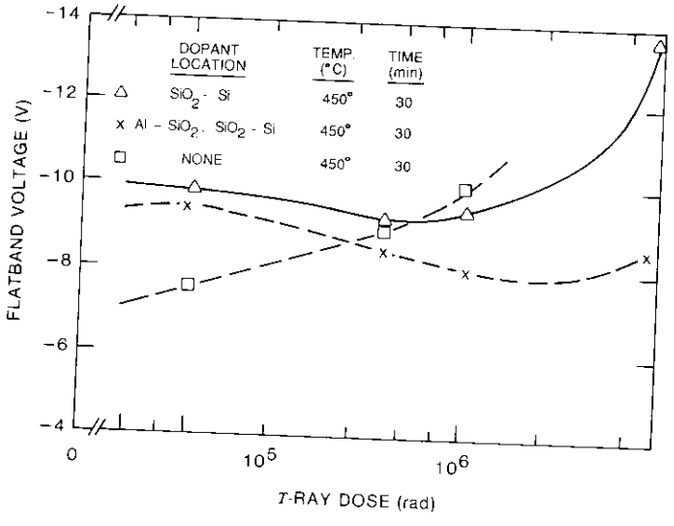

Figure 3. V_{fb} vs *Dose for Various 140-nm Oxides*

Dielectric layering and thickness effects

The thickness of both the total dielectric and the individual layers within the dielectric can influence the electrical and radiation characteristics of doped PECVD MOS devices. The total thickness effect is shown in Figure 4, in which several different structures are compared. The dielectric thicknesses, d, of 50, 120, and 400 nm are composed of 3, 5, and 13 layers, respectively. With the exception of unheated samples, V_{fb} is roughly proportional to thickness. This implies that charge is stored uniformly in the dielectrics and that heat tends to reduce the stored charge. Such reduction in V_{fb} with decreasing thickness and increasing anneal temperature means that both problems encountered early in the work (high V_{fb} and thermal instability) have been overcome.

The application of heat with aluminum present has another effect on the oxide properties. Figure 5 depicts the impact on the PECVD oxide of a postmetalization anneal (PMA) step at 450°C/30 min. The increase of nitrogen in the region near the silicon interface is attributed to relaxation of stress during the redistribution, and matches the stress profile peaks reported in the literature for a SiO_2-Si interface [6]. The apparent interdiffusion of the silicon and oxygen seen after the PMA step could be real or could be an artifact of a microscopically nonuniform ion etch rate resulting from changes in the internal oxide structure. The observed high concentration of oxygen in the silicon surface is unlikely; however, since the Auger measurements were

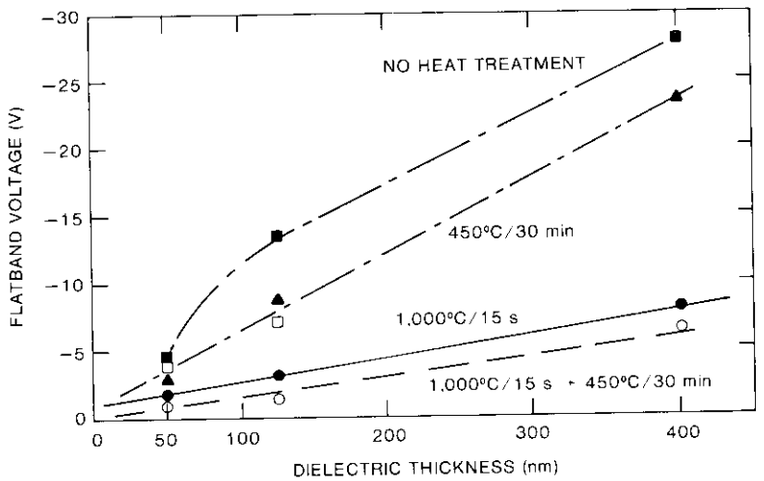

Figure 4. V_{fb} *Dependence on Total Thickness of Dielectric Layer*

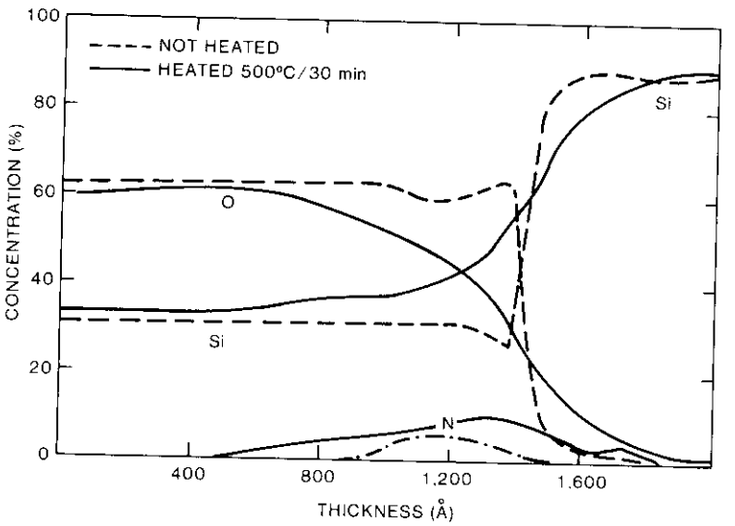

Figure 5. *Auger Profiles of Oxygen, Silicon, and Nitrogen in a PECVD Oxide Before and After Heating*

made on approximately 1-μm spots, any nonuniformities must be smaller than 1 μm. Thus, it becomes important to identify the presence and extent of any interdiffusion or microscopic nonuniformities in future layers.

Figure 6 shows the Auger profile of a 140-nm, multiple-layer film with a high-temperature anneal prior to application of the aluminum contacts. The excellent definition of these layers indicates reduced mixing of silicon and oxygen at the silicon surface, compared to the annealed sample of Figure 5. However, the greater presence of nitrogen in the first oxide layer, and particularly at the silicon interface, supports the earlier observations of the same effect. The effects of nitrogen during oxide processing and in the resulting layer have been reviewed elsewhere [7],[8].

Other effects can result from layering the dielectric in a MOS structure. The less-permeable nitride layers may contribute to device hardness in ways other than as the potential barrier used to trap radiation-generated carriers. The layers may prevent mobile ions such as hydrogen and fluorine from escaping, so that these ions might recombine with radiation-induced interface defects and thereby neutralize them. The nitride layers are seen to contribute nitrogen to the oxide layer adjacent to the silicon. Because the PECVD oxide and nitride layers are rich in hydrogen (which may be liberated during irradiation), they may be a nearly infinite source of hydrogen to heal damage as it is generated. The different structure and thermal expansion coefficients

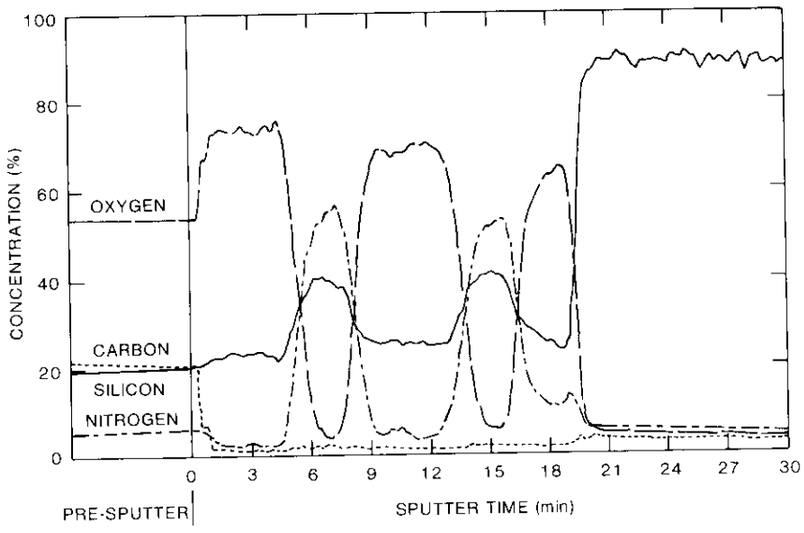

Figure 6. *Auger Profile of Multilayer Structure Heated to 900°C for 15 seconds*

probably will alter the stress within the various dielectric layers, and even in the silicon itself.

Other considerations

The contact material used during all of the work reported here was aluminum. The thinnest dielectric layers were 50 nm, and the silicon used was limited to FZ refined material. Because present IC technology employs polysilicon gate contacts, less than 30-nm oxides, and crucible-grown [Czochralski (CZ)] silicon, changes must be made in gate metal, oxide thickness, and substrate material to make the present process compatible with current commercial processes.

The conversion to polysilicon would not be difficult because, for 50-nm dielectrics, a high-temperature step (>900°C prior to metalization) which is necessary to activate the doped polysilicon also was found to improve the MOS electrical characteristics to the same extent as a low-temperature (450°C) PMA step. However, data are insufficient to consider the process compatible with IC technology without some testing of MOS structures that actually use the polysilicon contacts and thinner dielectric layers. Initial tests with CZ silicon have displayed differences when compared to FZ silicon in the same run. These differences must be examined further.

Conclusions

This study has demonstrated that low surface-state densities ($<10^{10}$ $eV^{-1}cm^{-2}$) can be attained with the application of low-temperature PECVD oxides. These oxides display charge trapping in the bulk, which improves radiation hardness to a level superior to that of undoped oxides.

Because trapped charges in PECVD oxides are released at low temperatures, thermally unstable devices will be created if other steps are not taken. The multiple layers within the MOS structures described here provide deep barriers that improve both thermal stability (no ΔV_{fb} under bias at 125°C for 24 hr) and radiation hardness ($\Delta V_{fb} < 1$ V after 6 Mrad under bias). Excellent radiation characteristics were observed for thin (50-nm), medium (100- to 150-nm), and thick (400-nm) structures utilizing both doped oxides and multiple layers.

The multilayer PECVD oxides survived the high temperatures (up to 1,100°C for 15 seconds or 1,000°C for 30 minutes) required for commercial IC processes. In addition, the PECVD oxide process provides a broad spectrum of variables with which to optimize a structure for a particular use.

Acknowledgments

The author wishes to thank D. Perez, R. Porter, T. Salerno, E. Sparks, and K. Wagner of COMSAT Laboratories for their excellent and enthusiastic participation in this program. The D_{it} measurements at NIST were made by P. Roitman, and at NRL were supervised by A. Revesz. The funding for this program was provided by the Intelsat Satellite Services Division of the Communications Satellite Corporation.

References

[1] K. Watanabe, M. Kato, T. Okabe, and M. Nagata, "Radiation Hardened Silicon Devices Using a Novel Thick Oxide," *IEEE Transactions on Nuclear Science*, Vol. NS-32, No. 6, December 1985, pp. 3971–3974.

[2] P. F. Schmidt, R. J. Jaccodine, C. H. Wolowodiuk, and T. Kook, "Chemically Enhanced Thermal Oxidation of Silicon," *Materials Letters*, Vol. 3, Nos. 5 and 6, April 1985, pp. 235–238.

[3] E. F. daSilva, Jr., Y. Nishioka, and T-P. Ma, "Radiation Response of MOS Capacitors Containing Fluorinated Oxides," *IEEE Transactions on Nuclear Science*, Vol. NS-34, No. 6, December 1986, pp. 1190–1195.

[4] K. Watanabe, M. Kato, T. Okabe, and M. Nagata, "Radiation Effects of Double Layer Dielectric Films," *IEEE Transactions on Nuclear Science*, Vol. NS-33, No. 6, December 1986, pp. 1216–1222.

[5] J. R. Swank *et al.*, "Physical Mechanisms Contributing to Device Rebound," *IEEE Transactions on Nuclear Science*, Vol. NS-31, No. 6, December 1984, pp. 1434–1438.

[6] V. Zekeriya and T-P. Ma, "Dependence of X-ray Generation of Interface Traps on Gate Metal Induced Interfacial Stress in MOS Structures," *IEEE Transactions on Nuclear Science*, Vol. NS-31, No. 6, December 1984, pp. 1261–1266.

[7] R. J. Jaccodine, "Nitridation Induced-Reactions in Si and SiO_2," *Material Research Society Symposia Proceedings*, Vol. 59, 1986, pp. 561–574.

[8] R. Sundareson, M. M. Matloubian, and W. E. Bailey, "Rapid-Nitridation of SiO_2 for Radiation-Hardened MOS Gate Dielectrics," *IEEE Transactions on Nuclear Science*, Vol. NS-33, No. 6, December 1986, pp. 1223–1227.

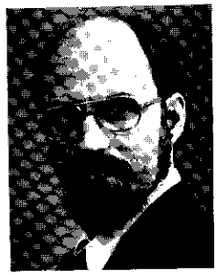

Andrew Meulenberg received his B.A. from the University of the South in 1962, and his Ph.D. in physics from Vanderbilt University in 1968. Since joining COMSAT in 1968, he has been responsible for defining and simulating the space environment encountered by synchronous satellites, studying the effects of this environment on spacecraft components, and investigating methods for protecting materials and components against radiation and its consequences. He is currently a Senior Scientist in the Analytical Chemistry and Failure Analysis Department.

CTR Note

Annotated bibliography of optical intersatellite link technology 1970–1988

R. G. MARSHALEK AND D. K. PAUL

(Manuscript received September 3, 1987, revised December 14, 1988)

Introduction

Optical intersatellite links (ISLs) have received considerable coverage in the literature, with earlier efforts concentrating on systems using the carbon dioxide gas laser or the neodymium-doped yttrium aluminum garnet (Nd:YAG) solid-state laser as the transmitter. Recent improvements in the optical power output and lifetime of semiconductor diode lasers have led to increasing interest in the use of the gallium aluminum arsenide (GaAlAs) laser in ISL applications. These developments have in turn led to in-depth investigations of the preferred optical technologies for ISLs in applications such as the INTELSAT global telecommunications network and data-relay systems for NASA.

The Optical Communications Department at COMSAT Laboratories has completed detailed assessments of the communications subsystem of ISLs for these two applications. As part of this effort, an in-depth literature search on optical ISL communications technology was completed at the systems and component levels. In this contribution, references on this subject are categorized into several technological areas, and a short annotation is provided for each. This compilation thereby summarizes both past and present activities relating to optical ISLs at a time when systems studies are essentially complete and hardware development of subsystems for ISLs is actively progressing throughout the United States and Europe.

Robert G. Marshalek, formerly with COMSAT, is a Principal Design Engineer with Ball Aerospace Systems Division, Boulder, Colorado.

Dilip K. Paul is Manager of the Optical Communications Department at COMSAT Laboratories.

To facilitate the use of this bibliography, the entries have been categorized into the following technological areas:

- Intersatellite Links—General
- Carbon Dioxide Laser ISLs
- Nd:YAG Laser ISLs
- GaAlAs Laser/Direct-Detection ISLs
- GaAlAs Laser/Heterodyne-Detection ISLs
- Diode Laser Sources
- Photodetectors
- Optical Receiver Design
- Modulation Formats
- Wavelength-Division Multiplexing
- High-Speed Systems
- Optical Background Radiation
- Radiation Effects

Intersatellite links—general

The items in this category discuss general features relating to optical ISLs, including potential applications, tradeoff analyses of various optical technologies, technology status, and the effect of pointing errors on ISL communications performance.

Agnieray, P., and J. D. Gayrard, "Study and Definition of an Optical Intersatellite Link Within a Satellite Cluster," 35th Congress of the International Astronautical Federation, Lausanne, Switzerland, October 7–13, 1984, Paper IAF-84-02.

Optical ISLs between satellites colocated in the same orbital slot are examined. The communications performance of such links is discussed for both conventional and regenerative satellites.

Barry, J. D., and G. S. Mecherle, "Beam Pointing Error as a Significant Design Parameter for Satellite-Borne, Free-Space Optical Communication Systems," *Optical Engineering*, Vol. 24, No. 6, November/December 1985, pp. 1049–1054.

This paper examines the issue of pointing errors between satellite-borne, free-space optical communications systems. Single-axis pointing error distribution is described as a Gaussian function and used to define a probability of burst error for the pointing subsystem. A relationship between the rms standard deviation of the pointing error distribution, the probability of burst error, and the Airy far-field beamwidth is deduced and used to show the limitations imposed on system beamwidth and antenna diameter by the burst error probability.

Begley, D. L., *et al.*, "Solid-State Laser Cross-Link Systems and Technology," *International Journal of Satellite Communications*, Vol. 6, No. 2, April–June 1988, pp. 91–105.

An overview of solid-state laser cross-link systems and technologies is presented. End-pumping of Nd:YAG lasers with semiconductor diode laser arrays has produced the highest efficiency (typically 6 to 9 percent of the total "wall-plug" efficiency) of all configurations tested thus far.

Caudill, L., "ACTS Laser Communication Experiment," Optical Technologies for Communication Satellite Applications, Los Angeles, California, January 21–22, 1986, *Proc. SPIE*, Vol. 616, p. 6 (abstract only).

Activities at NASA/Goddard Space Flight Center related to laser communications technology are described. The activities include the component development program at NASA/Goddard, details of the Advanced Communications Technology Satellite (ACTS) Laser ISL Communications Experiment scheduled for the 1990–1992 time frame, and brief mention of the Tracking and Data Acquisition System (TDAS) study performed by Ball Aerospace Systems Division and COMSAT Laboratories. Funding problems have subsequently led to termination of the ACTS Laser ISL Communications Experiment.

Forster, D. C., *et al.*, "Wide-Band Laser Communications in Space," *IEEE Journal of Quantum Electronics*, Vol. QE-8, No. 2, February 1972, pp. 263–272.

The CO_2 and Nd:YAG technologies are evaluated for use in a 1-Gbit/s ISL. The two systems are compared with respect to communications performance, weight/cost burden, and critical technological areas requiring further development.

***International Journal of Satellite Communications*, Special Issue on Intersatellite Links, Vol. 6, No. 2, April–June 1988.**

This special issue contains a number of overview papers on optical intersatellite links. Both systems and technology issues are discussed.

Katzman, M., "Laser Space Communication Technology Status," Control and Communication Technology in Laser Systems, San Diego, California, August 25–26, 1981, *Proc. SPIE*, Vol. 295, pp. 2–9.

The status of laser space communications technology in the early 1980s is assessed. Included are a discussion of the various available laser transmitters and a review of the state of development of modulation formats and technniques, optics design, and optical receivers.

Klein, B. J., and J. J. Degnan, "Optical Antenna Gain. 1: Transmitting Antennas," *Applied Optics*, Vol. 13, No. 9, September 1974, pp. 2134–2140.

Degnan, J. J., and B. J. Klein, "Optical Antenna Gain. 2: Receiving Antennas," *Applied Optics*, Vol. 13, No. 10, October 1974, pp. 2397–2401.

Degnan, J. J., and B. J. Klein, "Optical Antenna Gain. 2: Receiving Antennas. Errata," *Applied Optics*, Vol. 13, No. 12, December 1974, p. 2762.

Klein, B. J., and J. J. Degnan, "Optical Antenna Gain. 3: The Effect of Secondary Element Support Struts on Transmitter Gain," *Applied Optics*, Vol. 15, No. 4, April 1976, pp. 977–979.

This series of papers gives detailed calculations of the gain of transmitting and receiving optical antennas, including the effect of central obscuration. The general expressions derived here can be used in conjunction with the range equation to model ISL communications performance.

Koepf, G., "Technologies for Intersatellite Optical Communications," ESA Workshop on Space Laser Applications and Technology, Les Diablerets, Switzerland, March 26–30, 1984, *Proc.*, pp. P71–P76.

Various technologies applicable in intersatellite optical communications are reviewed. Advances in the areas of laser sources are discussed, including RF-excited CO_2 lasers, diode-pumped Nd:YAG lasers, optical power combining, and phased-array formation with GaAlAs lasers. A tradeoff is then presented between the selected systems with respect to mass, volume, prime power, and tracking requirements.

Koepf, G. A., *et al.*, "Analysis of Burst Error Occurrence on Optical Intersatellite Link (ISL) Design," Optical Technologies for Communication Satellite Applications, Los Angeles, California, January 21–22, 1986, *Proc. SPIE*, Vol. 616, pp. 129–136.

A method is described for analyzing the effect of tracking errors on the performance of optical ISLs. For a representative link configuration, it is concluded that link impairments due to burst errors can be limited to acceptable levels.

Lee, Y. S., "Technology Assessment for Implementation of Optical Intersatellite Link," IEEE International Conference on Communications, Denver, Colorado, June 14–18, 1981, *Conf. Rec.*, pp. 15.4.1–15.4.4.

The reliability of a diode-pumped Nd:YAG laser is assessed. In addition, key technological areas requiring further development and upgrading for the successful implementation of a diode-pumped Nd:YAG ISL system are identified.

Lee, Y. S., and R. E. Eaves, "Implementation Issues of Intersatellite Links for Future INTELSAT Requirements," IEEE International Conference on Communications, Boston, Massachusetts, June 19–22, 1983, *Conf. Rec.*, pp. E1.3.1–E1.3.7.

Microwave and optical systems are considered for both intracluster and interregional ISLs in future INTELSAT systems. The intracluster optical ISL uses a GaAlAs diode laser transmitter, whereas the interregional link considers both the frequency-doubled Nd:YAG laser and the GaAlAs diode laser.

Lutz, H., "Optical Inter-Satellite Links," *ESA Bulletin*, No. 45, February 1986, pp. 74–80.

This article reviews the development programs relating to optical ISLs which are being funded by the European Space Agency (ESA). ESA plans to use optical ISLs to link two telecommunications satellites in geostationary orbit, and for the high-speed transmission of data from a low earth-orbiting platform to the envisaged European Data-Relay Satellite. Prime consideration has been given to the CO_2 laser and the GaAlAs semiconductor laser for use in these ISLs. Initial activities concentrated on the definition of suitable system concepts, the elaboration of fundamental design solutions, and the experimental evaluation of basic laser communications principles. Development has progressed to the point where most of the critical units needed for the manufacture of a CO_2 laser ISL are at the laboratory breadboard stage.

Marshalek, R. G., and G. A. Koepf, "Comparison of Optical Technologies for Intersatellite Links," Optical Technologies for Communication Satellite Applications, Los Angeles, California, January 21–22, 1986, *Proc. SPIE*, Vol. 616, pp. 29–48. (A revision and expansion of this paper was published in *Optical Engineering*, Vol. 27, No. 8, August 1988, pp. 663–676.)

Six selected optical technologies are evaluated for use in a full-duplex communications link between geostationary satellites. The salient features of the various technologies are described, and their communications performance is analyzed to determine antenna diameter requirements for various modulation formats. Both digital and analog traffic from three wideband transponders are considered.

McIntyre, C., *et al.*, "Optical Components and Technology in Laser Space Communications Systems," *Proc. IEEE*, Vol. 58, No. 10, October 1970, pp. 1491–1503.

The optical properties of passive components commonly used in space optical communications systems are described. These passive components can be effectively and reliably used to implement acquisition, tracking, point-ahead, and background-noise-suppression functions. In addition, the systems can approach diffraction-limited performance to minimize transmitted beam divergence (*i.e.*, make efficient use of available optical transmitter power) and maximize tracking sensitivity.

***Proc. SPIE*, Vol. 756, "Optical Technologies for Space Communications Systems," Los Angeles, California, January 15–16, 1987.**
***Proc. SPIE*, Vol. 810, "Optical Systems for Space Applications," The Hague, The Netherlands, March 30–April 1, 1987.**
***Proc. SPIE*, Vol. 842, "Fiber Optics Reliability: Benign and Adverse Environments," San Diego, California, August 17–18, 1987.**
***Proc. SPIE*, Vol. 885, "Free Space Laser Communication Technologies," Los Angeles, California, January 11–13, 1988.**
***Proc. SPIE*, Vol. 992, "Fiber Optics Reliability: Benign and Adverse Environments II," Boston, Massachusetts, September 6–8, 1988.**
***Proc. SPIE*, Vol. 996, "High Data Rate Atmospheric and Space Communications," Boston, Massachusetts, September 8–9, 1988.**

These conference proceedings discuss up-to-date developments in optical ISL technology in the United States and Europe.

Sachdev, D. K., "Satellite Communication Technology Challenges for the 80's," AIAA 8th Communications Satellite Systems Conference, Orlando, Florida, April 20–24, 1980, *Proc.*, pp. 433–444.

This survey paper highlights some of the major technological developments in the satellite communications field anticipated during the 1980s, including ISLs, digital networks, on-board processing, and reconfigurable multiple-beam antennas. The emphasis is on those technology development programs which hold the promise of significantly increasing the spectrum utilization efficiency, capacity, and flexibility of next-generation satellite systems.

Sachdev, D. K., and T. Chidambaram, "Intersatellite Links for International Communications," IEEE International Conference on Communications, Denver, Colorado, June 14–18, 1981, *Conf. Rec.*, pp. 70.2.1–70.2.6.

This paper presents an overview of the INTELSAT R&D program in the 1978 to 1980 time frame as related to ISLs, including system studies and technology development. Potential applications of ISLs within a multisatellite communications system are discussed.

Sebacher, K. S., *et al.*, "Laser Crosslink Configurations for RF Satellite Communications Systems," IEEE Military Communications Conference, Boston, Massachusetts, October 20–23, 1985, *Conf. Rec.*, pp. 4.2.1–4.2.6.

The advantages of adding laser crosslinks to RF satellite communications systems are described. The characteristics of the required RF/optical interfaces on board the satellites are then discussed. Finally, terminal configurations that provide reliable, accurate laser communications are described for frequency-division multiple-access (FDMA) and time-division multiple-access (TDMA) traffic.

Sinha, A. K., "Optical Intersatellite Links," *COMSAT Technical Review*, Vol. 10, No. 2, Fall 1980, pp. 369–395.

A tradeoff analysis is presented for an ISL between geostationary satellites which uses a frequency-doubled Nd:YAG transmitter laser. The link performance is presented as a function of such parameters as angular separation between satellites, aperture diameter, data rate, and duty cycle. Some of the results are then compared with those obtained for ISL systems using CO_2, GaAs, HeNe, and Nd:YAG laser transmitters.

Svorec, R. W., "Parametric Performance Analysis of Spaceborne Laser Communication Systems," Control and Communication Technology in Laser Systems, San Diego, California, August 25–26, 1981, *Proc. SPIE*, Vol. 295, pp. 66–74.

General link performance calculations are given for an ISL based on either a GaAs diode laser (1 Mbit/s) or a frequency-doubled Nd:YAG laser (1 Gbit/s). Link performance is calculated with and without the presence of an optical background from starlight or the sun.

Svorec, R. W., and F. R. Gerardi, "Space Laser Communications," *Photonics Spectra*, Vol. 18, No. 4, April 1984, pp. 78–81.

This paper discusses several of the characteristic features and requirements of optical ISLs. It also mentions an ISL system approach which uses a transmitter source consisting of an InGaAsP semiconductor diode laser followed by a Nd:YAG optical power amplifier. This transmitter design was suggested by M. Katzman of the Aerospace Corporation.

Tucker, J. B., "Lasers to Bridge Satellites," *High Technology*, Vol. 6, No. 7, July 1986, pp. 56–59.

This general overview discusses the optical ISL systems under development in West Germany, France, and the United States.

Welti, G. R., "Intersatellite Link for Multiple Access Telephony," IEEE Electronics and Aerospace Systems Convention (EASCON), Arlington, Virginia, September 25–27, 1978, *Convention Record*, pp. 432–440.

This is an early publication on ISLs for INTELSAT applications. A bidirectional ISL is analyzed with carrier frequencies of 25 and 32 GHz, using FM remodulation of a composite baseband signal which consists of three 40-MHz frequency-division multiplex (FDM)/FM transmission channels. An implementation approach for the ISL (10° satellite separation) is described, and weight and power requirements are analyzed.

Carbon dioxide laser ISLs

The references in this category discuss the carbon dioxide gas laser communications technology and its use in ISL applications. Areas discussed include general systems studies, hardware development activities, CO_2 laser development and lifetime, and developments on heterodyne receivers. Much of the work reported in this area has been funded by NASA and by the European Space Agency (ESA).

Bonek, E., and H. Lutz, "CO_2 Laser Communication Technology for Intersatellite Data Links," *ESA Journal*, Vol. 5, No. 2, 1981, pp. 83–98.

A detailed description is given of CO_2 laser communications technology as developed through ESA funding. A representative data link between a low-altitude, remote-sensing satellite and a geostationary data-relay platform is analyzed in detail to illustrate how CO_2 technology could eventually be implemented. Analytical results are given to show the influence of ISL system parameters on the weight, prime power, and size of a satellite-borne CO_2 laser terminal.

Bonek, E., *et al.*, "Optical PLLs See the Light," *Microwaves and RF*, Vol. 22, No. 12, December 1983, pp. 65–70.

This review article discusses the basic principles of optical homodyne receivers, with emphasis on receivers for CO_2 laser communications systems. Design specifics are given for an optical phase-locked loop (PLL), which is an essential element of a homodyne receiver.

Cheo, P. K., and R. Wagner, "Infrared Electrooptic Waveguides," *IEEE Journal of Quantum Electronics*, Vol. QE-13, No. 4, April 1977, pp. 159–164.

The design, fabrication, and performance of low-loss, infrared, optical waveguides suitable for broadband electrooptic modulation of high-power CO_2 lasers are described.

Christensen, C. P., *et al.*, "Transverse Electrodeless RF Discharge Excitation of High-Pressure Laser Gas Mixtures," *IEEE Journal of Quantum Electronics*, Vol. QE-16, No. 9, September 1980, pp. 949–954.

Self-sustained discharge excitation of CO_2, Xe, F, and HF laser transitions using a transverse electrodeless RF configuration operating at an RF frequency of 30 MHz is investigated. Homogeneous, long-duration excitation of high-pressure laser gas mixtures is demonstrated, and the operating characteristics associated with the four laser species in the discharge environment are explored.

Degnan, J. J., "The Waveguide Laser: A Review," *Applied Physics*, Vol. 11, No. 1, September 1976, pp. 1–33.

This paper reviews the fundamental physical principles of waveguide gas and liquid lasers, and the current technological state of these devices. Applications of waveguide lasers and a wide variety of laser configurations are also discussed. Areas examined include the properties of modes in hollow dielectric waveguides of circular, rectangular, and planar cross section; various approaches to optical feedback, including internal and external mirror Fabry-Perot-type resonators, hollow waveguide distributed-feedback structures, and ring resonant configurations; and the design and optimization of waveguide gas lasers.

Goodwin, F. E., and R. T. Luke, "Millimeter Wave and Laser Satellite Communications System Comparison," International Conference on Lasers, Orlando, Florida, December 11–15, 1978, *Proc.*, pp. 349–360.

Millimeter-wave and CO_2 laser technologies are compared for use in ISL applications. A 100-Mbit/s link is considered between a low-orbit, data-gathering satellite and a geosynchronous data-relay satellite, and weight and power estimates are generated for both technologies.

Laakmann, K. D., "Transverse RF Excitation for Waveguide Lasers," International Conference on Lasers, Orlando, Florida, December 11–15, 1978, *Proc.*, pp. 741–743.

Cathodeless transverse RF excitation in waveguide lasers has been successfully demonstrated and shown to alleviate many of the problems associated with high-pressure, self-sustained discharges. This RF excitation scheme allows a considerable reduction in device complexity and size, as well as an improvement in performance compared to longitudinal DC excitation.

Laakmann, K. D., "Problems and Status of Reliability in RF-Excited Waveguide Lasers," Laser and Laser Systems Reliability, Los Angeles, California, January 28–29, 1982, *Proc. SPIE*, Vol. 328, pp. 2–6.

The history and status of RF-excited CO_2 waveguide lasers manufactured by Laakmann Electro-Optics, Inc., are outlined. Specific problems such as gas leaks, outgassing, and optics damage, as well as solutions to these problems, are discussed. It is concluded that no major problems remain in the tubes, so that 97 percent of them should perform at specified power for at least 1,000 hours of operation over a year. This still falls far short of the lifetime requirements for an optical ISL application.

Leeb, W. R., and A. L. Scholtz, "Single-Mode Laser Frequency Modulation," *IEEE Journal of Quantum Electronics*, Vol. QE-13, No. 11, November 1977, pp. 925–929.

The frequency response of an internally frequency-modulated single-mode laser is analyzed using a method based on the combined concepts of

an active Fabry-Perot interferometer and internal phase modulation. For modulating frequencies that are lower than the cavity mode spacing, the laser generates an ideally frequency-modulated signal. At higher modulating frequencies, the sideband amplitude *vs* modulating frequency characteristics exhibit oscillatory behavior.

Leeb, W. R., and A. L. Scholtz, "Homodyne Receiver Concepts for CO_2 Laser Intersatellite Links," Optical Technologies for Communication Satellite Applications, Los Angeles, California, January 21–22, 1986, *Proc. SPIE*, Vol. 616, pp. 84–91.

A laboratory breadboard model of a 140-Mbit/s optical linear phase-locked-loop homodyne receiver for detection of CO_2 laser radiation is described. A measurement of receiver sensitivity for a phase-shift-keyed modulation format is reported which is 4 dB above the theoretical value.

Malk, E. G., and I. A. Ramsay, "Reliability Factors in Gas Lasers," Laser and Laser Systems Reliability, Los Angeles, California, January 28–29, 1982, *Proc. SPIE*, Vol. 328, pp. 7–14.

Factors influencing the reliability of helium-neon and sealed-off waveguide CO_2 lasers are discussed. For the CO_2 lasers, the lifetime degradation factors are identified as CO_2 dissociation, contaminant buildup, cathode sputtering, mirror degradation, and hermetic seal defects or deterioration. Life tests have been performed that resulted in commercial waveguide CO_2 laser lifetime expectancies in excess of 1 year.

McElroy, J. H., "Carbon Dioxide Laser Systems for Space Communications," IEEE International Conference on Communications, San Francisco, California, June 8–10, 1970, *Conf. Rec.*, pp. 22–27 to 22–37.

This early publication from NASA discusses the use of CO_2 lasers for space communications links. An analysis is presented for CO_2 laser links from a synchronous satellite to the ground, from a low-altitude satellite to a synchronous satellite, from a synchronous satellite to a synchronous satellite, and from a Mars probe to either a ground station or a synchronous satellite. The key technological areas of the CO_2 link are also reviewed.

McElroy, J. H., *et al.*, "Spaceborne CO_2 Laser Communication Systems," IEEE Electronics and Aerospace Systems Convention (EASCON), Washington, D.C., September 29–October 1, 1975, *Convention Record*, pp. 176-A to 176-P.

A NASA-funded program to develop the technology for CO_2 laser ISLs is described in detail. This program included component, subsystem, and system development relating to spaceborne CO_2 laser communications systems, and led to the development of an engineering model transceiver capable of transmitting and receiving data at 300 Mbit/s. This paper is a preliminary version of the extended paper by J. H. McElroy *et al.*, published in *Proc. IEEE*, February 1977.

McElroy, J. H., *et al.*, "CO_2 Laser Communication Systems for Near-Earth Space Applications," *Proc. IEEE*, Vol. 65, No. 2, February 1977, pp. 221–251.

This classic reference gives a detailed description of the NASA-sponsored research program on CO_2 ISLs undertaken from 1971 to 1975. The component and subsystem developments, link communications performance, and system weight/power requirements are discussed. This program effectively established the technical feasibility of spaceborne CO_2 laser communications systems, including links between low-earth orbit and geosynchronous satellites, and between two geosynchronous satellites.

Philipp, H. K., *et al.*, "Costas Loop Experiments for a 10.6 μm Communications Receiver," *IEEE Transactions on Communications*, Vol. COM-31, No. 8, August 1983, pp. 1000–1002.

A Costas-type, nonlinear phase-locked loop for use as a CO_2 laser communications receiver at 10.6 μm is described. The ability of the optical Costas loop to regenerate the carrier of a binary phase-shift-keyed input signal and to perform coherent demodulation is demonstrated at a data rate of 20 Mbit/s.

Reiland, W., *et al.*, "Optical Intersatellite Communication Links: State of CO_2 Laser Technology," Optical Technologies for Communication Satellite Applications, Los Angeles, California, January 21–22, 1986, *Proc. SPIE*, Vol. 616, pp. 69–76.

This paper describes the baseline design of an optical ISL communications system using CO_2 laser technology, and reports on the status of the relevant technologies and the various ongoing hardware development activities. This program, funded by ESA and the German Aerospace Establishment/Ministry of Research and Technology (DFVLR), is aimed primarily toward laboratory breadboarding and full operational testing of the system, with the potential of space-qualifying all hardware components for experimental in-flight testing in the early 1990s. Because of recent increased interest in direct-detection semiconductor diode laser technology, a slowdown is noted in ESA's CO_2 laser technology program.

Scholtz, A. L., *et al.*, "Realization of a 10-μm Homodyne Receiver," *Journal of Lightwave Technology*, Vol. LT-5, No. 4, April 1987, pp. 625–632.

A 140-Mbit/s, DC-coupled, phase-locked-loop (PLL) homodyne optical receiver at 10.6 μm is reported. Locking of the PLL receiver to a 3-nW carrier is demonstrated. Phase-modulated 140-Mbit/s input signals with sideband powers as low as 0.12 nW were demonstrated at a 10^{-6} bit error rate, corresponding to a receiver sensitivity some 3 dB above the shot noise limit. This was achieved using a HgCdTe photovoltaic detector and preamplifier mechanically cooled to 80 K. This receiver system is part of a breadboard of an ISL data link.

Nd:YAG laser ISLs

The following papers describe the Nd:YAG solid-state laser communications technology and its use in ISL applications. Areas discussed include general systems studies, space-qualifiable hardware development activities, and ground-to-ground and aircraft-to-ground transmission tests performed for the United States Air Force (USAF), a major funding source in this technology.

Barry, J. D., *et al.*, "1000-Mbit/s Intersatellite Laser Communication System Technology," *IEEE Transactions on Communications*, Vol. COM-24, No. 4, April 1976, pp. 470–478.

The major technological advances which were achieved in developing a 1-Gbit/s Nd:YAG laser engineering feasibility model are described.

Chinn, S. R., *et al.*, "Low-Threshold Transversely Excited NdP_5O_{14} Laser," *Applied Optics*, Vol. 15, No. 6, June 1976, pp. 1444–1449.

The lasing threshold and optical power conversion efficiency of a transversely excited, continuous-wave (CW) NdP_5O_{14} laser were measured with 0.58-μm excitation from a dye laser and 0.8-μm excitation from a semiconductor laser. Using an AlGaAs double-heterostructure diode laser pump, quasi-CW lasing was obtained in NdP_5O_{14} with typically 7-mW threshold power and 7-percent efficiency. This lasing medium has potential application in a duplex ISL which uses a Nd:YAG laser in the opposite direction.

Denton, R. T., *et al.*, "Lithium Tantalate Light Modulators," *Journal of Applied Physics*, Vol. 32, No. 4, March 1967, pp. 1611–1617.

Baseband optical intensity modulators fabricated using single-domain $LiTaO_3$ as the modulating material are described. A broadband transistor driver-amplifier was developed, and 80-percent intensity modulation was achieved in a double-pass modulator from DC to 220 MHz.

Mason, R. S., "Laser Communication via an Atmospheric Link," National Telecommunications Conference, Houston, Texas, November 30–December 4, 1980, *Conf. Rec.*, pp. 27.1.1–27.1.9.

A detailed description is given of the prototype Nd:YAG transceiver system developed by McDonnell-Douglas Astronautics Company for the USAF LASERCOM program. Descriptions of the transceiver components, several system-related issues, and the acquisition sequence are included. Finally, several tests established by the USAF to evaluate the transceiver system performance are described. Of particular interest are the 1-Gbit/s ground-to-ground and aircraft-to-ground transmission tests, with the latter including a demonstration of full acquisition and mutual tracking.

Maynard, J. A., *et al.*, "Multi-Gigabit Laser Communications for Satellite Cross-Links," 4th International Conference on Digital Satellite Communications, Montreal, Canada, October 23–25, 1978, *Proc.*, pp. 155–159.

An approach is discussed for extending a 1-Gbit/s Nd:YAG engineering feasibility model to multigigabit-per-second applications. No major developments are required for extension to an even higher data rate capability.

Rice, R. R., and G. H. Burkhart, "Efficient Mode-Locked Frequency-Doubled Operation of an Nd:$YAlO_3$ Laser," *Applied Physics Letters*, Vol. 19, No. 7, October 1971, pp. 225–227.

Short mode-locked pulses are observed from a frequency-doubled Nd:$YAlO_3$ laser, with a second harmonic conversion efficiency of 50 percent. The laser was mode-locked and frequency-doubled by using a single $Ba_2NaNb_5O_{15}$ crystal. This lasing medium has potential application in a duplex ISL that uses a Nd:YAG laser in the opposite direction.

Rice, R. R., *et al.*, "A Barium Sodium Niobate Acousto-Optic Mode Locker/Frequency Doubler (AOML/FD) for Nd:YAG," *Journal of Applied Physics*, Vol. 47, No. 7, July 1976, pp. 3045–3053.

The use of a single $Ba_2NaNb_5O_{15}$ crystal to acousto-optically mode-lock and frequency-double a Nd:YAG laser is reported. The characteristics of a TEM_{oo} Nd:YAG laser frequency-doubled and mode-locked at 500 MHz using the AOML/FD are described. Furthermore, some of the AOML/FD units have been shock and vibration tested to prototype space-qualifiable model acceptance levels for use in an engineering feasibility model USAF laser space communications subsystem. Long life, high reliability, and rugged construction are demonstrated.

Roland, J. R., and C. E. Whited, "Air Force Space Laser Communications," International Telemetering Conference, Los Angeles, California, November 14–16, 1978, *Proc.*, Vol. 14, pp. 339–346.

This paper provides a general review of the Air Force Space Laser Communications Program which led to development of a 1-Gbit/s Nd:YAG communications system in the mid-1970s, with potential applications in satellite-to-satellite and satellite-to-aircraft links. The status of the technology, airborne flight demonstrations, system characteristics, and potential system applications are discussed.

Ross, M., *et al.*, "Measured Performances of 1 Gbps Short Pulse Laser Communication and Acquisition and Tracking Systems," National Telecommunications Conference, Atlanta, Georgia, November 26–28, 1973, *Conf. Rec.*, pp. 30A-1 to 30A-7.

The brassboard performance of both the communications subsystems and the acquisition and tracking subsystems for a 1-Gbit/s Nd:YAG laser space communications system is presented. For the communications tests, both multiple-channel TV and 1-Gbit/s pseudorandom data were transmitted, remotely synchronized, and detected at the receiver. The TV signal was converted to a serial digital pulse train and reconstructed after detection. For the acquisition and tracking subsystem, the brassboard demonstrated coarse acquisition, fine acquisition, and fine tracking automatically.

Ross, M., "Direct Photodetection Space Laser Communications," IEEE Electronics and Aerospace Systems Convention (EASCON), Washington, D.C., September 29–October 1, 1975, *Convention Record*, pp. 174-A to 174-H.

The 1-Gbit/s Nd:YAG laser/direct photodetection space communications system is described in detail. Critical components such as the laser, modulator, detector, high-speed electronics, and acquisition and tracking system are discussed.

Ross, M., *et al.*, "Space Optical Communications With the Nd:YAG Laser," *Proc. IEEE*, Vol. 66, No. 3, March 1978, pp. 319–344.

This classic reference describes the Nd:YAG laser space communications system developed at McDonnell-Douglas Astronautics Company and the Air Force Avionics Laboratory under funding from the U.S. Air Force. System components and an engineering feasibility model of the 1,000-Mbit/s system are described in detail.

Ross, M., *et al.*, "Space Laser Communications Systems for the Eighties," AIAA 8th Communications Satellite Systems Conference, Orlando, Florida, April 20–24, 1980, *Proc.*, pp. 739–745.

A series of communications field tests are described which are intended to extend the laboratory results previously obtained for the 1-Gbit/s Nd:YAG

laser communications system. These include ground-to-ground, aircraft-to-ground, and aircraft-to-satellite link tests. Results are given for the ground-to-ground tests, which demonstrated the performance of the 1-Gbit/s laser communications system through the atmosphere over a 2.1-km range.

Sharp, E. J., *et al.*, "High-Efficiency Nd^{3+}:$LiYF_4$ Laser," *Journal of Applied Physics*, Vol. 44, No. 12, December 1973, pp. 5399–5401.

Pulsed room-temperature laser action is reported in Nd^{3+}:$LiYF_4$ at 1.053 μm. The performance of the Nd^{3+}:$LiYF_4$ crystal is measured and compared to Nd^{3+}:YAG data taken in the same laser cavity. This lasing medium has potential application in a duplex ISL that uses a Nd:YAG laser in the opposite direction.

Siegman, A. E., and J. Heritier, "Analysis of Mode-Locked and Intracavity Frequency-Doubled Nd:YAG Laser," *IEEE Journal of Quantum Electronics*, Vol. QE-16, No. 3, March 1980, pp. 324–335.

Analytical and computer studies of the continuous-wave, mode-locked, and intracavity frequency-doubled Nd:YAG laser are presented. Simple analytical results for on-resonance pulse shape, pulse width, signal intensity, and harmonic conversion efficiency in terms of basic laser parameters are derived. Agreement is found between the analytical model and experimental studies.

Smith, R. J., *et al.*, "100 mW Laser Diode Pumped Nd:YAG Laser," Advances in Laser Engineering and Applications, San Diego, California, July 31–August 1, 1980, *Proc. SPIE*, Vol. 247, pp. 144–148.

This paper reports on a Nd:YAG laser that uses continuous-wave, room temperature injection lasers as pump sources. It was constructed and proven capable of 100-mW polarized output at 1.06 μm, with a prime power input to the injection laser arrays of 25 W. The potential for stable, long-life operation, together with its low power consumption, makes this laser an ideal source for space-borne applications.

Whitmer, R. F., "A 1-Gbps Laser Communication System Using QPSK Modulation," National Telecommunications Conference, Atlanta, Georgia, November 26–28, 1973, *Conf. Rec.*, pp. 30C-1 to 30C-4.

The performance of a Nd:YAG laser link using a QPSK-subcarrier intensity modulation format is evaluated experimentally. Under full operation with two asynchronous 500-Mbit/s input data streams, the laser link performs within 3 dB of the predicted performance at a 10^{-6} bit error rate.

Wolf, J. D., *et al.*, "Application of Nd:YAG Optical Communications Technology for Aircraft to Satellite Links," IEEE Electronics and Aerospace Systems Convention (EASCON), Arlington, Virginia, October 9–11, 1979, *Convention Record*, pp. 286–294.

A functional description is given for a general-purpose satellite laser receiver which allows users in a wide area of uncertainty to access a low-data-rate (~100-bit/s) multiple-access receiver. The integrated package also allows a high-data-rate (1-Gbit/s) communications link to be established from aircraft to a satellite. The geographic coverage advantages of small optical antennas in flush-mounted aircraft installations are shown for typical satellite orbits.

GaAlAs laser/direct-detection ISLs

The following references discuss the use of a GaAlAs semiconductor diode laser and a direct-detection optical receiver in ISL applications. Funding in this area is largely from ESA and NASA.

Barnoski, M. K., ed., *Fundamentals of Optical Fiber Communications*, 2nd ed., New York: Academic Press, 1981.

Basch, E. E., ed., *Optical-Fiber Transmission*, Indianapolis, Indiana: Howard W. Sams & Co., 1986.

Kressel, H., ed., *Semiconductor Devices for Optical Communications*. Vol. 39 of *Topics in Applied Physics*, Berlin: Springer-Verlag, 1980.

Personick, S. D., *Optical Fiber Transmission Systems*, New York: Plenum Press, 1981.

Centro Studie Laboratori Telecommunicazioni (CSELT), *Optical Fibre Communication*, New York: McGraw-Hill, 1981.

These textbooks cover various aspects of direct-detection optical communications systems, with an emphasis on fiber optic applications. Because much of the material discussed is of a general nature, it is also useful in evaluating the performance of optical ISLs.

Barry, J. D., and G. S. Mecherle, "LPI Optical Communication System," IEEE Military Communications Conference, Los Angeles, California, October, 21–24, 1984, *Conf. Rec.*, pp. 259–262.

This paper reports on the development and demonstration of a GaAlAs direct-detection, free-space optical communications system with low probability of intercept (LPI) properties. The 20-kbit/s LPI prototype system has been used to establish a link between a company roof house and a helicopter at a range of 8 to 10 miles.

Frecon, L., and E. Sein, "Optical Intersatellite Data Links With Semiconductor Laser," 35th Congress of the International Astronautical Federation, Lausanne, Switzerland, October 7–13, 1984, Paper No. IAF-84-69.

The fundamentals of a diode laser space data link are reviewed for both direct-detection and heterodyne-detection systems. Three links are analyzed in detail: a return data link between a low-earth orbiter and a geostationary relay satellite, a two-way link between geostationary satellites, and a return link from a planetary probe toward a relay satellite. Direct-detection systems are considered in each case, and weight and power requirements are estimated for the first two missions.

Frecon, L., *et al.*, "The Use of Optical Intersatellite Links for the European Relay System," Optical Technologies for Communication Satellite Applications, Los Angeles, California, January 21–22, 1986, *Proc. SPIE*, Vol. 616, pp. 49–68.

Details of the ESA-sponsored European Data Relay System (DRS) are discussed. This program is scheduled to provide optical telecommunications links between low-earth orbiting spacecraft and the DRS satellite positioned in geosynchronous orbit, and between two DRS satellites. Implementation of this program is scheduled for the 1993–1994 time frame. A detailed baseline design for the optical links in the DRS is also presented. This design is based on GaAlAs semiconductor diode laser transmitters and direct-detection receivers with silicon avalanche photodiodes.

Seaman, W. A., Jr., and R. A. Lewis, "Free-Space Laser Communication Terminals," IEEE Military Communications Conference, Boston, Massachusetts, October 20–23, 1985, *Conf. Rec.*, pp. 94–97.

This paper reports on the development of free-space laser communications terminals capable of acquiring and communicating over a 100-mi range at a data rate of up to 19.2 kbit/s. The communications subsystem of the terminals uses a GaAlAs diode laser array source, a 256-slot pulse-position modulation (PPM) format, and a quadrant of direct-detection silicon avalanche photodiode (APD) receivers. The acquisition, tracking, and communications functions of these terminals were recently demonstrated in an aircraft-to-aircraft link over an 80-km range (see *Laser Focus*, Vol. 22, No. 7, July 1986, pp. 40–42).

Sein, E., *et al.*, "400-Mbit Optical Telecommunications Link Between a Geostationary Satellite and a Low Earth Orbiter," Conference on Lasers and Electro-Optics, Baltimore, Maryland, May 21–24, 1985, *Technical Digest*, pp. 30–31.

A 400-Mbit/s optical link between a low-earth orbiter and a geostationary satellite is considered. The link uses wavelength-division multiplexing of two 200-Mbit/s channels operating at wavelengths of 0.82 and 0.85 μm, and direct-detection receivers. Details of the link performance and the optical system layout are presented.

GaAlAs laser/heterodyne-detection ISLs

The references in this category address the use of a GaAlAs diode laser and a heterodyne-detection optical receiver in ISL applications. Areas examined include critical system and technology issues, phase and frequency tracking considerations, heterodyne receiver development, and transmitter and local oscillator laser linewidth requirements. The USAF is a major sponsor of work in this area.

Abbas, G. L., and V. W. S. Chan, "Optimal Design and Performance of a Dual-Detector Optical Heterodyne Receiver for Local Oscillator Noise Suppression," IEEE Global Telecommunications Conference, San Diego, California, November 28–December 1, 1983, *Conf. Rec.*, pp. 12.5.1–12.5.6.

Abbas, G. L., *et al.*, "A Dual-Detector Optical Heterodyne Receiver for Local Oscillator Noise Suppression," *Journal of Lightwave Technology*, Vol. LT-3, No. 5, October 1985, pp. 1110–1122.

These papers discuss optical heterodyne receivers that use two photodetectors in a balanced-mixer configuration. Such a design suppresses excess photodetection noise resulting from wideband amplitude fluctuations of the local oscillator laser, and can provide near quantum-limited performance. The ultimate receiver sensitivity achievable in such noise-cancelling receivers is analyzed, and suggestions are provided for optimum receiver designs.

Abbas, G. L., *et al.*, "Near Quantum-Limited Operation of a GaAlAs Laser-Heterodyne Communication System," Conference on Lasers and Electro-Optics, Baltimore, Maryland, May 21–24, 1985, *Technical Digest*, pp. 52–53.

Experimental results are reported for a frequency-shift keyed optical heterodyne communications system using GaAlAs diode lasers as both the source and the local oscillator. The system data rate is continuously variable between 50 and 250 Mbit/s, and a communications performance within 1 to 2 dB of the ideal is reported.

Alexander, S. B., "Design of Wide-Band Optical Heterodyne Balanced Mixer Receivers," *Journal of Lightwave Technology*, Vol. LT-5, No. 4, April 1987, pp. 523–537.

Design and characterization techniques for balanced mixer optical receivers are discussed, assuming a heterodyne communications system based on semiconductor diode lasers. Simple circuit models illustrating the noise performance, small signal gain, and bandwidth of the receiver are developed. An example design is given for an optical heterodyne receiver operating within 1 dB of the quantum limit, with a +1-dB flat bandwidth of 1 GHz. The design and measurement techniques presented are applicable to most optical heterodyne balanced mixer applications.

Brain, M. C., *et al.*, "Performance Requirements for Devices and Components for Field Application of Coherent Optical Communications Systems," High Frequency Optical Communications, Cambridge, Massachusetts, September 23–24, 1986, *Proc. SPIE*, Vol. 716, pp. 153–161.

This paper reviews the performance required of devices and components for coherent systems, and considers the developments needed to bridge the gap between laboratory demonstration and field application.

Chan, V. W. S., "Coherent Optical Space Communications System Architecture and Technology Issues," Control and Communication Technology in Laser Systems, San Diego, California, August 25–26, 1981, *Proc. SPIE*, Vol. 295, pp. 10–17.

Important optical communications system architectures and critical system and technology issues that affect ISL designs are examined. Coherent (heterodyne or homodyne) systems are compared to incoherent (direct-detection) systems in the context of space communications, including a discussion of the advantages and disadvantages of each approach.

Chan, V. W. S., *et al.*, "Heterodyne Lasercom Systems Using GaAs Lasers for ISL Applications," IEEE International Conference on Communications, Boston, Massachusetts, June 19–22, 1983, *Conf. Rec.*, pp. E1.5.1–E1.5.7.

Chan, V. W. S., "Space Coherent Optical Communication Systems—An Introduction," *Journal of Lightwave Technology*, Vol. LT-5, No. 4, April 1987, pp. 633–637.

Critical technology and system issues for space optical heterodyne communications systems using GaAlAs diode lasers are discussed. Based on present state-of-the-art technologies, it is concluded that an efficient optical ISL can be realized with a few years of development.

Cohen, S. C., "Heterodyne Detection: Phase Front Alignment, Beam Spot Size, and Detector Uniformity," *Applied Optics*, Vol. 14, No. 8, August 1975, pp. 1953–1959.

This paper extends the results given in the Fink paper (*Applied Optics*, Vol. 14, No. 3, p. 689) to include combinations of Airy, Gaussian, uniform signal, and local oscillator distributions. Effects of nonuniformities in the detector quantum efficiency are also analyzed.

Fink, D., "Coherent Detection Signal-to-Noise," *Applied Optics*, Vol. 14, No. 3, March 1975, pp. 689–690.

General expressions are derived for the signal-to-noise ratio of an optical heterodyne receiver in terms of the distribution functions of the signal and local oscillator (LO) fields and the size and shape of the detector. Two cases are considered: the signal and LO are matched Airy functions, and the signal is an Airy function and the LO is uniform over a circular detector.

***Journal of Lightwave Technology*, Special Issue on Coherent Communications, Vol. LT-5, No. 4, April 1987.**

This special issue gives an up-to-date review of progress in coherent optical communications systems. Many of the items discussed are pertinent to a CO_2 heterodyne-detection ISL, and more particularly to a GaAlAs heterodyne-detection ISL communications subsystem.

Kaufmann, J. E., "Phase and Frequency Tracking Considerations for Heterodyne Optical Communications," International Telemetering Conference, San Diego, California, September 28–30, 1982, *Proc.*, pp. 123–136.

This paper examines a phase-locked loop approach to provide phase tracking in an optical binary phase-shift keying (BPSK) heterodyne communications system, and two forms of frequency tracking for an M-ary frequency-shift keying (MFSK) heterodyne system. Using a statistical model for laser frequency instability, the performance of these schemes is calculated by linear analysis of the tracking loop in the small-error regime.

Kaufmann, J. E., and L. L. Jeromin, "Optical Heterodyne Intersatellite Links Using Semiconductor Lasers," IEEE Global Telecommunications Conference, Atlanta, Georgia, November 26–29, 1984, *Conf. Rec.*, pp. 28.4.1–28.4.8.

Optical heterodyne communications systems are considered for ISL applications. Key system design issues and the expected performance of such systems are discussed. Heterodyne receiver and transmitter technology using semiconductor diode lasers is also summarized.

Kazovsky, L. G., "Impact of Laser Phase Noise on Optical Heterodyne Receivers," Conference on Lasers and Electro-Optics, Baltimore, Maryland, May 21–24, 1985, *Technical Digest*, pp. 32–33.

Kazovsky, L. G., "Performance Analysis and Laser Linewidth Requirements for Optical PSK Heterodyne Communications," *Journal of Lightwave Technology*, Vol. LT-4, No. 4, April 1986, pp. 415–425.

Kazovsky, L. G., "Impact of Laser Phase Noise on Optical Heterodyne Communication Systems," *Journal of Optical Communications*, Vol. 7, No. 2, June 1986, pp. 66–78.

In these papers, the impact of transmitter and local oscillator laser phase noise on the performance of optical heterodyne communications receivers is analyzed in terms of the system signal-to-noise ratios and bit error rates. The analysis results in the determination of laser linewidth requirements for a variety of modulation and demodulation techniques. Amplitude-shift keyed, frequency-shift keyed, and phase-shift keyed systems are considered.

Kimura, T., and Y. Yamamoto, "Review: Progress of Coherent Optical Fiber Communication Systems," *Optical and Quantum Electronics*, Vol. 15, No. 1, January 1983, pp. 1–39.

This review of coherent fiber optic communications systems addresses such areas as modulation and demodulation techniques, frequency stabilization of diode lasers, AM and FM quantum noises and their reduction, and expected system performance and future problems.

Lowney, S. D., and D. V. L. Marquis, "Frequency Acquisition and Tracking for Optical Heterodyne Communication Systems," *Journal of Lightwave Technology*, Vol. LT-5, No. 4, April 1987, pp. 538–550.

A frequency acquisition and tracking system for optical heterodyne communications systems that use semiconductor diode lasers is described, with emphasis on frequency acquisition. Analytical models for acquisition and tracking are used to predict performance; the probability of incorrect acquisition is predicted for the frequency acquisition system; and rms error is predicted for the frequency tracker. Experimental data are presented and compared to the analytic results.

Okoshi, T., and K. Kikuchi, "Heterodyne-Type Optical Fiber Communications," *Journal of Optical Communications*, Vol. 2, No. 3, September 1981, pp. 82–88.

Okoshi, T., "Heterodyne and Coherent Optical Fiber Communications: Recent Progress," *IEEE Transactions on Microwave Theory and Techniques*, Vol. MTT-30, No. 8, August 1982, pp. 1138–1149.

Okoshi, T., "Recent Progress in Heterodyne/Coherent Optical-Fiber Communications," *Journal of Lightwave Technology*, Vol. LT-2, No. 4, August 1984, pp. 341–345.

These review papers discuss the basic characteristics of coherent fiber optic communications systems. Several of the issues addressed are relevant for free-space coherent optical communications.

Okoshi, T., "Recent Advances in Coherent Optical Fiber Communication Systems," *Journal of Lightwave Technology*, Vol. LT-5, No. 1, January 1987, pp. 44–52.

Recent advances in research on coherent optical fiber communications systems are reviewed, with emphasis on those results reported in 1984 and 1985. Bit error rate measurements are reported for amplitude-shift keying (ASK), frequency-shift keying (FSK), phase-shift keying (PSK), and differential phase-shift keying (DPSK) systems, and the state-of-the-art of polarization-state stabilization technique is discussed.

Smith, D. W., "Coherent Fiberoptic Communications," *Laser Focus*, Vol. 21, No. 11, November 1985, pp. 92–106.

The characteristics of coherent optical communications systems are reviewed, and future developments needed to realize the full potential of this technology are briefly addressed.

Swanson, E. A., and V. W. S. Chan, "Spatial Tracking System for Heterodyne Optical Communication," IEEE Military Communications Conference, Los Angeles, California, October 21–24, 1984, *Conf. Rec.*, pp. 253–258.

Swanson, E. A., and V. W. S. Chan, "Heterodyne Spatial Tracking System for Optical Space Communication," *IEEE Transactions on Communications*, Vol. COM-34, No. 2, February 1986, pp. 118–126.

The performance of an optical spatial tracking system which uses heterodyne detection is presented. The system is assumed to operate in its linear region, use semiconductor lasers, and use a squaring loop to combat the frequency noise caused by the lasers. Preliminary experimental results are also presented.

Yamamoto, Y., and T. Kimura, "Coherent Optical Fiber Transmission Systems," *IEEE Journal of Quantum Electronics*, Vol. QE-17, No. 6, June 1981, pp. 919–935.

This paper presents a comprehensive review of coherent fiber optic transmission systems, addressing such items as system configuration, modulation-demodulation technology, source frequency noise, transmission capacity, and repeater spacing.

Diode laser sources

The references in this category discuss the general properties of semiconductor diode laser sources, with emphasis on those properties of utmost importance in a free-space optical communications system. The areas stressed are high-power transmitters using either a single diode or power-combining of several diodes, diode reliability, and diode modulation characteristics.

Barry, J. D., "Design and System Requirements Imposed by the Selection of GaAs/GaAlAs Single-Mode Laser Diodes for Free Space Optical Communications," *IEEE Journal of Quantum Electronics*, Vol. QE-20, No. 5, May 1984, pp. 478–491.

Several important properties of GaAlAs semiconductor diode lasers are discussed and related to the use of such sources in a free-space optical communications system. It is concluded that the operating features of the GaAlAs diode laser impose restrictions on the system design and generate additional requirements for the development and use of the system.

Barry, J. D., *et al.*, "Thermally Accelerated Life Testing of Single-Mode, Double-Heterostructure, AlGaAs Laser Diodes Operated Pulsed at 50 mW Peak Power," *IEEE Journal of Quantum Electronics*, Vol. QE-21, No. 4, April 1985, pp. 365–376.

The results of life tests on single-spatial-mode, double-heterostructure, channeled-substrate-planar AlGaAs diode lasers under thermally accelerated conditions are reported. The diodes were operated pulsed under constant drive current conditions at 50-mW peak power, 25-ns pulse width, and 1-percent duty cycle, with ambient test temperatures of 40°, 55°, and 70°C. Diode performance parameters related to space applications, such as pulse width, peak power, wavelength spectrum, spatial mode, and threshold current, were periodically monitored for over 14,000 hours. An activation energy of about 0.39 eV was deduced, with a predicted median life of about 5×10^4 hours at 20°C.

Basov, N. G., "Dynamics of Injection Lasers," *IEEE Journal of Quantum Electronics*, Vol. QE-4, No. 11, November 1968, pp. 855–864.

This is the first theoretical paper which attempts to provide a clear understanding of the dynamic performance of semiconductor injection diode lasers. Laser instabilities and performance under high-speed modulation are discussed.

Begley, D. L., *et al.*, "Selection of Laser Diode Beam Combining Techniques for Free Space Communications," Optical Technologies for Communication Satellite Applications, Los Angeles, California, January 21–22, 1986, *Proc. SPIE*, Vol. 616, pp. 276–280.

The results of an extensive trade study of various techniques for combining multiple-diode laser beams are presented. Each of the candidate concepts was tested against a stringent set of criteria, and a dichroic reflection combiner was selected for further development into flight-qualifiable hardware.

Botez, D., "Single-Mode AlGaAs Diode Lasers," *Journal of Optical Communications*, Vol. 1, No. 2, November 1980, pp. 42–50.

The major types of AlGaAs laser structures that operate single-mode in continuous-wave operation are reviewed, and the principles of spatial mode stabilization are presented. The performance of these structures is described, and experimental results relevant to single-mode operation are given. In addition, the dynamic behavior of the devices is briefly discussed.

Botez, D., "Single-Mode Lasers for Optical Communications," Future Trends in Fiber Optic Communications, Arlington, Virginia, May 4–5, 1982, *Proc. SPIE*, Vol. 340, pp. 32–49.

Major types of single-mode diode laser devices are grouped and described, including low-power (3–7 mW/facet) and high-power (10–40 mW/facet) lasers. The low-power laser section contains principles of mode stabilization and a treatment of AlGaAs and InGaAsP buried-mesa, nonplanar-substrate, and laterally lossy device structures. The high-power laser section discusses the various means of achieving high-power, reliable, single-mode operation, and describes the major types of high-power AlGaAs devices.

Brouwer, R. P., *et al.*, "Lateral Modes and Self-Oscillations in Narrow-Stripe Double-Heterostructure GaAlAs Injection Lasers," *IEEE Journal of Quantum Electronics*, Vol. QE-17, No. 5, May 1981, pp. 694–701.

Measurements of the radiation field, the mode spectrum, and the power characteristic of narrow-stripe, proton-bombarded, double-heterostructure, GaAs-GaAlAs injection lasers are presented. A correlation is observed between these properties and the presence of self-oscillations. Lasers that display self-oscillations are found to have different lateral gain distributions than lasers which do not oscillate.

Carlin, D. B., *et al.*, "High-Power Diode Lasers for Optical Communications Applications," IEEE Military Communications Conference, Boston, Massachusetts, October 20–23, 1985, *Conf. Rec.*, pp. 109–114.

The state of high-power laser technology is reviewed, and the communications system implications of high-power laser devices are discussed. Promising power output capabilities are reported for channeled-substrate-planar devices.

Casey, W. L., "Design of a Wideband Free-Space Lasercom Transmitter," Optical Technologies for Communication Satellite Applications, Los Angeles, California, January 21–22, 1986, *Proc. SPIE*, Vol. 616, pp. 92–99.

A GaAlAs laser transmitter is described which dichroically combines six single-mode diode lasers to provide 250-mW peak power in a 100-Å bandpass. The diode laser mount accommodates lasers from various manufacturers, and includes an impedance matching network for the laser, and a thermistor and heater for diode laser closed-loop temperature control. The modulator-driver for the transmitter supplies a 500-Mbit/s Manchester-encoded signal to its six outputs, each of which is separately adjustable in amplitude and phasing.

Dean, B. A., and M. Dixon, "Functional Life Testing of Multimoded Lasers for Digital Communications Applications," Laser and Laser Systems Reliability, Los Angeles, California, January 28–29, 1982, *Proc. SPIE*, Vol. 328, pp. 35–41.

The need to evaluate the performance of semiconductor lasers with respect to operating system requirements is discussed. Multimoded GaAlAs lasers were aged in transmitter circuits under both continuous-wave (CW) and pulsed conditions, and functional life tests subject to stringent failure criteria such as average optical power, extinction ratio, self-pulsation frequency, optical noise level, and pattern dependence were performed.

The threshold current and external quantum efficiency of lasers aged under pulsed conditions remained comparable to those observed in CW measurements, and were not the cause of transmitter failure. The dominant failure mechanisms observed were large changes in the average power due to front-to-back facet mistracking, and extinction ratio degradation arising from both the growth of spontaneous power and a decrease in average power. To correct these problems, use of an optical tap to eliminate mistracking and a circuit strategy which eliminates extinction ratio degradation by feedback control of both the DC bias and the modulation drive are suggested.

Einhorn, A. J., *et al.*, "Diagnostic Testing for Evaluation of Semiconductor Lasers for Space Communications," Laser and Laser Systems Reliability, Los Angeles, California, January 28–29, 1982, *Proc. SPIE*, Vol. 328, pp. 28–34.

Several techniques are described for evaluating the physical and optical properties of diode lasers to determine the long-term stability of these sources in a space communications system. Physical diagnostics include techniques for the examination of mechanical, electrical, and material characteristics, and for the identification of facet contamination. Laser beam diagnostics include the far-field pattern, total absolute power, beam wander, longitudinal mode structure, beam polarization, and wavefront characteristics.

Einhorn, A. J., and J. D. Barry, "Review of Reliability Improvements of GaAlAs Laser Diodes," *Microelectronics and Reliability*, Vol. 22, No. 4, 1982, pp. 769–780.

The 10- to 100-fold improvement in laser diode lifetime achieved between 1975 to 1980 is reviewed. This improvement can be attributed to a much better understanding of the factors which cause degradation, and to the implementation of methods such as facet coating, substrate materials selection, production process control, new device structures, and new alloys to retard these effects.

Ettenberg, M., and H. Kressel, "The Reliability of (AlGa)As CW Laser Diodes," *IEEE Journal of Quantum Electronics*, Vol. QE-16, No. 2, February 1980, pp. 186–196.

The major factors affecting the reliability of (AlGa)As continuous-wave (CW) diode lasers are reviewed. The degradation modes of facet mirror damage, contact degradation, and internal damage are discussed in terms of present knowledge of their effect on device performance, their origin, and their reduction or elimination.

Evans, G., and J. Leary, "Issues Impacting the Application of Semiconductor Lasers in Space Communications," Control and Communication Technology in Laser Systems, San Diego, California, August 25–26, 1981, *Proc. SPIE*, Vol. 295, pp. 26–40.

Evans, G., *et al.*, "Applications of Semiconductor Lasers in Space Communications," *Optical Engineering*, Vol. 22, No. 2, March/April 1983, pp. 247–255.

Techniques for combining individual semiconductor lasers for use as a laser communications transmitter are discussed. The geometries, aging

characteristics, radiation effects, and lifetimes of semiconductor lasers are reviewed, and the resulting effects on the laser communications transmitter are assessed.

Harnagel, G. L., *et al.*, "Accelerated Aging of 100-mW CW Multiple-Stripe GaAlAs Lasers Grown by Metalorganic Chemical Vapor Deposition," *Applied Physics Letters*, Vol. 46, No. 2, January 1985, pp. 118–120.

Lifetime characteristics of multistripe, multi-quantum-well lasers operating in the 810-nm region at 100-mW continuous-wave (CW) and at heat sink temperatures of 30°, 70°, and 100°C are reported. Dark-line defect formation during early burn-in; gradual degradation at lower temperatures; and an increase in thermal resistance for high-temperature, long-term testing are observed. For the devices showing a gradual degradation, a median lifetime of 22,000 hours at 30°C, with a mean time to failure of 31,000 hours, is projected.

Imai, H., *et al.*, "Long-Lived High-Power GaAlAs DH Laser Diodes," *IEEE Journal of Quantum Electronics*, Vol. QE-16, No. 3, March 1980, pp. 248–250.

Results of aging tests on high-power (up to 20-mW/facet), facet-coated, GaAlAs, double-heterostructure (DH) diode lasers are reported. The median lifetime is found to decrease with the inverse square of the optical power.

Katz, J., "Semiconductor Optoelectronic Devices for Free Space Optical Communications," International Telemetering Conference, San Diego, California, September 28–30, 1982, *Proc.*, pp. 137–144. (Also published in *IEEE Communications Magazine*, Vol. 21, No. 9, September 1983, pp. 20–27.)

Following a brief review of the properties of individual AlGaAs injection lasers, more complex devices are described. These include monolithic integration configurations of the lasers with their electronic driving circuitry, the power-combining methods of diode lasers, and electronic methods for steering the radiation patterns of diode lasers and diode laser arrays.

Lau, K. Y., *et al.*, "Nonlinear Distortions in the Current-Modulation of Nonself-Pulsing and Weakly Self-Pulsing GaAlAs/GaAs Injection Lasers," *Optics Communication*, Vol. 34, No. 3, September 1980, pp. 424–428.

The dynamic instabilities in semiconductor injection lasers, and the associated nonlinear distortions in current modulation, are reported for buried-heterostructure lasers.

Lau, K. Y., *et al.*, "Gigabit/s Rate Bipolar Pulse Modulation of Semiconductor Injection Lasers," *Optics Communication*, Vol. 35, No. 3, December 1980, pp. 337–341.

Drive circuit considerations for high-speed bipolar pulse modulation of semiconductor injection lasers are discussed.

Lau, K. Y., *et al.*, "Direct Modulation of Semiconductor Lasers at $f >$ 10 GHz by Low Temperature Operation," *Applied Physics Letters*, Vol. 44, No. 3, February 1984, pp. 273–275.

Using a 175-μm-long buried-heterostructure laser fabricated on a semi-insulating substrate operating at -50°C, a direct modulation bandwidth in excess of 10 GHz was achieved for optical output power levels up to 3-mW continuous-wave.

Lau, K. Y., and A. Yariv, "Intermodulation Distortion in a Directly Modulated Semiconductor Injection Laser," *Applied Physics Letters*, Vol. 45, No. 10, November 1984, pp. 1034–1036.

The intermodulation characteristics of diode lasers capable of being modulated at multigigahertz frequencies are studied. The intermodulation product is found to initially increase at a rate of 40 dB/decade as the modulation frequency is increased, but settles to a steady value of approximately -45 dBc, which is satisfactory for many applications. The experimental results are well explained by a theory based on perturbative analysis of laser dynamics.

Lau, K. Y., and A. Yariv, "Ultra-High Speed Semiconductor Lasers," *IEEE Journal of Quantum Electronics*, Vol. QE-21, No. 2, February 1985, pp. 121–137.

Recent progress on semiconductor lasers with direct modulation bandwidths beyond 10 GHz is described, and issues related to the application of these lasers in actual systems are addressed. The possibility of further extending the modulation bandwidth of semiconductor lasers is also examined.

Linke, R. A., *et al.*, "High Speed Laser Driving Circuit and Gigabit Modulation of Injection Lasers," Single Mode Optical Fibers Conference, San Diego, California, August 23–24, 1983, *Proc. SPIE*, Vol. 425, pp. 123–126.

Circuit design considerations for high-speed modulation drivers of injection lasers are experimentally assessed. The optical power penalties are compared for several single-mode diode laser structures modulated at speeds ranging from 100 Mbit/s to low Gbit/s.

Mecherle, G. S., "Laser Diode Combining for Free Space Optical Communication," Optical Technologies for Communication Satellite Applications, Los Angeles, California, January 21–22, 1986, *Proc. SPIE*, Vol. 616, pp. 281–291.

Issues regarding the combining of diode lasers for application to free-space optical communications systems are examined. Design considerations include high throughput efficiency, diffraction-limited angular divergence, and reasonable volume constraints. Methods to incorporate the combiner into the communications system, including power combining, multiplexing parallel independent channels, and a generalized matrix modulation scheme, are compared. Power combining is found to offer the best tradeoff between performance and complexity, except for systems severely limited by background radiation or component bandwidth.

Nagano, K., *et al.*, "Sinusoidal Modulation Characteristics of BH Lasers," *Transactions of the IECE* (Japan), Vol. E-61, No. 6, June 1978, pp. 441–445.

Sinusoidal modulation characteristics of narrow-stripe, low-threshold, single-transverse-mode, buried-heterostructure (BH) lasers are measured with respect to frequency response, spectrum broadening, and nonlinear distortion. These lasers are reported to show a flat frequency response to 2 GHz, with less spectrum broadening than conventional wide-stripe lasers, and a low second-order distortion, typically −50 dB below the fundamental level. The feasibility of using BH lasers as promising optical sources with linear and wideband modulation capabilities is demonstrated.

Okoshi, T., and K. Kikuchi, "Frequency Stabilization of Semiconductor Lasers for Heterodyne-Type Optical Communication Systems," *Electronics Letters*, Vol. 16, No. 5, February 1980, pp. 179–181.

An automatic frequency control experiment using a Peltier cooler element is described in which the frequency fluctuation of a GaAlAs diode laser is reduced below 10 MHz.

Paul, D. K., "High-Power Semiconductor Diode Lasers: Reliability Data and Lifetest Methodology," Fiber Optics Reliability: Benign and Adverse Environments, San Diego, California, August 17–18, 1987, *Proc. SPIE*, Vol. 842, pp. 86–94.

This paper summarizes the development of high-power semiconductor diode lasers. Structural and material considerations, as well as a lifetest methodology appropriate for high-power devices, are discussed. Also included are lifetest data of representative state-of-the-art, high-power diode lasers.

Smith, R. J., "Wideband Lasercom Transmitter Performance," Optical Technologies for Communication Satellite Applications, Los Angeles, California, January 21–22, 1986, *Proc. SPIE*, Vol. 616, pp. 100–104.

The dichroic combination of directly modulated GaAlAs lasers is shown to be a valid approach to achieving a high-brightness, high-data-rate, free-space laser communications transmitter. Temporal, spectral, and spatial qualities of the emitted beam are found to be intact from 0.1 to 1.0 Gbit/s.

Tucker, R. S., and D. J. Pope, "Microwave Circuit Models of Semiconductor Injection Lasers," *IEEE Transactions on Microwave Theory and Techniques*, Vol. MTT-31, No. 3, March 1983, pp. 289–294.

Small-signal, two-port circuit models of packaged commercial broad-stripe and buried-heterostructure AlGaAs diode lasers are developed. The high-frequency circuit model based on the single-mode diode laser rate equations uses appropriate parameters for the heterojunction I-V and space charge characteristics, package, and substrate parasitics. A standard microwave circuit analysis program is used to calculate the reflection coefficient and modulation behavior of diode lasers operated at high speed. The calculations agree well with the measured data of various packaged commercial devices.

---

van der Ziel, J. P., *et al.*, "Mode-Locked Picosecond Pulse Generation From High Power Phase-Locked GaAs Laser Array," *Applied Physics Letters*, Vol. 44, No. 4, February 15, 1984, pp. 357–359.

This letter reports on successful mode-locking of a phase-locked array of GaAs lasers in an external cavity. This yielded optical pulses as short as 61 ps full width at half-maximum, with a peak power of 1.1 W and an average power of 70 mW. The array consisted of 10 lasers, each 3-μm wide with 9-μm center-to-center spacing, and emitted a stable, double-lobed, far-field pattern characteristic of the out-of-phase coupling between neighboring lasers.

Wada, M., *et al.*, "A High-Power, Single-Mode Laser With Twin-Ridge-Substrate Structure," *Applied Physics Letters*, Vol. 42, No. 10, May 1983, pp. 853–854.

The structure of stripe-geometry lasers is reported, in which a double-heterostructure with a very thin active layer is fabricated on a substrate with two parallel ridges. This structure is shown to be very attractive for high-power (100 mW/facet maximum), single-mode GaAlAs diode lasers.

Walther, F. G., and J. E. Kaufmann, "Characterization of GaAlAs Laser Diode Frequency Noise," 6th Topical Meeting on Optical Fiber Communication, New Orleans, Louisiana, February 28–March 2, 1983, *Digest*, pp. 70–71.

This paper reports on measurements of the frequency noise spectra of 5- and 15-mW GaAlAs diode lasers over a 100-MHz frequency range. The measured spectra were used to calculate the heterodyne line shape, which was found to include deviations from a pure Lorentzian form. The line shapes of the two diodes were also experimentally measured and found to be in good agreement with the calculations.

Yamaguchi, S., and M. Suzuki, "Simultaneous Stabilization of the Frequency and Power of an AlGaAs Semiconductor Laser by Use of the Optogalvanic Effect of Krypton," *IEEE Journal of Quantum Electronics*, Vol. QE-19, No. 10, October 1983, pp. 1514–1519.

The output power and frequency of AlGaAs semiconductor lasers have been simultaneously stabilized by using feedback loops in both the temperature controller and the injection current source. The optical output power level under a frequency-stabilized condition is held constant within 1 μW for a period of 20 minutes, and the laser frequency shift is held to within 2 MHz in the optical power dynamic range of 0.7 to 1.6 mW.

Yoshida, J., *et al.*, "Degradation Behavior of AlGaAs DH Laser Diodes Aged Under Pulsed Operating Conditions," *IEEE Journal of Quantum Electronics*, Vol. QE-18, No. 5, May 1982, pp. 879–884.

Degradation behavior of AlGaAs double heterostructure (DH) diode lasers operating pulsed at 70°C and 5-mW/facet optical output power are reported. The effect on degradation characteristics caused by pulsed duty cycle and DC bias magnitude variation is clarified. Pulsed operation is reported to be less harmful than continuous-wave operation.

Photodetectors

The following references describe the general properties of photodetectors, including recent developments concerning reduction of the effective ionization ratio, which decreases the excess noise in avalanche photodiodes (APDs).

Capasso, F., *et al.*, "New Very Low Noise Multilayer and Graded-Gap Avalanche Photodiodes for the 0.8- to 1.8-μm Wavelength Region," Future Trends in Fiber Optic Communications, Arlington, Virginia, May 4–5, 1982, *Proc. SPIE*, Vol. 340, pp. 50–55.

Experimental and theoretical results on low-noise APDs are reviewed. The structures discussed are super lattices, graded band-gap detectors, staircase or graded-gap multilayer APDs, and channeling APDs. Low excess noise factors are achieved by enhancing the impact ionization rates ratio.

Capasso, F., *et al.*, "Staircase Solid-State Photomultipliers and Avalanche Photodiodes With Enhanced Ionization Rates Ratio," *IEEE Transactions on Electron Devices*, Vol. ED–30, No. 4, April 1983, pp. 381–390.

The theory of the staircase APD is presented, and recent results on a new class of APDs with an enhanced ratio of ionization coefficients are reviewed. Experimental and theoretical results on other structures (super lattice, channeling, graded-gap APDs) with high ionization rate ratios are also reviewed, and design considerations for a long-wavelength multilayer APD are presented.

Capasso, F., "Multilayer Avalanche Photodiodes and Solid-State Photomultipliers," *Laser Focus*, Vol. 20, No. 7, July 1984, pp. 84–101.

A technique called band-gap engineering is described which is used to develop APDs for the 1.3- and 1.55-μm fiber optic transmission wavelengths. The devices designed by this technique provide internal avalanche gain with low excess noise, and effectively function as solid-state analogs to photomultiplier tubes.

Goedbloed, J. J., and E. T. J. M. Sheets, "Very Low Noise Silicon Planar Avalanche Photodiodes," *Electronics Letters*, Vol. 14, No. 3, February 1978, pp. 67–69.

Silicon APDs with effective ratios of carrier ionization rates of 0.008 to 0.014 are described.

Green, S. I., "Testing High-Speed Detectors." *Laser Focus*, Vol. 14, No. 9, September 1978, pp. 60–66.

Results on receiver performance at 500 and 400 Mbit/s are presented at 0.532 and 1.064 μm, respectively, for optical receivers using either photomultipliers or APDs. One type of photomultiplier is found to offer the best performance in a pulsed digital communications system in the visible region; however, the advantage over APDs is small. At 1.064 μm, the APD is found to provide superior performance with regard to receiver sensitivity. The measured results at 0.532 μm are also reported in S. I. Green, "Gigabit Detectors for Visible Space Laser Communications," International Telemetering Conference, Los Angeles, California, November 14–16, 1978, *Proc.*, pp. 333–337.

Melchior, H., *et al.*, "Photodetectors for Optical Communication Systems," *Proc. IEEE*, Vol. 58, No. 10, October 1970, pp. 1466–1486.

The characteristics of high-sensitivity photodetectors suitable for wide-bandwidth optical communications systems are summarized. Photodiodes, photomultipliers, and photoconductive detectors for wavelengths from 0.3 to 10.6 μm are discussed.

Melchior, H., "Sensitive High Speed Photodetectors for the Demodulation of Visible and Near Field Infrared Light," *Journal of Luminescence*, Vol. 7, 1973, pp. 390–414.

The principles of operation, the basic construction, and the operational characteristics of photomultipliers, solid-state photodiodes, and APDs are described. Tradeoffs involving the optimization of quantum efficiency, speed of response, internal current gain, and sensitivity to weak light signals are treated in detail for silicon photodiodes.

Müller, J., "Photodiodes for Optical Communication," *Advances in Electronics and Electron Physics*, Vol. 55, L. Marton and C. Marton, eds., New York: Academic Press, 1981, pp. 189–308.

This review paper discusses the fundamental operating principles of optical detectors and receivers for the 0.8- to 1.7-μm wavelength range. This

theoretical treatment is followed by discussions on material selection and solid-state photodiode designs.

Pearsall, T. P., "Photodetectors for Optical Communication," *Journal of Optical Communications*, Vol. 2, No. 2, June 1981, pp. 42–48.

The performance characteristics of five photodiodes suitable for optical fiber communications systems are calculated based on measured parameters of both the photodiode and the preamplifier. The materials considered are Si, Ge, $Al_{0.14}Ga_{0.86}Sb$, $Ga_{0.47}In_{0.53}As$, and $Ga_{0.27}In_{0.73}As_{0.60}P_{0.40}$. The silicon APDs are shown to be the most sensitive, due principally to their low-noise properties.

Petschacher, R., *et al.*,"Error-Rate Measurements on a 1-Gbit/s Fibre-Optic Communications Link," *Electronics Letters*, Vol. 14, No. 22, October 1978, pp. 711–713.

Experimental and calculated results are reported on the bit error rate performance of a 1-Gbit/s fiber optic communications link. The link utilizes a GaAlAs double-heterostructure injection laser, a 1.6-km single-mode fiber, and a silicon APD.

Stillman, G. E., and C. M. Wolfe, "Avalanche Photodiodes," *Semiconductors and Semimetals*, Vol. 12, R. K. Willardson and A. C. Beer, eds., New York: Academic Press, 1977, pp. 291–393.

This article discusses the basic principles of APDs. Areas addressed include the avalanche gain mechanism, multiplication noise, electron and hole ionization coefficients, and device structures. The performance of APDs in various materials is summarized, and problem areas requiring further research are noted.

Webb, P. P., *et al.*, "Properties of Avalanche Photodiodes," *RCA Review*, Vol. 35, No. 2, June 1974, pp. 234–278.

The basic properties of APDs are reviewed, including expressions for calculating the avalanche gain, signal-to-noise ratio, detector excess noise factor, diode linearity and saturation, noise equivalent power, quantum

efficiency, impulse response time, and frequency response. Several commercially available APDs are compared, and their advantages and disadvantages are discussed.

Optical receiver design

Various aspects of designing high-sensitivity optical receivers are described in these references.

Brain, M., and T.–P. Lee, "Optical Receivers for Lightwave Communication Systems," *Journal of Lightwave Technology*, Vol. LT-3, No. 6, December 1985, pp. 1281–1300.

This review concentrates on describing the principles of operation and the details of the development of long-wavelength (1.3- and 1.55-μm) PIN photodiode and avalanche photodiode receivers. Bipolar phototransistors and photoconductive detectors are also considered, as are the receiver requirements for coherent optical systems. The paper concludes with a broad comparison of various receiver designs.

Jain, V. K., *et al.*, "Design of an Optimum Optical Receiver," *Journal of Optical Communications*, Vol. 6, No. 3, September 1985, pp. 106–112.

This paper gives a systematic approach to the design of an optimum optical receiver for on-off-keyed signals. The receiver design requires a minimum in received optical power for a given communications performance, and is optimized for available avalanche and PIN photodiodes.

Muoi, T. V., "Receiver Design for Digital Fiber Optic Transmission Systems Using Manchester (Biphase) Coding," *IEEE Transactions on Communications*, Vol. COM-31, No. 5, May 1983, pp. 608–619.

The sensitivity of an optical receiver in a digital communications system using Manchester coding is analyzed. Based on the Gaussian approximation, expressions are developed to predict the receiver sensitivity for both PIN and avalanche photodiodes. Experimental results for the sensitivity of a 250-Mbit/s Manchester receiver are then presented for both high-impedance

and transimpedance preamplifier designs. Tradeoffs between Manchester and nonreturn-to-zero (NRZ) coding are discussed in terms of receiver sensitivity and ease of implementation, and the Manchester system is found to be an attractive alternative to NRZ coding, particularly when an avalanche photodiode is used.

Muoi, T. V., "Receiver Design for High-Speed Optical-Fiber Systems," *Journal of Lightwave Technology*, Vol, LT-2, No. 3, June 1984, pp. 243–267.

Optical receiver design is viewed in terms of high receiver sensitivity, wide dynamic range, transparency to the operating bit rate, unrestricted data format, and fast acquisition time. Design tradeoffs between conflicting receiver requirements are considered, with an emphasis on the sensitivity of high-capacity, long-wavelength transmission systems for telecommunications applications.

Muoi, T. V., "Extremely Sensitive Direct Detection Receiver for Laser Communications," Conference on Lasers and Electro-Optics, Baltimore, Maryland, April 26–May 1, 1987, *Digest*, pp. 302–304.

This paper reports on a 325-Mbit/s direct-detection receiver with a sensitivity of 110 photons/bit for a 10^{-9} bit error rate. The receiver operates in the 0.8- to 0.9-μm wavelength range and uses a silicon avalanche photodiode and transimpedance preamplifier design. The sensitivity of this receiver compares very favorably with some of the best sensitivities obtained in coherent detection systems.

Ogawa, K., "Considerations for Optical Receiver Design," *IEEE Journal on Selected Areas in Communications*, Vol. SAC-1, No. 3, April 1983, pp. 524–532.

Digital receiver design in long-wavelength fiber optic systems is reviewed from a practical viewpoint. Noise sources and degradation factors which constrain overall receiver performance are discussed, and the expected sensitivities of several detector-preamplifier combinations are compared. The sensitivity power penalties due to the bandwidth of the optical source and transmission media, and to imperfections in the design of the optimized filter, are also discussed.

Personick, S. D., "Receiver Design for Digital Fiber Optic Communication Systems," *Bell System Technical Journal*, Vol. 52, No. 6, July–August 1973, pp. 843–886 (in two parts).

This classic reference presents a systematic approach to the design of a digital optical receiver. Areas addressed include the selection of a suitable front-end preamplifier and biasing circuitry for the photodetector, as well as variations in the receiver sensitivity with the bit rate, the received optical pulse shape, and the desired baseband-equalized output pulse shape. Numerical results on receiver sensitivity as a function of the design parameters are provided for a specific receiver design.

Personick, S. D., "Receiver Design for Optical Fiber Systems," *Proc. IEEE*, Vol. 65, No. 12, December 1977, pp. 1670–1678.

This tutorial review of the theory and practice of receiver design for optical fiber communications systems discusses such topics as the fundamental limitations on performance, the design and performance limitations of laboratory receivers, and practical design tradeoffs and their effect on the performance of real system receivers.

Modulation formats

The papers in this category describe the modulation formats best suited to free-space laser communications systems. Formats for both direct-detection and heterodyne-detection systems are included.

Abshire, J. B., "Performance of OOK and Low-Order PPM Modulations in Optical Communications When Using APD-Based Receivers," *IEEE Transactions on Communications*, Vol. COM-32, No. 10, October 1984, pp. 1140–1143.

On-off keying and low-order pulse-position modulation (PPM) signaling are compared in terms of bit error probability *vs* required signal counts per bit for direct-detection avalanche photodiode (APD) receivers. Plots of the error probabilities are given as a function of signal level, APD effective ionization ratio, background level, and APD gain. The results assume a Gaussian model for the avalanche gain statistics and indicate that quaternary

PPM (QPPM) requires approximately 3 dB less signal than on-off keying (OOK), while binary PPM (BPPM) requires the same or slightly more signal than OOK for the same bit error rate performance.

Davidson, F., "Free-Space Direct Detection Optical Communication With Color Coded PPM Signaling," IEEE Global Telecommunications Conference, Atlanta, Georgia, November 26–29, 1984, *Conf. Rec.*, pp. 944–948.

Davidson, F., "Direct-Detection Optical Communication With Color Coded Pulse Position Modulation Signaling," *IEEE Transactions on Communications*, Vol. COM-33, No. 3, March 1985, pp. 273–276.

The performance characteristics of a direct-detection optical communications system are analyzed in which the transmitter outputs a light pulse of 1-ns duration at one of N possible optical center frequencies. This signaling scheme, known as color-coded pulse-position modulation (CCPPM), consists of selecting both a time slot in which to send the light pulse and the color of the pulse to be sent. It has two advantages over ordinary (single-color) PPM signaling. First, fewer comparators are needed to determine which of the possible symbols has been received (same throughput rate assumed in each case). Second, at constant channel throughput capacity, the optimal energy efficiency (as measured by the channel capacity per received photon) is higher. It is also shown that the CCPPM signaling scheme can be used in conjunction with Reed-Solomon coding to obtain high-data-rate, reliable communications under conditions of optimal energy efficiency.

Gagliardi, R. M., and S. Karp, *Optical Communications*, New York: John Wiley & Sons, 1976.

This general textbook gives an analytical study of optical communications. Mathematical models of optical components are developed and used to determine the design equations, limitations to system performance, and technological tradeoffs involved in an optical communications system.

Gagliardi, R. M., "Error Probabilities in Lasercom PPM Systems," National Telecommunications Conference, New Orleans, Louisiana, November 29–December 3, 1981, *Conf. Rec.*, pp. B10.1.1–B10.1.2.

In this paper, bit error probability equations for optical pulse-position modulation (PPM) systems are listed. Uncoded and coded PPM systems are considered with hard-decision, soft-decision, and threshold-detection receivers.

Garrett, I., "Pulsed-Position Modulation for Transmission Over Optical Fibers With Direct or Heterodyne Detection," *IEEE Transactions on Communications*, Vol. COM-31, No. 4, April 1983, pp. 518–527.

Digital pulse-position modulation (PPM) systems are analyzed where the receiver is optimized in terms of the received pulse for both wrong slot and false alarm errors. Direct-detection and heterodyne-detection receivers are considered, and timing extraction is also discussed.

Goell, J. E., "Input Amplifiers for Optical PCM Receivers," *Bell System Technical Journal*, Vol. 53, No. 9, November 1974, pp. 1771–1793.

A description of the noise performance of an optical link using an on-off keying modulation format and a direct-detection receiver is given. The noise factors in the receiver are described for both field-effect and bipolar transistor front-end amplifiers, and the effective noise currents of the two preamplifier types are compared as a function of bit rate.

Hubbard, W. M., "Utilization of Optical-Frequency Carriers for Low- and Moderate-Bandwidth Channels," *Bell System Technical Journal*, Vol. 52, No. 5, May–June 1973, pp. 731–765.

This tutorial paper explores the use of optical-frequency carrier systems for transmission over low- to moderate-bandwidth channels (a few kHz to ~100 MHz). Analog intensity modulation, pulse-position modulation, delta modulation, and pulse-code modulation are considered. Only direct-detection receivers are discussed.

Jeromin, L. L., and V. W. S. Chan, "Modulation Design for Heterodyne Optical Communication System," IEEE Global Telecommunications Conference, San Diego, California, November 28–December 1, 1983, *Conf. Rec.*, pp. 412–415.

The modulation performance of an optical communications system using a semiconductor laser and heterodyne detection is described. Phase and frequency noise in semiconductor lasers causes spectral spread, producing a nonzero-linewidth signal. This limits modulation choices and degrades the communications performance when compared with a zero-linewidth system. A simple analytical model is presented to estimate the performance of an optical communications system using M-ary, frequency-shift keyed (FSK) modulation and noncoherent heterodyne detection. The model predicts a bit error rate floor caused by crosstalk introduced by the frequency noise of the semiconductor laser, and predicts performance when background noise is also present. Estimates agree well with the results of a Monte Carlo simulation of the actual system.

Jeromin, L. L., and V. W. S. Chan, "*M*-ary FSK Performance for Coherent Optical Communication Systems Using Semiconductor Lasers," *IEEE Transactions on Communications*, Vol. COM-34, No. 4, April 1986, pp. 375–381.

This paper describes the design and performance of an M-ary, frequency-shift-keyed (MFSK) signaling and demodulation scheme for an optical communications system which uses semiconductor lasers and heterodyne detection. Frequency or phase noise in semiconductor lasers causes spectral spreading, producing a nonzero-linewidth laser signal. This degrades communications performance when compared with a system using an ideal laser with zero linewidth. Theoretical estimates of the bit error rate performance of an MFSK system are compared with Monte Carlo simulations.

Jeromin, L. L., and D. Welford, "The Effect of Spurious Intensity Modulation in Semiconductor Diode Lasers on the Performance of Optical Heterodyne Frequency Shift-Keyed Communications Systems," *Journal of Lightwave Technology*, Vol. LT-4, No. 6, June 1986, pp. 590–595.

Analytical expressions for the bit error rate of an MFSK, heterodyne optical communications system with noncoherent demodulation are derived, including the effects of spurious intensity modulation and finite laser linewidth. The system performance degradation (power penalty) is calculated for both an InGaAsP distributed-feedback laser and a GaAlAs channeled-substrate-planar laser as a function of the chirp-to-modulated-power ratio and the data

rate for binary, 4-, and 8-ary FSK systems. The power penalties at data rates below 400 Mbit/s are less than 1 dB for both lasers, but a sharp increase in the power penalties of both lasers is reported for data rates approaching 1 Gbit/s.

Karp, S., and R. M. Gagliardi, "The Design of a Pulse-Position Modulated Optical Communication System," *IEEE Transactions on Communication Technology*, Vol. COM-17, No. 6, December 1969, pp. 670–676.

The system performance of an optical M-ary pulse-position modulation (MPPM) link in terms of error probabilities and information rates is derived with respect to key parameters such as power levels, number of PPM signals, pulse width, and bandwidths. Both background radiation and receiver thermal noise are included.

Kreutel, R. W., *et al.*, "Optical Transmission Technology in Satellite Communications," *COMSAT Technical Review*, Vol. 10, No. 2, Fall 1980, pp. 321–367.

Optical communications technology is reviewed with emphasis on satellite communications applications. Of particular interest are the derived expressions describing the communications performance of digital and analog optical links, which can be used to assess the communications performance of an optical ISL.

Kobayashi, S., *et al.*, "Modulation Frequency Characteristics of Directly Optical Frequency Modulated AlGaAs Semiconductor Laser," *Electronics Letters*, Vol. 17, No. 10, May 1981, pp. 350–351.

Kobayashi, S., *et al.*, "Direct Frequency Modulation in AlGaAs Semiconductor Lasers," *IEEE Journal of Quantum Electronics*, Vol. QE-18, No. 4, April 1982, pp. 582–595.

Experimental measurements of the direct FM modulation characteristics in an AlGaAs diode laser from DC to 5.2 GHz are reported. For modulation frequencies below 10 MHz, thermal effects are predominant. Above 1 GHz, resonance peaks are observed, with a center frequency that depends on the bias current. In the range from 10 MHz to 1 GHz, the frequency deviation

is essentially frequency-independent, indicating the usefulness of the device in a coherent optical transmission system with an FM format.

Lee, G. M., and E. A. Paddon, "Modulation Formats for High Data Rate Optical Communications," Western Electronic Show and Convention (WESCON), San Francisco, California, August 24–27, 1971, *Proc.*, Paper 6/1.

Models for digital baseband and digital subcarrier optical modulation systems are developed and used to obtain expressions for bit error rate performance as a function of received optical power. Emphasis is placed on systems operating at data rates of 1 Gbit/s or greater. In particular, the modulation formats discussed are well suited to a space optical link which uses the Nd:YAG laser.

Lee, G. M., *et al.*, "A Comparison of Multi-User Optical Space Communication Systems," National Telecommunications Conference, Atlanta, Georgia, November 26–28, 1973, *Conf. Rec.*, pp. 30E-1 to 30E-6.

Digital baseband and subcarrier noncoherent optical communications systems are compared on the basis of required laser power. The baseband approach is shown to be superior for both RF and optical users. Both demodulating and nondemodulating repeaters are considered.

Lee, G. M., *et al.*, "Bit Error Probability for Baseband and Subcarrier Optical Communication Systems," *IEEE Transactions on Communications*, Vol. COM-22, No. 1, January 1974, pp. 55–61.

Digital baseband and digital subcarrier noncoherent optical communications systems are considered. Expressions are developed for the bit error probability of optical subcarrier systems which use a nonlinear polarization modulator and either a one-detector or two-detector receiver. The expressions are evaluated numerically, and the results are used to compare the one- and two-detector subcarrier systems with the corresponding one- and two-detector baseband systems. The modulation formats considered are well suited for Nd:YAG laser links.

Lee, G. M., *et al.*, "Pulse Quaternary Modulation," National Electronics Conference, Chicago, Illinois, October 16–18, 1974, *Proc.*, Vol. 29, pp. 163–167.

Pulse quaternary modulation is described, and several suboptimum receiver designs are considered for using this format for binary data transmission. A comparison of the receiver designs on the basis of bit error rate *vs* received optical power indicates that there is little difference in their performance for reasonable background counts and achievable modulator extinction ratios. Experimental results are presented which show that the system operates within 2.7 dB of an ideal photoelectron counter for a 1-Gbit/s data rate.

Lee, G. M., and G. W. Schroeder, "Optical Pulse Position Modulation With Multiple Positions per Pulsewidth," *IEEE Transactions on Communications*, Vol. COM-25, No. 3, March 1977, pp. 360–364.

The required laser power to achieve a given probability of bit error using pulse-interval modulation (PIM) (discrete pulse-position modulation) is determined, assuming the pulse resolution is much smaller than a laser pulsewidth. Both analytic and computer simulation results are presented.

Lesh, J., "Power Efficient Optical Communications for Space Applications," International Telemetering Conference, San Diego, California, September 28–30, 1982, *Proc.*, pp. 109–113.

The progress to date is described on a project to design, build, and demonstrate in the laboratory an optical communications system capable of conveying 2.5 bits of information per effective received photon. Such high power efficiencies reduce the need for photon collection at the receiver and greatly reduce the requirements for optical pointing accuracy at both the transmitter and the receiver. A longer range program to demonstrate even higher photon efficiencies is also described.

Mercherle, G. S., "Impact of Laser Diode Performance on Data Rate Capability of PPM Optical Communication," IEEE Military Communications Conference, Boston, Massachusetts, October 20–23, 1985, *Conf. Rec.*, pp. 115–121

A model is developed for an avalanche photodiode receiver which is shown to have dominant noise contributions from signal-dependent excess noise and thermal noise at high data rates. For a link using pulse-position modulation (PPM), the optimum choice of PPM word size is dependent on the source peak-to-average power ratio. Several commercially available single-transverse-mode diode lasers (20-mW average power) were found to have peak-to-average power ratios of about 8, indicating that they could be used in 4-ary or 8-ary PPM systems.

Morris, D. J., *Pulse Code Formats for Fiber Optical Data Communications*, New York: Marcel Dekker, 1983.

This textbook provides a comprehensive discussion of the pulse code formats commonly used in data communications, with emphasis on those formats well suited to fiber optic systems. Each format is described in detail, and their benefits and liabilities are compared. State diagrams are also presented which display data clearly and highlight many important features.

Okoshi, T., *et al.*, "Computation of Bit-Error Rate of Various Heterodyne and Coherent-Type Optical Communication Systems," *Journal of Optical Communications*, Vol. 2, No. 3, September 1981, pp. 89–96.

The receiver sensitivities in various heterodyne optical communications systems are determined as functions of the information transmission rate and the mixer diode parameters. The results are compared with those for a system using an intensity modulation format (on-off keying) and a direct-detection receiver.

Osterwalder, J. M., and B. J. Rickett, "Frequency Modulation of GaAlAs Injection Lasers at Microwave Frequency Rates," *IEEE Journal of Quantum Electronics*, Vol. QE-16, No. 3, March 1980, pp. 250–252.

Direct frequency modulation of GaAlAs diode lasers is reported at frequencies up to 2.25 GHz, with a modulation index of 2.4. A simple Fabry-Perot cavity model is used to represent the active laser medium and to calculate the static frequency shift expected by laser bias current changes. The calculated shift is then compared with measured frequency shifts of typical lasers and found to be in good agreement.

Pratt, W. K., "Communication Receivers," *Laser Communication Systems*, New York: John Wiley and Sons, 1969.

An analysis of direct-, heterodyne-, and homodyne-detection optical communications receivers is presented, including derivations of expressions for the signal-to-noise ratios at the receiver outputs. Detector shot noise and thermal noise due to resistive elements are considered, and all other noise sources are assumed to be negligible.

Ryan, C. R., and G. Meyer, "Transceiver Electronics for a 1 Gbit/s PGBM Optical Communication System," National Telecommunications Conference, Atlanta, Georgia, November 26–28, 1973, *Conf. Rec.*, pp. 30B-1 to 30B-4.

Theoretical and experimental results are given for the electronics portion of a 1-Gbit/s pulse-gated binary modulation (PGBM) optical communications system. A performance level of approximately 1.5 dB from the theoretical was observed experimentally, with the degradation in performance attributed to the nonoptimum predecision filter, threshold errors, and timing errors of the decision circuit. Computer simulations were performed to determine the effect of these error sources.

Saito, S., *et al.*, "Optical FSK Heterodyne Detection Experiments Using Semiconductor Laser Transmitter and Local Oscillator," *IEEE Journal of Quantum Electronics*, Vol. QE-17, No. 6, June 1981, pp. 935–941.

Frequency-modulated GaAlAs laser signals at 100 to 200 Mbit/s are demodulated by optical heterodyne detection using a temperature-stabilized GaAlAs laser local oscillator and a square-law detector, followed by electrical frequency discrimination circuitry. Short-term and long-term beat frequency stability of the free-running laser transmitter and local oscillator are described. In addition, the direct frequency modulation characteristics of the GaAlAs transmitter are studied by observing the intermediate frequency spectra.

Saito, S., *et al.*, "*S/N* and Error Rate Evaluation for an Optical FSK-Heterodyne Detection System Using Semiconductor Lasers," *IEEE Journal of Quantum Electronics*, Vol. QE-19, No. 2, February 1983, pp. 180–193.

Receiving performance is evaluated for an optical frequency-shift-keyed (FSK) heterodyne detection system in which GaAlAs lasers are used as both the transmitter and local oscillator. Noise and error rate performance are measured under feedback stabilization of the intermediate signal frequency (IF) and electrical equalization of the diode laser FM modulation frequency characteristics. Since system performance is limited by both AM and FM quantum noise in the transmitter and local oscillator lasers, only a 2-dB receiver sensitivity improvement over a direct-detection system with intensity modulation is observed for a 200-Mbit/s signal.

Taub, H., and D. L. Schilling, *Principles of Communications Systems*, New York: McGraw-Hill, 1971.

This textbook discusses the fundamental principles of communications systems. The general material presented here can be used as necessary in formulating link budget analyses of an optical ISL.

Welford, D., and S. B. Alexander, "GaAlAs Semiconductor Diode Laser 4-ary Frequency Shift Key Modulation at 100 Mbit/s," *Electronics Letters*, Vol. 21, No. 1, January 3, 1985, pp. 12–13.

The 4-ary, frequency-shift-keyed (FSK) modulation of a GaAlAs diode laser by injection current modulation is demonstrated at a rate of 100 Mbit/s. The injection current modulator has a modular design which allows expansion to *M*-ary FSK with independent control of each tone frequency.

Welford, D., and S. B. Alexander, "Magnitude and Phase Characteristics of Frequency Modulation in Directly Modulated GaAlAs Semiconductor Diode Lasers," *Journal of Lightwave Technology*, Vol. LT-3, No. 5, October 1985, pp. 1092–1099.

This paper describes experimental measurements, based on the use of RF network analyzers, of both the magnitude and phase of the FM transfer function of several semiconductor diode lasers. The small-sized injection current-to-frequency modulation characteristics of channeled-substrate-planar, buried-heterostructure, and transverse-junction-stripe GaAlAs diode lasers over the frequency range of 100 Hz to 1,300 MHz were studied, since these devices are potential candidates for the transmitter of a frequency-shift-keyed, optical heterodyne communications system.

The measured FM transfer functions are discussed in terms of thermal and carrier-density modulation mechanisms. The data show the presence of thermal FM at low frequencies and carrier-density FM at high frequencies for all three laser structures, when biased well above threshold. The thermal FM was observed to be nearly independent of bias current, while the carrier-density FM decreases with increasing bias current due to gain clamping effects.

Yamamoto, Y., "Receiver Performance Evaluation of Various Digital Optical Modulation-Demodulation Systems in the 0.5–10 μm Wavelength Region," *IEEE Journal of Quantum Electronics*, Vol. QE-16, No. 11, November 1980, pp. 1251–1259.

Error-rate characteristics of various digital optical modulation-demodulation schemes using direct-detection and heterodyne-detection receivers are evaluated, taking into account such parameters as data rate, optical carrier wavelength, photodetector performance, optical local oscillator power, and multilevel codes. Amplitude-shift keyed, frequency-shift keyed, and phase-shift keyed systems are considered, with direct modulation of the optical carrier and intensity modulation of the optical carrier by a subcarrier signal.

Wavelength-division multiplexing

Wavelength-division multiplexing and demultiplexing (WDM) are important concepts in optical ISLs with applications for incoherent power combining, transmission of several independent optical channels through a single transmit telescope, and dichroic separation of the transmit and receive optical beams. The following references describe the properties of optical multiplexing and demultiplexing elements and WDM systems.

Gibson, D. R., and P. H. Lissberger, "Optical Properties of Narrowband Spectral Filter Coatings Related to Layer Structure and Preparation," *Applied Optics*, Vol. 22, No. 2, January 15, 1983, pp. 269–281.

The optical properties of 35 all-dielectric spectral filter coatings for the visible spectrum were investigated and correlated with the deposition coatings of the constituent layers of cryolite and zinc sulfide, and with the processes that occur when the coatings are exposed to the atmosphere. It is shown that experimental measurements of transmittance and reflectance over the passband

wavelengths are accurately described theoretically only if account is taken of absorption in the layers, scattering at the rough boundaries, and changes in the refractive indices of the layers due to water penetration.

Gourley, P. L., *et al.*, "Single-Crystal, Optical Interference Filters and Integrated High Reflector/Photodiode Using Multilayers of GaP and $GaAs_xP_{1-x}$," *Applied Physics Letters*, Vol. 49, No. 5, August 1986, pp. 242–244.

Single-crystal optical interference filters (high reflectors and antireflectors) with alternating quarterwave-thick layers (300–600 Å) of GaP and $GaAs_xP_{1-x}$ were developed using metallo-organic chemical vapor deposition (MOCVD). The measured reflectance ranged from 0.80 to 0.90 at selected wavelengths from 460 to 750 nm. The filter linewidth was quite narrow, typically 100 Å. The reflectance at a selected wavelength could be varied by a factor of 10, despite the relatively small index difference between layers and the modest number of periods in the filters. To ensure reflectance values approaching 0 and 100 percent, a large number of interfaces and very strict control of uniformity were required.

In addition to the filter development on III–V semiconductor material, an integrated optical detector was fabricated in which a photodiode and an electrically active high reflector were grown sequentially in a single growth run. The interest in pursuing such filters is that these materials are already well established for electrical devices, so that integration of such optically/electrically active structures with other devices is feasible.

Kersten, R. T., and M. Rocks, "Wavelength Division Multiplexing in Optical Communication Systems," *Journal of Optical Communications*, Vol. 3, No. 3, September 1982, pp. 93–100.

Taking into account parameters of realized components for WDM systems with multimode graded index fibers, it is shown that such a system has no advantage compared with a single-wavelength system operating at an optimum wavelength. A WDM system is proposed with very small optical frequency separation of some gigahertz, in connection with a single-mode fiber and a heterodyne receiver. The components for such a futuristic system can be realized by using integrated optics.

Larsson, A., *et al.*, "High-Speed Dual-Wavelength Demultiplexing and Detection in a Monolithic Superlattice p-i-n Waveguide Detector Array," *Applied Physics Letters*, Vol. 49, No. 5, August 1986, pp. 233–235.

High-speed, dual-wavelength demultiplexing and detection in a monolithic linear array of superlattice photodetectors with a waveguide configuration are demonstrated. The wavelength selectivity is based on the quantum-confined Stark effect. Increasing the applied reverse bias to the PIN photodiode causes an electric field-induced decrease in the confinement energies of the quantized states in the conduction and valence bands. The shift in the near-band-edge absorption to lower energies with increasing reverse bias is larger than the Franz-Keldysh effect seen in bulk material. The sharpness of the absorption edge is also preserved because the band discontinuities prevent ionization of the excitons, even at high electric fields. This effect is useful for optical modulators, self-electrooptic effect devices (SEED), actively Q-switched quantum-well lasers, and tunable photodetectors. In this device, wavelength-multiplexed optical signals can be demultiplexed directly into different electrical channels.

Improved wavelength selectivity and increased crosstalk attenuation are achieved due to enhanced electroabsorption in the superlattice PIN diodes that constitute the detector. The superlattice consists of 100-Å GaAs wells and 50-Å $Al_{0.25}Ga_{0.75}As$ barriers, and is surrounded by undoped graded superlattice buffers, each with a total thickness of 385 Å. The two detectors are 20-μm wide and 20- and 50-μm in length, and the separation is 10 μm. The linear array of photodiodes was defined by proton implantation, which provides high electrical isolation (>1 GΩ) and low capacitance (0.7 pF) of the individual diodes. The total capacitance of each diode was 0.9 pF at the operating bias, which implies a resistance/capacitance (RC) time constant in the 100-ps range. The detector geometry provides optical waveguiding perpendicular to the layers, and is compatible with integrated optoelectronics. Experiments were conducted at 1 Gbit/s and 500 Mbit/s, with dual wavelengths of 840 and 870 nm. Electrical crosstalk attenuation for 30-nm interchannel spacing was typically 30 dB, and the detector sensitivity was 0.2 and 0.12 A/W with −5 and −15 V reverse bias, respectively. The corresponding quantum efficiencies are 30 and 17 percent, which includes losses due to coupling, reflection, and scattering. An improved responsivity and narrow interchannel spacing, without sacrificing the crosstalk, is possible through device optimization.

Macleod, H. A., *Thin-Film Optical Filters*, New York: American Elsevier, Inc., 1969.

This reference book provides an introduction to thin-film optical filters for the manufacturer and the user. The basic mathematics involved in thin-film devices is discussed, and specific devices such as beam splitters, edge filters, and bandpass filters are described in detail. This is followed by discussions on production and monitoring methods, the specification of filters, and environmental effects.

Mahlein, H. F., "Fiber-Optic Communication in the Wavelength-Division Multiplex Mode," *Fiber and Integrated Optics*, Vol. 4, No. 4, 1983, pp. 339–372.

The physical design, operating principle, and properties of various micro-optical WDM couplers are surveyed, and the criteria on which their practical application depends are defined.

Minowa, J., and Y. Fujii, "Dielectric Multilayer Thin-Film Filters for WDM Transmission Systems," *Journal of Lightwave Technology*, Vol. LT-1, No. 1, March 1983, pp. 116–120.

The design and manufacture of dielectric bandpass filters for WDM applications are discussed. Included are descriptions of the filter requirements in WDM systems, the design and manufacture of bandpass filters according to the specified requirements, and the characteristics of fabricated filters.

Title, A. M., *et al.*, "Drift in Interference Filters. Part 1," *Applied Optics*, Vol. 13, No. 11, November 1974, pp. 2675–2679.
Title, A. M., "Drift in Interference Filters. Part 2: Radiation Effects," *Applied Optics*, Vol. 13, No. 11, November 1974, pp. 2680–2684.

Experimental results are presented on the drift in peak transmission wavelength of optical interference filters that results from thermal and radiation effects. These papers concentrate on ZnS-cryolite filters, which are commonly used in the visible region; however, the qualitative results are useful for thin-film filters designed to operate in other spectral regions.

Tomlinson, W. J., "Wavelength Multiplexing in Multimode Optical Fibers," *Applied Optics*, Vol. 16, No. 8, August 1977, pp. 2180–2194.

Various WDM system designs that might be used with multimode fiber transmission systems are considered. Following a review of the basic characteristics of various multiplexer devices, the required dimensions and material properties for angularly dispersive and thick-grating devices are determined.

Watanabe, R., *et al.*, "Optical Multi/Demultiplexers for Single-Mode Fiber Transmission," *IEEE Journal of Quantum Electronics*, Vol. QE-17, No. 6, June 1981, pp. 974–981.

Two types of optical multi/demultiplexers are described for a bidirectional, single-mode fiber optic transmission system in the wavelength region from 1 to 1.5 μm. The first type consists of four bandpass filters and a short-wavelength pass or long-wavelength pass filter. The second type, known as the filter-grating type, consists of two bandpass filters and a grating.

Welsh, F. S., and T. S. Stakelon, "Optical Frequency Control for Wavelength Multiplexed Systems," 35th Annual Frequency Control Symposium, Ft. Monmouth, New Jersey, May 1981, *Proc.*, pp. 525–531.

This paper describes limitations on wavelength-multiplexed system channel capacity resulting from instabilities of available diode laser sources and characteristics of optical filters and gratings. The requirements for improved source stability and multiplexer performance are also outlined, and resulting opportunities for large-capacity systems are described.

High-speed systems

Several references are given which review digital systems and components capable of operating at multigigabit-per-second rates.

Albrecht, W., *et al.*, "Optical Digital High-Speed Transmission: General Considerations and Experimental Results," *IEEE Journal of Quantum Electronics*, Vol. QE-18, No. 10, October 1982, pp. 1547–1559.

Laboratory experiments on digital optical transmission systems at bit rates of 1 and 2 Gbit/s are described. These systems use a silicon avalanche photodiode receiver and include complete circuits for clock and signal regeneration.

Baack, C., ed., *Optical Wideband Transmission Systems*, Boca Raton, Florida: CRC Press, 1986.

Practical and theoretical aspects of high-bit-rate systems (1 to 2 Gbit/s) for long-range transmission are explored in depth. The functions of individual components and system performance are discussed.

Cormier, D., "High-Speed Digital ICs," *EDN*, Vol. 30, No. 19, August 22, 1985, pp. 110–126.

This article is an overview of integrated circuit technologies suitable for systems operating with data rates on the order of 1 Gbit/s. Included are silicon technologies such as emitter-coupled logic (ECL) bipolar, complementary metal-oxide semiconductor (CMOS), and advanced low-power Schottky designs, and GaAs technologies. For ultra-high-speed applications, GaAs promises to outperform any silicon technology.

Ferry, D. K., ed., *Gallium Arsenide Technology*, Indianapolis, Indiana: Howard W. Sams and Co., 1985.

An excellent recent book that provides in-depth discussions on material growth, device fabrication, and high-speed/wide-bandwidth applications, by experts drawn from industry, academia, and government laboratories. A chapter on the physics of submicron/ultrasubmicron dimensions explores the limits of ultrasmall electronics for high-density, high-speed GaAs devices.

Goodfellow, R. C., *et al.*, "Optoelectronic Components for Multigigabit Systems," *IEEE Journal of Lightwave Technology*, Vol. LT-3, No. 6, December 1985, pp. 1170–1179.

This is a survey of the optoelectronic components required for implementation of optical communications systems operating at multigigabit-per-second data rates. Included are discussions on integrated circuits, high-speed

optical sources, external modulators, high-speed receivers, and limitations in fiber optic link lengths due to dispersion. It is speculated that increasing speed and complexity will drive technology to higher optoelectronic integration levels.

Hinckling, R. M., "High-Speed GaAs ICs," Reliability Considerations in Fiber Optic Applications, Cambridge, Massachusetts, September 25–26, 1986, *Proc. SPIE*, Vol. 717, pp. 82–84.

Practical considerations related to the utilization of off-the-shelf GaAs digital ICs in high-speed applications (~500 Mbit/s), including reliability, thermal management, and interconnection issues, are presented.

Hutcheson, L. D., "High-Speed Optical Interconnect Development," High Frequency Optical Communications, Cambridge, Massachusetts, September 23–24, 1986, *Proc. SPIE*, Vol. 716, pp. 32–40.

Rapid progress in very large-scale integration/very high-speed integrated circuit (VLSI/VHSIC) technology has improved on-chip density and speed, while the packaging of these high-speed chips is becoming extremely difficult and in some cases limits system performance. This paper reviews the concepts and technology for advanced optical interconnects which will allow a dramatically improved system throughput in high-speed computing applications.

Kane, M., *et al.*, "GaAs 8:1 Multiplexer and 1:8 Demultiplexer Chip Set for High-Speed Transmission of Television and Digital Data," High Frequency Optical Communications, Cambridge, Massachusetts, September 23–24, 1986, *Proc. SPIE*, Vol. 716, pp. 131–138.

Recent advances in processing and circuit technology have made possible the medium-scale integration of high-speed ICs with production-oriented repeatability. By using depletion-mode buffered field-effect transistor (FET) logic technology, GaAs 8:1 multiplexer and 1:8 demultiplexer circuits were designed and fabricated as single-chip subsystems capable of operating at data rates up to 1.7 Gbit/s. The multiplexer and demultiplexer are packaged in 44-lead multilayer ceramic packages with 50-Ω transmission lines on all I/O pins and on-package decoupling capacitors. Typical transition time for the output data is 150 ps, and power dissipation is 2 W for both chips.

Microwaves & RF, **Vol. 25, No. 3, March 1986.**

This issue is devoted to GaAs technology and commercial digital integrated circuits. It provides an up-to-date examination of GaAs IC technology and markets, including discussions with vendors, testing techniques, and descriptions of work on silicon NMOS devices. The latter devices compete with GaAs counterparts in terms of speed, yet offer low power consumption.

Prucnal, P. R., "All-Optical Ultra-Fast Networks," Fiber Telecommunications and Computer Networks, Cambridge, Massachusetts, September 23–24, 1986, *Proc. SPIE*, Vol. 715, pp. 42–47.

The use of optical signal processing and novel optical architectures in networks is discussed. Examples of two experimental all-optical passive star networks are presented: asynchronous code-division multiple access (spread-spectrum), and fixed assignment time-division multiple access (at 500 Mbit/s). An active star network, utilizing an all-optical, self-routing, strictly nonblocking photonic switch, is also presented. The feasibility of future photonic networks with 10-Gbit/s capacity is discussed.

Spadaro, J. J., "Ultrafast Chips Shoot for Commercial Sockets," *Electronic Products*, Vol. 28, No. 11, November 1, 1985, pp. 42–46.

This article is a review of recent commercially available GaAs logic devices which indicates the rapid development (both achieved and anticipated) in this technological area.

Optical background radiation

Optical background radiation is important in direct-detection ISLs because the background adds noise to the received signal, which can substantially degrade the signal-to-noise ratio or bit error rate of the communications link. The following references quantify the optical background resulting from the sun, planets, moon, and stars.

Bell, E. E., "Spectral Radiance of Sky and Terrain at Wavelengths Between 1 and 20 μm. Part II. Sky Measurements," *Journal of the Optical Society of America*, Vol. 50, No. 12, December 1960, pp. 1313–1320.

Quantitative data are presented to illustrate the infrared spectral radiance of the sky under a variety of situations. A qualitative discussion of the dominant spectral features based on a simple model of the atmosphere is given to show the importance of the emission and scattering processes, and the effect of angle of elevation, angle of azimuth, sun angle, and cloud cover.

***Geophysical Activity Reports, World Data "A" for Solar-Terrestrial Physics*, Boulder, Colorado: U.S. Department of Commerce, NOAA, and Environmental Data and Information Services.**

This is a continuously updated collection of Geophysical Activity Reports compiled by the U.S. Department of Commerce and NOAA for environmental data and information services.

Kondratev, K. Y., *Radiation Characteristics of the Atmosphere and the Earth's Surface*, NASA TTF-678, New Delhi, India: Amerind Publishing Co., 1973.

This excellent reference discusses atmospheric radiation and earth albedo observed in various geographic locations and under various environmental conditions. Several models for estimating background radiation are also discussed.

Liou, K. N., *An Introduction to Atmospheric Radiation*, New York: Academic Press, 1980.

A comprehensive analysis of the observed atmospheric radiation under various atmospheric conditions throughout the world is presented. Solar spectral irradiance as a function of height, and a profile of the average intensity of solar energy reflected by the earth, are included.

Meisenholder, G. W., "Planet Illuminance–Range and Phase Angle," Jet Propulsion Laboratory, Pasadena, California, Report No. JPL-TR-32-361, November 1962. NTIS No. N63-13443.

The background power density curves for the moon, planets, and stars are estimated for the worst-case scenario of normal incidence.

Pratt, W. K., "Background Radiation," *Laser Communication Systems*, New York: John Wiley and Sons, 1969.

A concise chapter on background radiation and its effect on laser communication links is provided.

Ramsey, R. C., "Spectral Irradiance From Stars and Planets Above the Atmosphere from 0.1 to 100 Microns," *Applied Optics*, Vol. 1, July 1962, pp. 465–471.

Using published data on star irradiances in the visible region, and assuming a blackbody distribution of energy, irradiances from stars and planets are calculated over the spectral range of 0.1 to 100.0 μm. Results are available in chart form for ready application to the space environment.

Valley, S. L., ed., *Handbook of Geophysics and Space Environments*, New York: McGraw-Hill, 1965.

This comprehensive and heavily referenced source book for solar electromagnetic radiation was compiled by the Air Force Cambridge Research Laboratory (AFCRL).

Radiation effects

The following papers describe the charged particles in the geostationary orbit, and the effect of this radiation environment on the performance of semiconductor sources and detectors. These considerations have led to radiation-hardened designs for the various optical components to minimize the impact of radiation on device lifetimes and ISL communications performance.

Aukerman, L. W., *et al.*, "Radiation Effects on Semiconductor Optical Devices for Space Communications," Laser and Laser Systems Reliability, Los Angeles, California, January 28–29, 1982, *Proc. SPIE*, Vol. 328, pp. 56–65.

A survey of published results is presented on radiation effects in diode lasers and photodiodes as applied to space communications. For diode lasers,

irradiation causes a speed-up of the aging characteristics, an increase in the threshold current, a shift in the lasing wavelength, a change in the mode structure, a decrease in the light output at constant current, and an increase in the turn-on time delay. However, these effects are not a significant problem at fluence levels under 10^{14} neutron/ cm^2, provided the diode laser is operated well above the threshold and is well heat-sinked. Furthermore, gamma irradiation should pose no threat to most types of diode lasers.

Photodiode detectors, on the other hand, and particularly avalanche photodiodes (APDs), are degraded by sustained ionizing radiation. The effect of radiation is either to decrease the responsivity or increase the noise, with the latter being more important. The radiation insensitivity of silicon PIN photodiodes can be improved by using direct bandgap material and employing a double-heterostructure design that blocks nearly all the minority carriers generated outside the depletion region. Such a design, if successfully applied to APDs, would be extremely valuable.

Aukerman, L. W., *et al.*, "Radiation Threshold Levels for Noise Degradation of Photodiodes," *Optical Engineering*, Vol. 23, No. 5, September/October 1984, pp. 678–684.

The radiation threshold doses and radiation dose rates for a PIN photodiode and an avalanche photodiode in a space environment are calculated. The calculations involve an assessment of the photodetector noise currents as a result of either a sustained ionizing dose rate or displacement damage. Experimental results which verify the models used are discussed.

Barnes, C. E., "Radiation-Hardened Optoelectronic Components: Sources," Optical Technologies for Communication Satellite Applications, Los Angeles, California, January 21–22, 1986, *Proc. SPIE*, Vol. 616, pp. 248–253.

The effects of various types of radiation on the sources used in practical optoelectronic systems are reviewed. The most severe radiation effects problem for LEDs and diode lasers is light output degradation due to permanent, radiation-induced lattice damage. However, this effect can be minimized by judicious modification of material and device parameters. For diode lasers, structures should be chosen which have low threshold currents and high maximum operating currents.

Johnston, A. H., and R. S. Caldwell. "Design Techniques for Hardened Fiber Optic Receivers," *IEEE Transactions on Nuclear Science*, Vol. NS-27, No. 6, December 1980, pp. 1425–1431.

Radiation-hardened design techniques for fiber optic receivers are discussed which consider transient ionization and permanent damage effects. The results indicate a fundamental tradeoff between optical sensitivity and transient ionization hardness that depends primarily on the bit rate and the physical characteristics of the detector. In addition, various input stage designs and modulation methods can be considered in order to optimize both optical sensitivity and radiation hardness.

Kalma, A. H., and W. H. Hardwick, "Radiation Testing of PIN Photodiodes," *IEEE Transactions on Nuclear Science*, Vol. NS-25, No. 6, December 1978, pp. 1483–1488.

PIN photodiodes representative of commercially available device types were radiation tested for total dose exposure up to 10^8 rad (Si), neutron fluence exposure up to 10^{14} n/cm^2, and ionizing pulse exposure up to 10^7 rad (Si)/s in 10-ms pulses and 10^{13} rad (Si)/s in 20-ns pulses. The first two tests examined permanent degradation effects, and the last test examined the transient response to ionizing radiation. Surface shunt paths were observed in all devices, which produced a decreased optical response and an increased dark current. In devices biased to less than full depletion, lifetime degradation was observed.

Mitchell, K. W., "Optimizing Photodetectors for Radiation Environments," *IEEE Transactions on Nuclear Science*, Vol. NS-24, No. 6, December 1977, pp. 2294–2297.

Maximum allowable radiation dose rates normalized to the incident optical signal intensity are determined for various photodiode materials at different wavelengths of interest as a function of the effective collection depth. Modeling indicates that thin active regions are necessary to increase the radiation insensitivity of photodiodes. Multipass detector structures and the use of high optical absorption coefficient materials significantly increase the optical quantum efficiency, and thus the maximum allowable radiation dose rate, for thin photodiodes.

Paul, D. K., "Panel Summary: Fiber Optics Reliability in Benign and Adverse Environments," Fiber Optics Reliability: Benign and Adverse Environments, San Diego, California, August 17–18, 1987, *Proc. SPIE*, Vol. 842.

Paul, D. K., "Panel Summary: Fiber Optics Reliability," Fiber Optics Reliability: Benign and Adverse Environments II, Boston, Massachusetts, September 6–8, 1988, *Proc. SPIE*, Vol. 992.

Fiber optic and optoelectronic reliability issues in benign and adverse environments are discussed by a group of distinguished panelists. The *Proceedings* also includes a number of contributed and invited papers on radiation effects in fiber optics and high-speed electronics.

Singh, R. S., and W. D. Raburn, "Reliability Considerations of Si and GaAs Active Components," Reliability Considerations in Fiber Optic Applications, Cambridge, Massachusetts, September 25–26, 1986, *Proc. SPIE*, Vol. 717, pp. 85–91.

The performance of silicon and gallium arsenide active components such as photodetectors, silicon metal-oxide semiconductor field-effect transistors (MOSFETs), and GaAs metal semiconductor FETs (MESFETs) operating in typical radiation environments (total-dose gamma, high-dose-rate gamma, high-energy heavy particles and neutrons) is measured. The effect on charge trapping and interface state generation in the silicon dioxide due to total-dose gamma radiation is reported. Various process optimization steps used to enhance the radiation immunity in silicon technology, and their relevance to high-reliability optical communications systems, are presented.

Stassinopoulos, E. G., "The Geostationary Radiation Environment," *Journal of Spacecraft*, Vol. 17, No. 2, March–April 1980, pp. 145–152.

The distribution of charged particles in the geostationary orbit is reviewed in terms of population domains, where trapped constituents (energetic electrons and protons) and transients (solar flare protons) have been considered. Synchronous geomagnetic geometry is discussed, and temporal and spatial variations of trapped particles are briefly reviewed. Finally, calculated results are presented for orbital flux integrations and dose and shielding evaluations. The data, given in graphic and tabular form, are explained and discussed.

Wiczer, J. J., *et al.*, "Transient Effects of Ionizing Radiation in Photodiodes," *IEEE Transactions on Nuclear Science*, Vol. NS-28, No. 6, December 1981, pp. 4397–4402.

This paper reports on photodiode structures designed and fabricated to reduce the amplitude of the noise current induced during exposure to ionizing-radiation environments, without significantly reducing the desired photodiode signal current. Photodiodes fabricated from AlGaAs, AlGaSb, and InGaAsP compound semiconductor materials are studied in the 0.7- to 1.4-μm wavelength range. These specially fabricated, radiation-insensitive photodiodes have also been compared with commercially available photodiodes in an ionizing-radiation environment.

Wiczer, J. J., *et al.*, "Permanent Damage Effects in Si and AlGaAs/GaAs Photodiodes," *IEEE Transactions on Nuclear Science*, Vol. NS-29, No. 6, December 1982, pp. 1539–1544.

This paper reports on permanent damage effects in photodiodes due to total-dose exposures of 10^8 rad (Si). The degradation of optical quantum efficiency and increases in photodiode leakage current in silicon PIN structures are compared with those in specifically designed and fabricated AlGaAs/GaAs photodiodes. Results indicate some degradation in quantum efficiency for both types of devices. Leakage currents were found to increase significantly after 10^8 rad in the silicon PIN structures, but to increase only slightly in the AlGaAs/GaAs structures.

Wiczer, J. J., "Radiation-Hardened Optoelectronic Components: Detectors," Optical Technologies for Communication Satellite Applications, Los Angeles, California, January 21–22, 1986, *Proc. SPIE*, Vol. 616, pp. 254–266.

Recent research in the area of radiation-hardened optical detectors is reviewed, including radiation effects on conventional silicon PIN photodiodes, special radiation-hardened silicon PIN photodiodes, and special double-heterojunction AlGaAs/GaAs photodiodes. It is shown that detectors can be fabricated which function acceptably after exposure to neutron fluences of 10^{15} n/cm^2, total-dose gamma exposure of 10^8 rad (Si), and flash x-ray environments of 10^8 rad/s (Si). Detector structures that can operate under these conditions, pre-rad and post-rad operational characteristics, and experimental conditions are described.

Translations of Abstracts

Liaisons intersatellites: application aux satellites de télécommunications commerciales

Y. S. LEE, A. E. ATIA ET D. S. PONCHAK

Sommaire

On décrit les caractéristiques fondamentales des systèmes de liaison intersatellites (LIS) et leur application aux télécommunications par satellite nationales, régionales et mondiales. On souligne également les avantages quantitatifs qu'offrent les LIS pour ce qui est de l'amélioration de l'utilisation de l'orbite, de l'occupation du spectre, du temps de propagation de la transmission (comparé aux liaisons à plusieurs bonds), de la couverture et de la connexité, outre la diminution du nombre d'antennes de stations terriennes qu'elles permettent. On détermine la rentabilité et les autres avantages au niveau des systèmes que présente l'utilisation des LIS, et l'on traite des questions techniques et de planification des systèmes liées à la mise en oeuvre des LIS.

Comparaison de technologies optiques pour les charges utiles de liaison intersatellites

Première Partie. Estimations de masse, d'énergie primaire et de volume

R. G. MARSHALEK

Sommaire

On compare six technologies optiques pour ce qui est des impératifs de masse, d'énergie primaire et de volume (MPV) de la charge utile de télécommunications d'une liaison intersatellites (LIS) dans le cas d'une interconnexion duplex entre deux satellites géostationnaires. Les sous-systèmes de télécommunications des charges utiles LIS sont